Intergovernmental Oceanographic Commission technical series

Time series of ocean measurements

Volume 4 - 1988

Unesco 1988

For bibliographic purposes this document should be cited as follows:

IOC. Time series of ocean measurements
Volume 4, 1988. *IOC Tech. Ser. 33*
Unesco, 1988

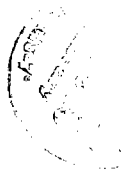

ISBN 92-3-102604-6

Published in 1988
by the United Nations Educational,
Scientific and Cultural Organization,
7. place de Fontenoy, 75700 Paris

Printed in Unesco's Workshops

Printed in France

Foreword

"Time series of ocean measurements" was instituted by the Intergovernmental Oceanographic Commission (IOC) in 1983 in response to the need expressed by the research community to demonstrate the importance and usefulness of time series data to the understanding of oceanic and atmospheric processes. The historical events, such as the Tokyo Time Series Meeting in 1981, and the decisions which have contributed to the promotion of time series of ocean measurements, are outlined in Volume 1 of the series (IOC Technical Series No. 24, Unesco 1983).

The primary purpose of this emphasis on time series is to support the World Climate Research Programme (WCRP) and to encourage the creation of data sets necessary for climate prediction. The WCRP entered a new phase in January 1985 when the first large-scale experiment with an ocean component - the study of the Interannual variability of the Tropical Oceans and Global Atmosphere (TOGA) - began.

The observational strategy of TOGA is to measure, for a ten-year period, the month-to-month variability of the temperature field and currents in the upper layer of the Tropical oceans in the latitude band 20°N to 20°S. The second large-scale WCRP endeavour, the World Ocean Circulation Experiment (WOCE), will begin later in the decade when oceanographic satellite systems, including at least one altimetric mission, are launched. The observational strategy for WOCE includes a global suite of *in-situ* observations for an initial five-year period including tide gauges, hydrography from research ships, expendable bathythermographs from ships of opportunity and drifting buoys. Several of the ongoing time series projects presented in this volume address the observational requirements of TOGA and WOCE and are assisting scientists in establishing the criteria for the TOGA and WOCE observational strategies. These projects also have the potential of extending TOGA and WOCE, as the representativeness of the discrete ten and five-year experimental periods will be checked against earlier and follow-on data.

The time series volumes are prepared by the Joint IOC/SCOR (Scientific Committee on Oceanic Research) Committee on Climatic Changes and the Ocean (CCCO). This volume was edited by Arthur G. Alexiou, a NOAA Consultant to the IOC.

The ideas and opinions expressed herein are those of the authors and do not necessarily represent the views of Unesco or IOC.

Finally, should you be interested in having an article published in this annual review, you are invited to submit an abstract to the Secretary, Unesco, Intergovernmental Oceanographic Commission, 7 place de Fontenoy, 75700 Paris, France.

List of Contributors

J.G.H. Dias
Grupo de Oceanografia
Departamento de Fisica/Centro de Geofisica
Universidade de Lisboa
Rua da Escola Politecnica, 58
1200 Lisboa, Portugal

J.R. Donguy
Groupe SURTROPAC
Antenne ORSTOM
BP 337
29273 Brest Cedex
France

A.F.G. Fiuza
Grupo de Oceanografia
Departamento de Fisica/Centro de Geofisica
Universidade de Lisboa
Rua da Escola Politecnica, 58
1200 Lisboa, Portugal

D.M. Legler
Mesoscale Air-Sea Interaction Group
Department of Meteorology
Florida State University
Tallahassee, FL 32306
United States of America

J.R.N. Lazier
Bedford Institute of Oceanography
Dartmouth, Nova Scotia
Canada

J.J. O'Brien
Mesoscale Air-Sea Interaction Group
Department of Meteorology
Florida State University
Tallahassee, FL 32306
United States of American

J.P. Rebert
Groupe SURTROPAC
Antenne ORSTOM
BP 337
29273 Brest Cedex
France

J-M. Verstraete
ORSTOM
Laboratoire d'Océanographie Dynamique et Climatologie
Institut Océanographique
195 Rue St Jacques
75005 Paris France

S. Zuta
Direccion General de Investigaciones Oceanograficas
Instituto del Mar
Callao, Peru

Contents

1 . Measurements from Instruments Moored in the Labrador Current 1978 -1986

John R.N. Lazier

Bedford Institute of Oceanography
Dartmouth, Nova Scotia, Canada

Introduction

The Labrador Current (Figure 1), flows over the continental shelf and slope of eastern Canada from northern Labrador at 60°N to the southern tip of the Grand Banks of Newfoundland at 43°N. From the surface to 1500m, and shoreward of the 2000m isobath, the current transports about $5\pm2\times10^6 m^3/s$ of cold, low-salinity water south from Baffin Bay, Hudson Bay, Foxe Basin and the West Greenland Current. The flow is easily recognized by its frigid temperatures and well known for the sea ice and icebergs it carries south during the winter and spring.

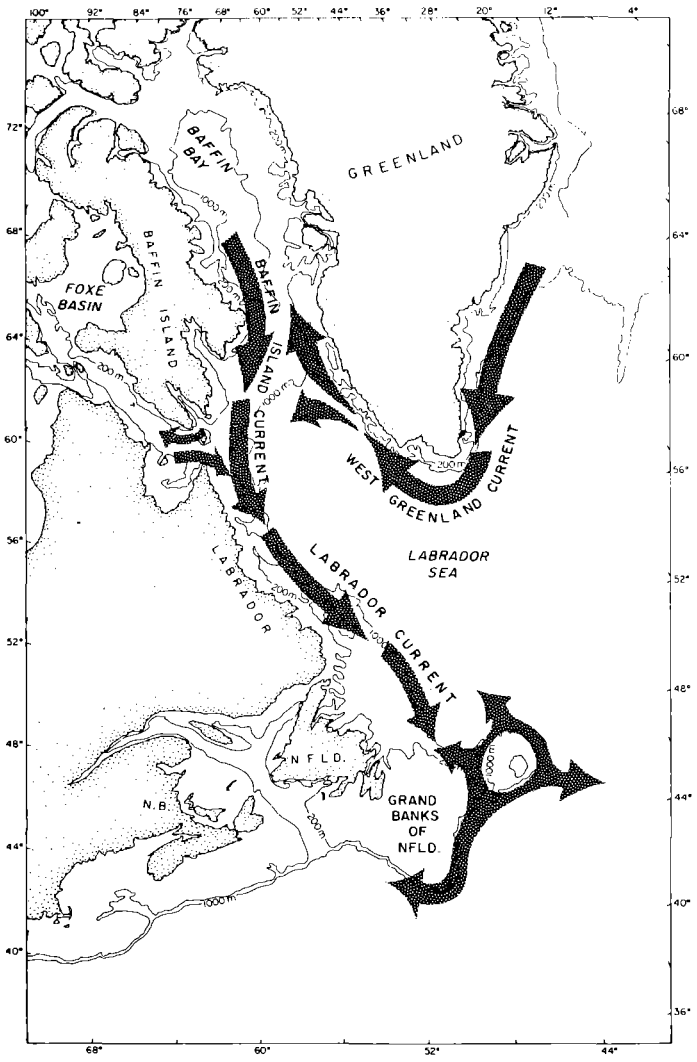

Figure 1. Location of the Labrador Current

The Current's economic importance prompted the Bedford Insitute of Oceanography (BIO) in 1978, to begin a ten year programme to measure some of the significant variables of the current with moored instruments in the vicinity of Hamilton Bank (Figure 2). The purpose of the programme is to determine the means and variations of the parameters important to hydrocarbon exploration and production, fisheries oceanography, climate studies, and understanding the dynamics of the flow. The Hamilton Bank area was chosen for the study because the current is well constrained by topography there, and because it is logistically convenient to Canada's major east coast ports.

This article contains short descriptions of the mooring programme, its successes and failures, the water mass structure across the current and two of the important low frequency signals that have been observed to date.

Mooring Programme

The mooring programme began in October 1978, with current meter moorings at sites 1, 2 and 3 (Figure 2). The first two sites are on the 200 and 300m, isobaths respectively and

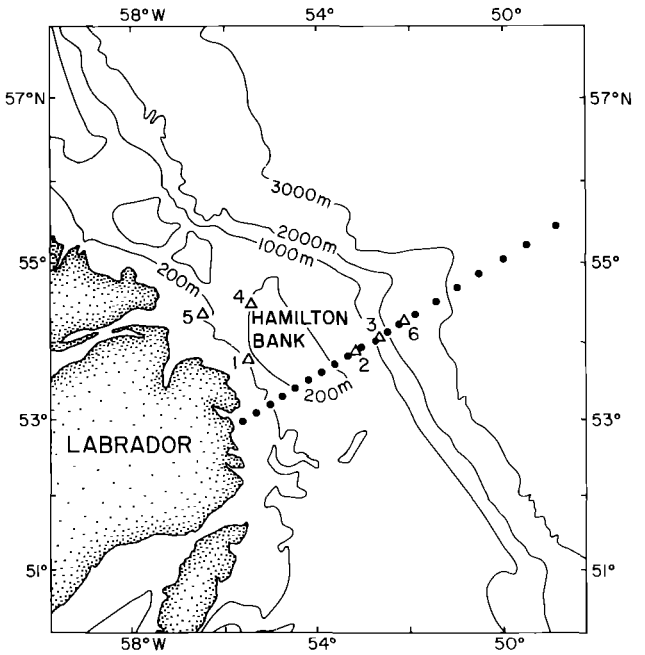

Figure 2. Current meter mooring sites (A) near Hamilton Bank Labrador 1978-1986, and CTD station positions (•) occupied in July 1985.

Figure 3.

Outlines of the three moorings placed at sites 1, 3 and 6 in August 1986.

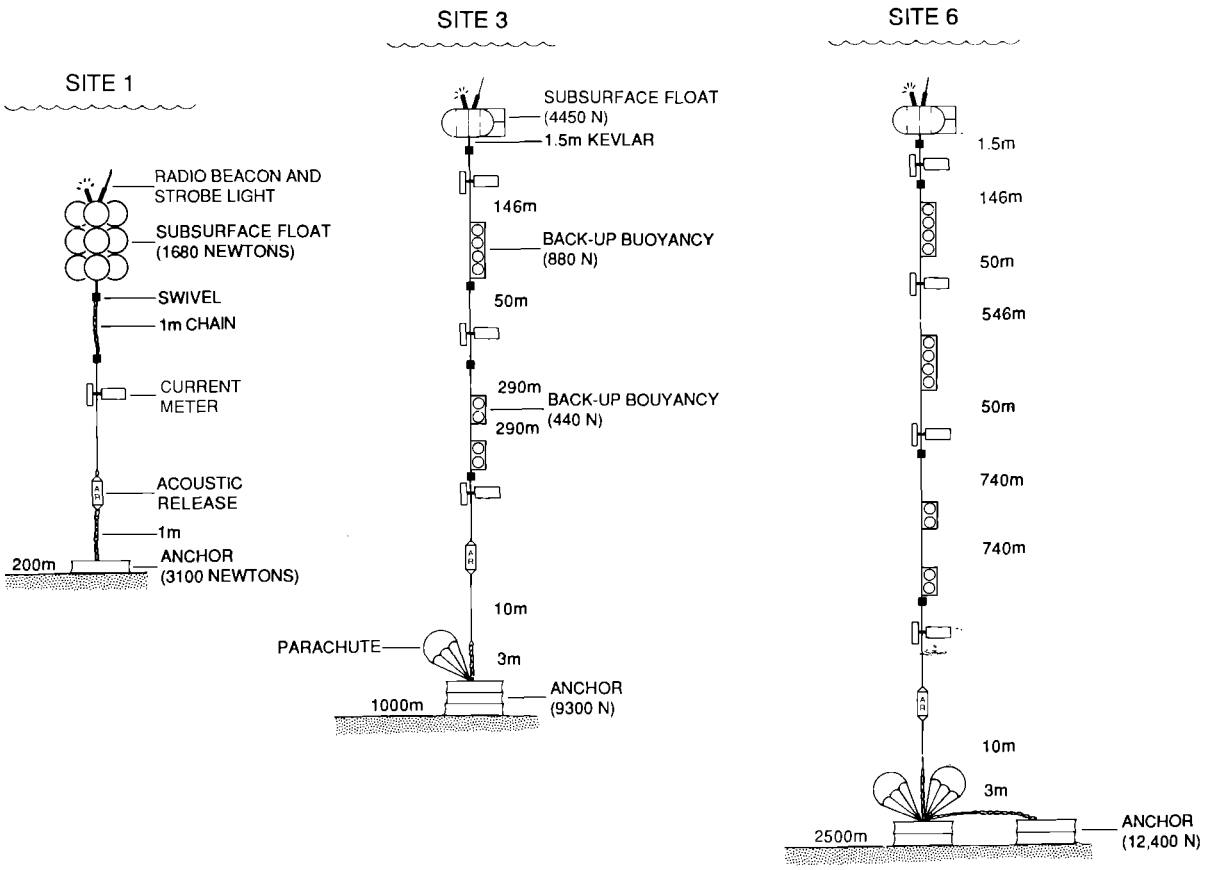

have one instrument each, about 4m, above the bottom (Figure 3). Site 3 is on the 100m isobath and began with instruments at 400m and 1000m. The upper meter was moved down to 600m, between 1981 and 1985 to decrease corrosion-induced losses, and in 1985 the mooring was changed to that shown in Figure 3. To date, seven current meters, five releases and nine floats have been lost of the 51, 35, and 35 respectively that have been deployed. Besides corrosion, icebergs, fishing activity and poor batteries have been suspected to cause losses. Since 1982, however, no equipment has been lost due, in part, to new digital releases with lithium batteries, Kevlar mooring line, and use of proven, safe mooring positions. Advances in shipboard acoustic communication equipment and nagivation equipment have also contributed to the decrease in losses by improving signal identification and the accuracy of mooring relocation.

The moorings at site 2 ended in 1980 because the location is too vulnerable to icebergs. Since that time the third mooring has been shifted around, and one year of data has been collected at each of sites 4, 5 and 6. The most recent mooring configurations are shown in Figure 3. The intervals over which data now exist at the eleven current meter positions are presented in Figure 4.

Throughout the programme Aanderaa RCM5 recording current meters have been used and, when possible, temperature and conductivity have been measured in addition to water velocity. These instruments are stated by the manufacturer to be accurate to ±0.01m/s or ±2% of speed, whichever is greater, ±5° in direction for speeds above .05 m/s, ±0.05°C in temperature and ±0.025 mmho/cm in conductivity. All sensors are calibrated at the Bedford Institute of Oceanography before and after each deployment.

Water Mass Structure

The water in the Labrador Current, especially over the Labrador continental shelf, is distinctly different in temperature and salinity from the water, at the same depth, in the Labrador Sea. The shelf water, having come via regions with an Arctic climate, is cold and of relatively low salinity compared to the warmer, saltier offshore water. Temperature and salinity sections across the shelf and slope (Figure 5), and the temperature versus salinity (θ-s) curves from the same data (Figure 6), illustrate the main features of these two main water masses. Over the shelf and in the open ocean, the horizontal gradients of both salinity and temperature are small compared to the large gradients found over the continental slope. It is here that the cold, low-salinity shelf water is separated by a region of high horizontal gradient from the warmer more saline waters of the open ocean, (Lazier, 1982). The θ-s curves of Figure 6 help to show how constant the water mass characteristics are in the two areas, and how rapid is the change from shelf to oceanic properties.

The high horizontal salinity gradient over the continental slope gives rise to a high horizontal density gradient which results, through the thermal wind relation, in a band of high

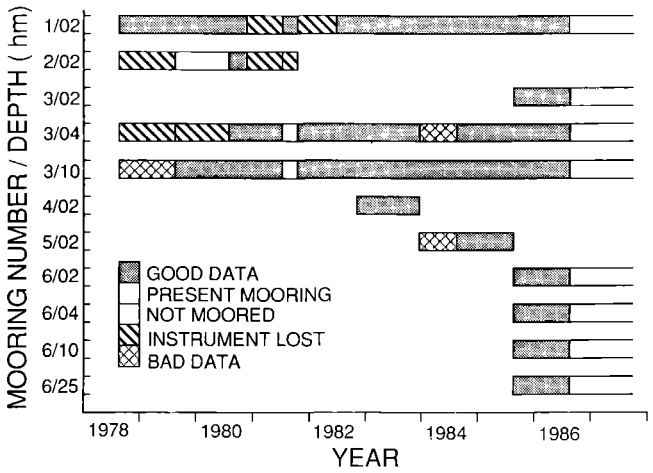

Figure 4. Data return from eleven instruments at six mooring sites from 1978-1986.

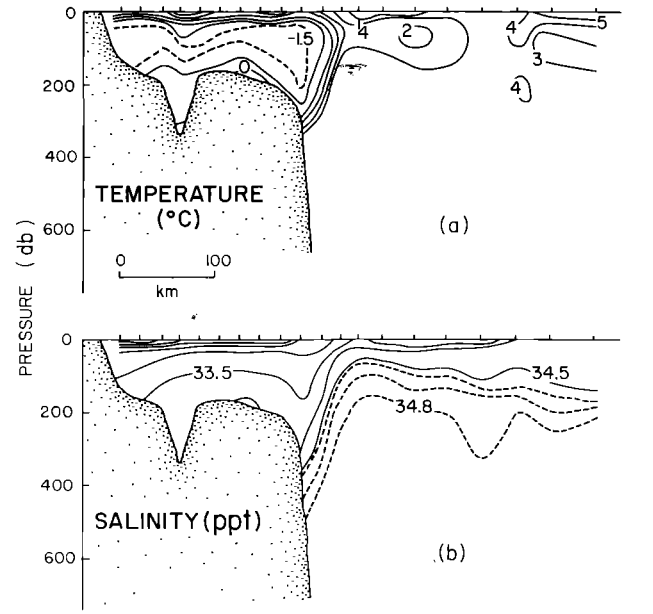

Figure 5. Vertical sections of temperature (a) and salinity (b) across the shelf and slope at Hamilton Bank. The data, obtained in July 1985 at the positions marked along the surface and in Figure 2, were acquired with a Guildline CTD accurate to ±.01°C and ±.005°/oo in salinity.

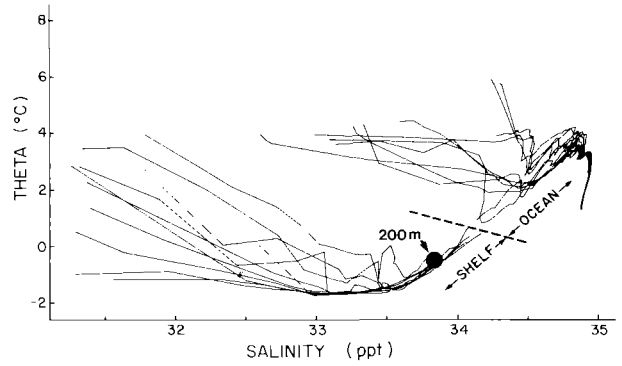

Figure 6. Temperature versus salinity curves from the CTD stations indicated in Figure 2. The approximate location of the 200m observations from over the shelf indicates the position, relative to the water masses, of the current meter at site 1. The division between the shelf and oceanic water masses is suggested by the line passing through 34.1 and 0.8°C.

vertical shear in the current. The consequence is a narrow (50 km) band of flow parallel to the isobaths with speeds, in the centre, up to~1.0 m/s at the surface diminishing to~0.1 m/s at 1000m. This strip of high speed flow is the main branch of the Labrador Current and carries 80% of the total transport of the current. The remaining transport takes place over the shelf in flows of .1-.2 m/s.

Results

Long series of data like these contain many valuable signals from relatively high frequency meteorologically forced oscillations through seasonal cycles to interannual changes that appear to be forced by temporary displacements of the mean circulation in the atmosphere. Over the next few years these signals will be analyzed and results will be published, but for this presentation just an outline of two important ones will be given: the annual variation in velocity of the main jet of the current and the interannual changes in temperature of the water over the shelf.

The velocity in the main jet of the Labrador Current is represented in Figure 7 by the monthly mean velocities at 600m, site 3, parallel to the isobaths. The curve indicates a significant seasonal variation from a minimum of 0.03 m/s in April to a maximum of 0.13 m/s in October. The recently recovered one year record from 200m at the same position shows a similar seasonal oscillation, but with a minimum of 0.05 m/s in April and a maximum of 0.29 m/s in October.

The seasonal change in velocity has been found to be coincident with a seasonal change in the horizontal pressure gradient across the front which separates the shelf and oceanic waters. The gradient changes because the seasonal steric height oscillation is greater over the shelf than in the open ocean. In the open ocean at Ocean Weather Ship BRAVO (56.5°N, 51°W) the steric height increases by approximately 0.048m from the late winter minimum to the late summer maximum. During the same time, the steric height over the shelf increases by approximately 0.132m. The difference, n, shown in Figure 7, approximates the variable part of the difference in sea level from the shelf to the open ocean, which, through the geostrophic and hydrostatic equations, predicts a velocity change close to that calculated for the surface waters from the site-3, current-meter records.

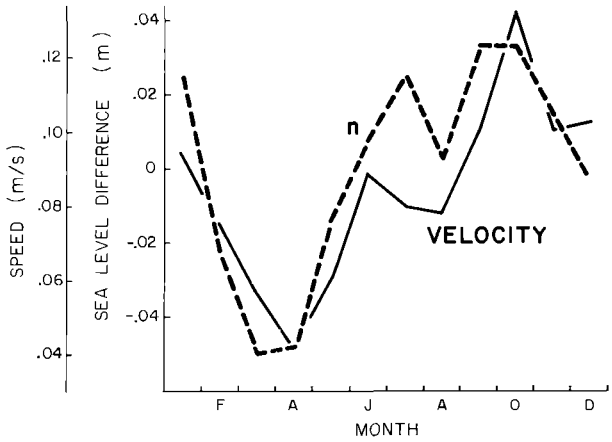

Figure 7. Monthly means of velocity at 600m, site 3, from 1980-1985 and estimates of the monthly values of the sea level differences (n) between the Labrador Shelf and the open ocean.

The steric height rises more over the shelf because the salinity (density) decreases more from winter to summer than in the open ocean. The difference arises because the fresh water, from land run-off and melting ice, flowing out of the Arctic regions is largely confined over the shelf by the succession of boundary currents such as the Labrador Current.

The other important signal found in the long records was observed at site 1. It is the significant cooling of the cold intermediate layer over the shelf from late 1982 to late 1985. The characteristics of the cold layer are shown in Figure 5a and in the θ-s plot of Figure 6. The position of the current meter, which is indicated on the θ-s plot, shows that the observations were obtained at the base of the intermediate cold layer.

The temperature record from 1978 to 1986 is shown in Figure 8 in the form of a monthly anomaly curve. A point on this curve is the difference between the monthly mean temperature and the average temperature calculated from all data collected in that month over all years in the record. The graph shows the temperature to be warmer, by approximately 1°C, during the first two years of the record than during the period from late 1982 to late 1985. The period from late 1980 to late 1982 is in doubt because of data loss during most of the period. The three-month record from the summer of 1981 and the start of the record in late 1982 are both relatively warm and suggest that the warmer period extended through those years too and that the cold period did not start until late 1982.

The cold period was also evident in other data from the area. Abnormally large amounts of ice were found during the winters of 1983/1984 and 1984/1985 over the Labrador Shelf, and CTD measurements obtained during the mooring-replacement cruises showed abnormally cold conditions throughout the water column right across the shelf.

The reasons for the unusually cold water are still being studied. Preliminary investigations show the years of cold water coinciding with years of exceptionally cold winters in the eastern Canadian Arctic. Since the mean wind direction is from the land to the water, it appears that unusually cold air is causing more heat than normal to leave the ocean throughout the eastern Arctic.

Summary

A ten-year programme to continuously measure important variables of the Labrador Current began in 1978. Eleven instrument positions on six moorings have been occupied for periods of from one to eight years. Early difficulties with losses due to corrosion and icebergs and/or fishing appear to have ended with the use of Kevlar mooring line, digital releases and safe mooring positions.

The measurements show the Labrador Current to have a significant annual signal in velocity and transport due, in part, to the large increase in freshwater runoff in the summer. Continuous data from the cold intermediate layer over the shelf show large interannual variations in heat content which seem linked to variations in the winter-time circulation of the atmosphere over the eastern Canadian Arctic.

References

Lazier, J.R., 1982. Seasonal variability of temperature and salinity in the Labrador Current. *Journal of Marine Research*, Vol. 40, Supplement, pp. 341-356.

Figure 8.

Anomaly of monthly mean temperatures recorded at 200m, site 1, between 1978 and 1986.

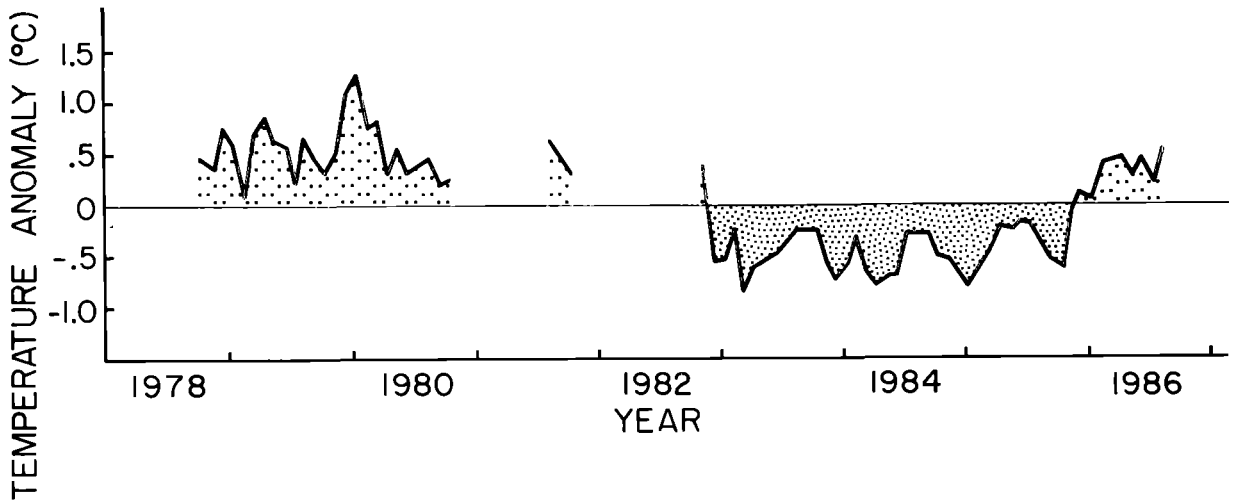

2 .Tropical Pacific Wind Stress Analysis for TOGA

D.M. Legler and J.J. O'Brien

Department of Meteorology
Florida State University Tallahassee, FL, USA

Introduction

Oceanographers have consistently documented important research objectives for TOGA which require analyzed wind-stress fields. It is conceivable to obtain these fields from four sources: analysis of ship and buoy observations, analysis of low-level cloud movements from satellites, analysis of meterological global models, and from scatterometers on polar orbiting satellites. This is a report on the TOGA efforts to prepare maps of "quick-look" ship winds and "research-quality" gridded wind analyses from ship winds and buoys.

Since many areas of the tropical oceans do not have sufficient ship and buoy data to sample the monthly fields adequately, the other three methods are thought by many scientists to be preferable. Sufficient data for monthly fields is generally believed to be a minimum of 10 observations in a 2^{o} latitude by 10^{o} longitude region. Recent ideas on the importance of 30-60-day waves suggest that an ideal research quality data set should have a minimum of 10 observations in a 2 x 5 degree region every five days. Only the wind scatterometers promise to meet this requirement. The low-level cloud data are also sparse over the tropics, particularly due to the lack of satellite coverage in large regions of no low clouds or excessive high clouds. Global meteorological models look promising, but it is widely believed that these models give poor performance in the tropics (due to lack of data?) and boundary layer models in most general circulation models (GCM's) are not physically adequate for good surface stress analysis. Scientists interested in TOGA are working to solve these problems.

TOGA has funded programmes in the U.S. and France to prepare analyses of wind stress fields in the entire Tropical Ocean. Florida State University produces wind stress analyses for the Pacific and Indian Oceans. Dr J. Servain, Orstom, Brest, produces analyses for the tropical Atlantic Ocean. This article will review the history and current status of the data anlysis prepared for the Pacific Ocean, 30^{o}S to 30^{o}N. We have determined that there is sufficient data from the Indian Ocean to prepare a monthly analysis on a 2 x 2 degree grid using a completely objective method. The technology for this is developed and in the future there will be an announcement on the availability of the Indian Ocean data.

The history of the Pacific project is interesting. Wyrtki and Meyers (1975a,b) binned the ship data for the period prior to 1970. They used 2 x 10 degree boxes for each month and eliminated high winds over 40 m/sec. In the mid-seventies, several people suggested that equatorial oceanic Kelvin waves were responsible for initiating El Nino's (Wyrtki, 1975; Hurlburt, Kindle and O'Brien, 1976; McCreary, 1976, etc.). Since oceanographers had never observed these giant Kelvin waves, the theory was dismissed by many as wrong. In order to convince the scientific community, the Mesoscale Air-Sea Interaction Group at Florida State University subjectively analyzed the monthly Wrytki-Meyers data for 1961-1970 and used it to simulate the El Nino's in 1963. 1965 and 1968-1969 (Busalacchi and O'Brien, 1981).

During the 1970's, the NORPAX project collected the Pacific Ocean wind data at Scripps. Dr Steve Pazan, Scripps, provided FSU with the binned data on a 2 x 10 grid. In 1980, we analyzed these data for 1971-1980. Two atlases are available (O'Brien and Goldenberg, 1982, and Legler and O'Brien, 1985). The FSU Pacific Model (Busalacchi, Takeuchi and O'Brien, 1984) was run with these winds and simulated the occurrence, timing and relative amplitude of the 1972 and 1976 El Nino's. These data have been used by many other investigators interested in TOGA to investigate various aspects of the interannual wind stress field over the Pacific and the results of ocean models driven with these winds for 20 years.

After the 1982-1983 El Nino, the U.S. TOGA Project Office funded FSU to prepare "quick-look" wind stress fields and run an experimental El Nino Forecast Model (Inoue and O'Brien, 1984). For the study, we analyzed monthly tropical Pacific winds for the period 1981-1985 using marine reports available through the National Climate Data Center, Asheville. The most recent months were analyzed using data from the National Meteorology Center/Climate Analysis Center. Recently, we decided to redo the analyses for 1961-1980 using the Comprehensive Ocean-Atmosphere Data Set (COADS) CMR5 data. At FSU we have developed improved techniques for the objective identification of bad data and poor analysis. FSU expects to have the 25-year data set (1961-1985) research-quality, gridded, wind-stress product available by July 1987. This data set will be extremely valuable for climate studies for TOGA.

We have compared our climatology with the GFDL climatology prepared by Hellerman and Rosenstein (1983). They compare very well within 20 degress of the equator using a drag coefficient of 1.7×10^{-3} and an air density of 1.2 kg m^{-3}. At higher latitudes, the non-linear drag coefficient used by GFDL yields higher stresses.

Data Analysis

At the end of each month, we receive from NMC/CAC a tape of global marine surface observations that were received over the global telecommunications system (GTS) during that month. These observations originate from merchant ships, buoys, and other marine observing stations. Combined, they total about 165,000 for any given month for the entire world.

The wind vector data in the tropical Pacific region, 30°N to 30°S, 120°E to 70°W, typically 25,000 observations monthly, are first converted to pseudo-stress. (A pseudo-stress vector is defined as the wind components multiplied by the wind magnitude). A pseudo-stress vector of 60 m^2s^{-2} corresponds to 1 dyne cm^{-2} assuming a drag coefficient of 1.4×10^{-3} and an air density of 1.2 $kg\,m^{-3}$). If any individual report of wind speed exceeds 40m s^{-1}, the report is deleted. These pseudo-stress vector components are then binned into 10° longitude by 2° latitude rectangles. In each rectangle with more than two observations, statistical theory is used to eliminate "bad" observations. For each rectangle with greater than two observations, but less than 11, the lowest and the highest component values are ignored. For locations with greater than 10 reports, the top and bottom 10% are removed for each stress component. New averages are then computed, and a three-standard-deviation test is used to eliminate any remaining outliers. The resulting scalar fields are then hand-contoured and checked by trained meteorologists. After digitization, the resulting 2° by 2° maps are given a final examination and additional wind reports, for example island stations, are used to verify the maps. Fields of the anomaly from the 23-year (1961-1983) mean month are also produced. This data is used at Florida State University to drive a numerical model (see Busalacchi and O'Brien, 1980, 1981) producing estimates of the upper ocean currents in the tropical Pacific. It is also used in predicting the occurrence of El Nino events (Incue and O'Brien, 1984; Inoue et al, 1985).

In the following calendar year, a more complete data set of marine reports is obtained from the National Climatic Data Center (NCDC). This set contains data already received via the GTS and supplemental reports that were received late. The increase in the number of observations in the tropical Pacific regions is about 10-25%. The analysis procedure is the same for this more complete data set, and the results constitute the 'research quality' product.

Interpretation of Late 1986 Data

During the last three months of 1986 (Figures 1a, 1b, 1c) the tropical Pacific winds displayed large month-to-month variations. In the western Pacific, off the east coast of Australia for example, the winds increased from weak south-easterlies in October to very strong south-easterlies in December. The anomalies also reflect this large variation.

Another example of the important variations of tropical Pacific winds is in the western equatorial Pacific where there was a decrease of easterly winds and an easterly shifting and intensification of equatorial westerlies, particularly for December 1986. Similar patterns were also noted in a previous case (Figure 2). Before the onset of the 1982-1983 El Nino, westerly anomalies strengthened and intesified eastward in early to mid-1982. These anomalies continued eastward through mid-1983, although the anomalies in the western equatorial Pacific changed to moderate during the mature stages of this episode. The early data in late 1986 indicated a similar strengthening of the equatorial westerlies, but the timing of the onset was different from that of the 1982-1983 event. Supporting data such as Peruvian coastal temperatures, indicated the beginning of an El Nino event.

Data Availability

The products described are available to anyone who desires them. Copies of the monthly analyses of stress and the computed currents are mailed directly to many researchers. Monthly stress analyses are available on magnetic tape for the period 1960 to the present month. The stress fields since November 1985 are available via an easy-to-use, dial-up computer system for U.S. scientists. For additional information, please contact us (telemail, J.OBRIEN/OCEAN; telephone (904) 644-4581; mail: Meteorology Annex, Florida State University, Tallahassee, FL 32306, U.S.A).

Acknowledgements

We would like to sincerely thank all the people who have analyzed the hundreds of maps necessary for this project. Thanks also to Jay Breidenbach for Figure 2 and to Rita Kuyfer for typing. This work has been supported by the National Science Foundation under grant OCE 8415986 and by NOAA grant NA 84AA-D-00049.

Figure 1.

Surface Pseudo-Stress Vectors for (a) October, (b) November, and (c) December 1986.
Pseudo-stress vectors are subjectively analyzed from ship winds,
digitized on a 2° grid and drawn on a 2° latitude, 4° longitude grid for display.
Contour interval of the vector magnitude is 20 m^2s^{-2}. Vectors of magnitude less than 9 m^2s^{-2} are not drawn.
The anomaly is a departure from the 23 year (1961-1983) monthly mean.
Contour interval of vector magnitude is 15 m^2s^{-2}. Vectors of magnitude less than 3 m^2s^{-2} are not drawn.

Figure 1a

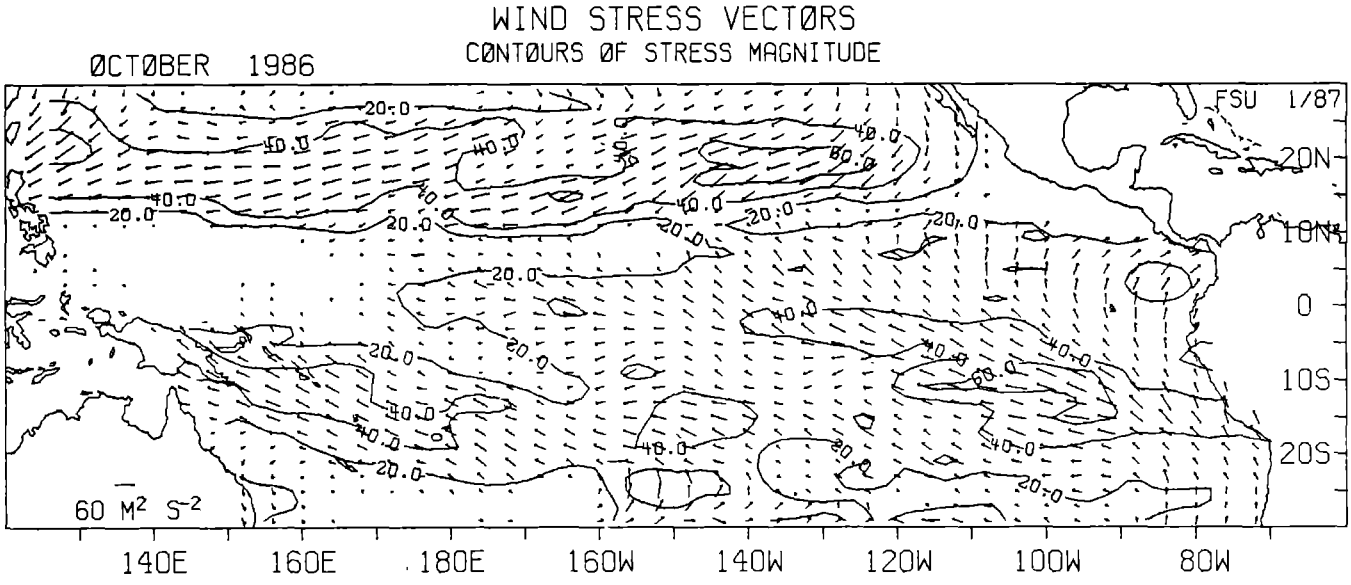

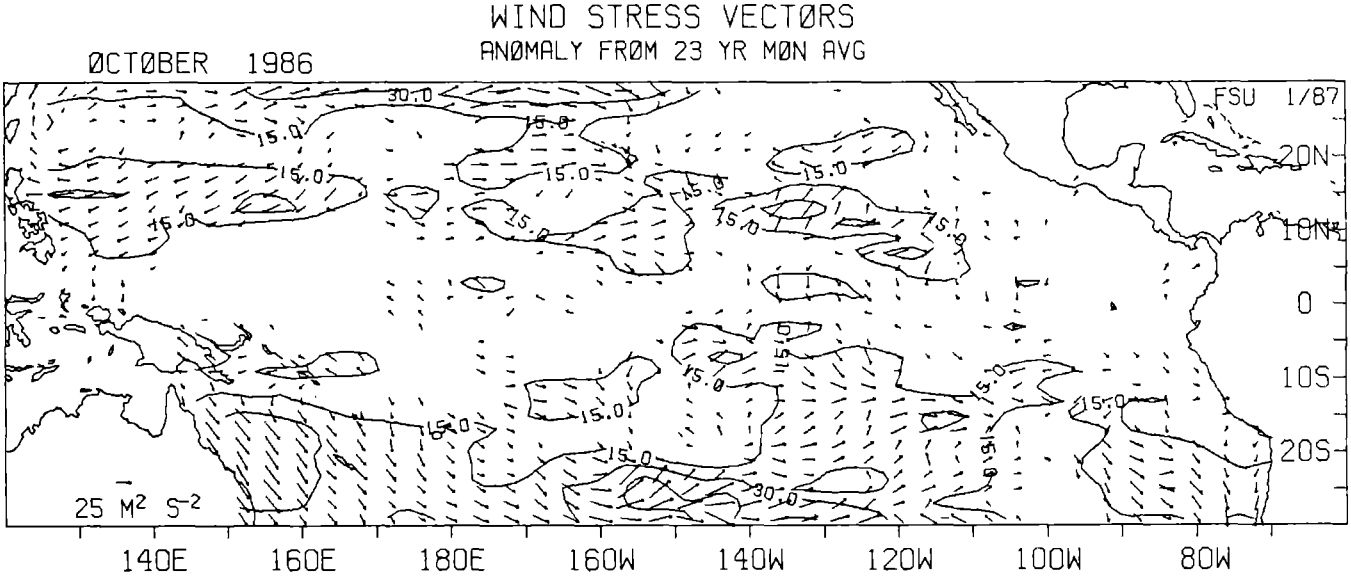

Figure 1b

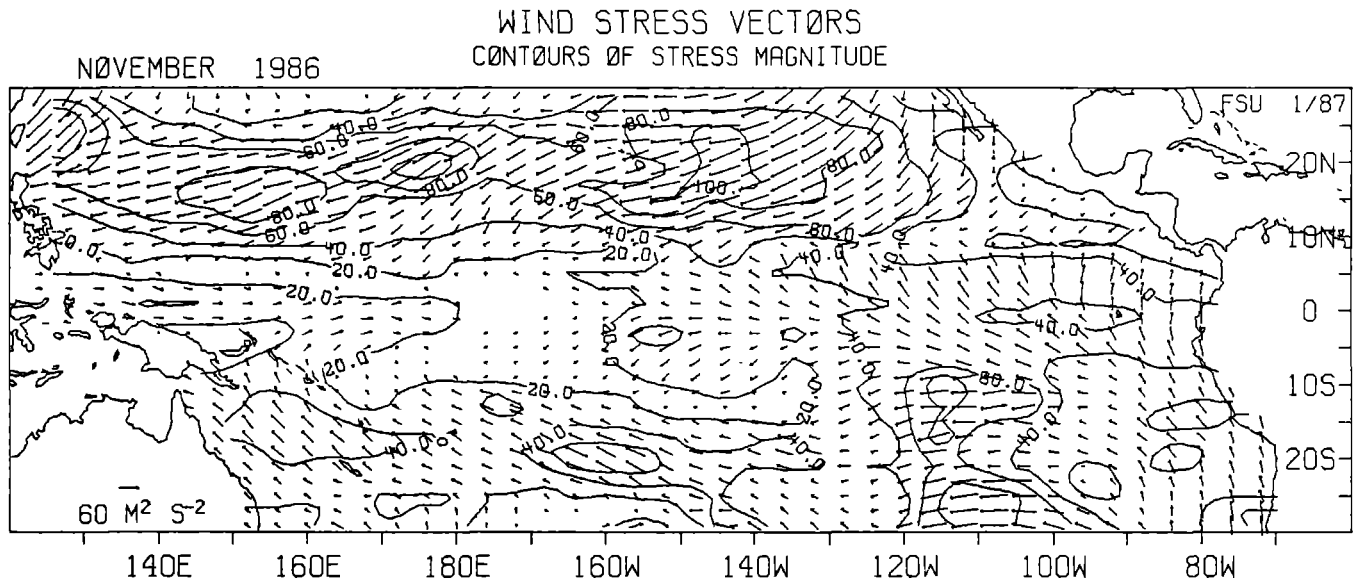
WIND STRESS VECTØRS
CØNTØURS ØF STRESS MAGNITUDE
NØVEMBER 1986
FSU 1/87
20N
10N
0
10S
20S
60 M² S⁻²
140E
160E
180E
160W
140W
120W
100W
80W

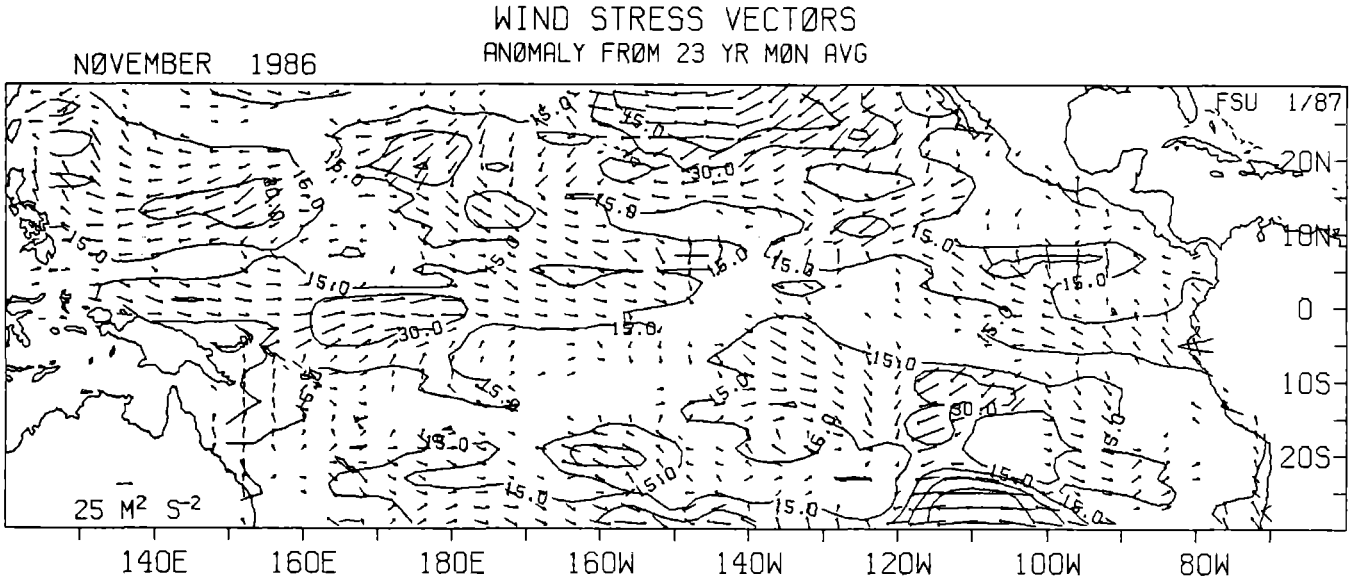
WIND STRESS VECTØRS
ANØMALY FRØM 23 YR MØN AVG
NØVEMBER 1986
FSU 1/87
20N
10N
0
10S
20S
25 M² S⁻²
140E
160E
180E
160W
140W
120W
100W
80W

Figure 1c

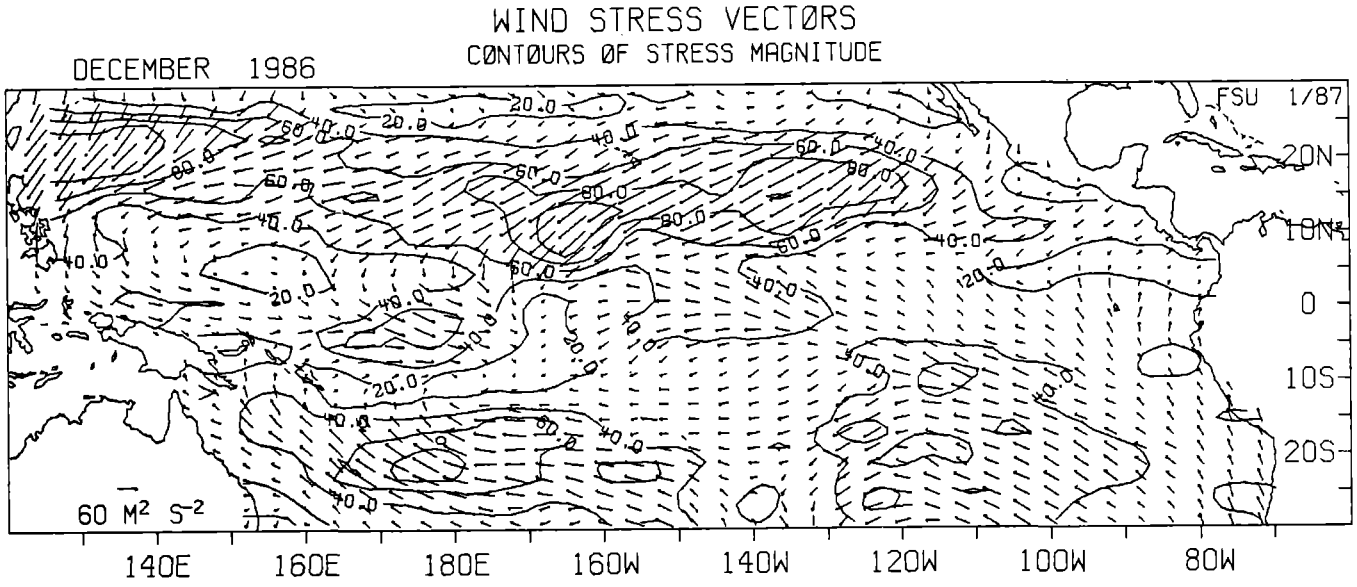
WIND STRESS VECTØRS
CØNTØURS ØF STRESS MAGNITUDE
DECEMBER 1986
FSU 1/87
20N
10N
0
10S
20S
60 M² S⁻²
140E
160E
180E
160W
140W
120W
100W
80W

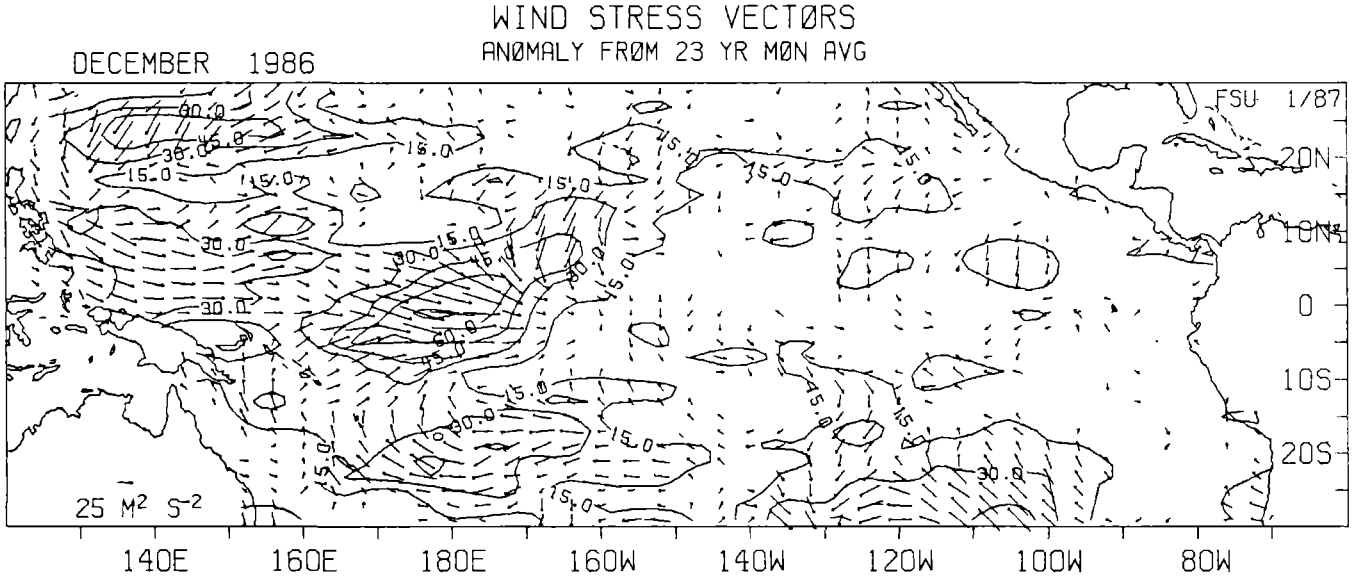
WIND STRESS VECTØRS
ANØMALY FRØM 23 YR MØN AVG
DECEMBER 1986
FSU 1/87
20N
10N
0
10S
20S
25 M² S⁻²
140E
160E
180E
160W
140W
120W
100W
80W

Figure 2.

Longitude-time diagram of pseudo-stress east-west component averaged
from 6S to 6N from January 1980 to December 1986.
A Hanning filter was applied in time and in longitude.
Solid lines indicate winds from the west, dashed lines indicate winds from the east.
Units are m^2s^{-2}, and the contour interval is 10 m^2s^{-2}.

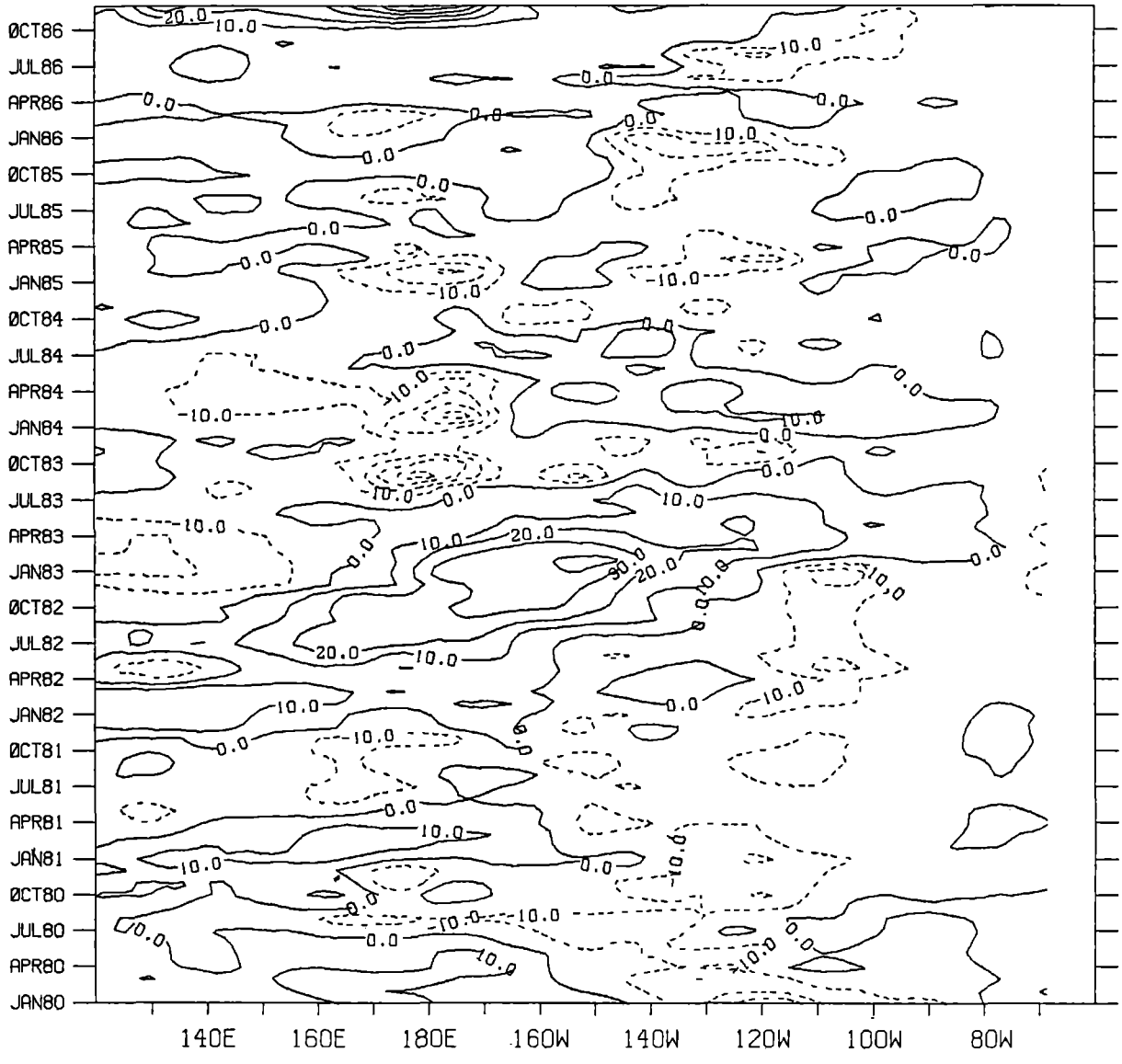

References

1. Busalacchi, A.J., and O'Brien J.J., 1980. The seasonal variability in a model of the tropical Pacific, *J. Phys. Oceanogr.*, 10, pp. 1929-1951.

2. Busalacchi, A.J., and O'Brien, J.J., 1981. Interannual variability of the equatorial Pacific in the 1960's. *J. Geophys. Res.*, 86, pp. 10,901-10,907.

3. Busalacchi, A.J., Takeuchi, K., and O'Brien J.J., 1984. Interannual variability of the equatorial Pacific-Revisited, *J. Geophys. Res.*, 88, pp. 7551-7562.

4. Hellerman, S., and Rosenstein, M., 1983. Normal monthly wind stress over the world ocean with error estimates. *J. Phys. Oceanogr.*, 13, pp. 1093-1104.

5. Hurlburt, H.E., Kindle, J.C., and O'Brien, J.J., 1976. A numerical similation of the onset of El Nino, *J. Phys.Oceanogr.*, 6(5), pp. 621-631.

6. Inoue, M., and O'Brien J.J., 1984. A forecasting model for the onset of a major El Nino, *Mon. Wea. Rev.*, 112, No.11, pp. 2326-2337.

7. Inoue, M., O'Brien, J.J., White, W.B., and Pazan, S., 1985. Interannual variability in the tropical Pacific prior to the onset of the 1982/1983 ENSO event, submitted to *J. Geophys. Res.-Oceans.*

8.Legler, D.M., O'Brien, J.J., 1985. Atlas of Tropical Pacific Wind-Stress Climatology 1971-1980, Florida State University, Tallahassee, 187 pp.

9.McCreary, J.P., Jr., 1976, Eastern tropical ocean response to changing wind systems: with application to El Nino, *J. Phys. Oceanogr.*, 6, pp. 632-645.

10.O'Brien, J.J., and Goldenberg, S.B., 1982, Atlas of Tropical Pacific Wind Climatology, 1961-1970, Florida State University, Tallahassee, 187 pp.

11.Wyrtki, K., 1975. El Nino The dynamic response of the equatorial Pacific Ocean to atmospheric forcing, *J. Phys. Oceanogr.*, 5, pp. 572-584.

12.Wyrtki, K., and Meyers G., 1975. The trade wind field over the Pacific Ocean, Part I: The mean field and the mean annual variation, *Hawaii Inst. Geophys.*, Rept. HIG-75-1, 26 pp.

13.Wyrtki, K., and Meyers, G., 1975. The trade wind field over the Pacific Ocean, Part II: Bimonthly fields of wind stress: 1950 to 1972, *Hawaii Inst. Geophys.*, Rept. HIG-75-2.

3. Meridional Circulation and Heat Transport in the Subtropical North Atlantic from One Year of XBT Measurements with a Voluntary Observing Ship

A.F.G. Fiuza and J.G.H. Dias

Grupo De Oceanografia, Departamento De Fisica
Universidade De Lisboa, Portugal

Introduction

The Oceanography Group of the University of Lisbon has been conducting the CLIVA Project (Climate and Variability of the North Atlantic) since 1983 with the following basic objectives:

1. to characterize means and fluctuations of sea temperatures and salinities from observations along a quasi-zonal transect in the subtropical North Atlantic;
2. to evaluate the ocean heat content and the relative contributions of mean and eddy components of the meridional heat and mass transports across that zonal section and to investigate their respective seasonal cycles and interannual variability;
3. to contribute to the international effort of systematic observations of the ocean with voluntary observing ships and to optimize the sampling strategy to be adopted in such programmes in the North Atlantic.

Results will be presented in this paper of the first complete year of observations accomplished during CLIVA.

Observations and Methods

After an initial period of equipment tests and trials at sea, corresponding to CLIVA sections nos. I, II and III (see Table 1), the observational phase of the project went on uninterrupted for about a year along transects from Portugal to the east coast of the USA aboard the small cargo *Mauricio de Oliveira*, belonging to the CTM shipping company (see Table 1).

Table 1

Dates and number of XBT and surface salinity observations obtained with the *Mauricio de Oliveira* during the first phase of the CLIVA Project.

CLIVA section no.	Dates	No.of XBT observations	No. of surface salinity samples
	1983:		
I	18 - 20 September	8	8
	1984:		
II	2 - 7 April	10	10
III	15 - 20 June	21	18
IV	3 - 13 August	39	39
V	28 Sep.-9 Oct.	43	43
VI	17 - 28 November	34	34
	1985:		
VII	19 Jan.-3 Feb.	55	48
VIII	14 - 24 March	39	39
IX	19 - 30 April	40	40
X	9 - 22 June	41	41
	TOTAL	330	320

An XBT hand-held launcher, connected to an analogue recording system, was used in this early stage of the project and XBT probes, mostly of the T-7 type, were dropped every six hours (0 - 6 - 12 - 18 GMT). Simultaneously, a sample of surface waterwas collected with a bucket for salinity determination and standard meteorological observations were made. The ship officers discretized the XBT traces and prepared BATHY/SHIP messages which were broadcast in near-real time to coastal stations and transmitted globally through the Global Telecommunication System (GTS), as a contribution to Integrated Global Ocean Services System (IGOSS).

At the ship's arrival in Lisbon, the salinity of the samples was determined by the project team by means of a high-precision AUTOSAL salinometer. Temperature records were checked, using TS diagrams and historical temperatures, then digitized (every 5m down to 100m, every 10m, from 100 to 300m, and every 20m, at deeper levels), and finally put on magnetic tape.

In order to generate the salinity field corresponding to the observed temperature field, a method described by Emery (1975) was used, in which the historical TS regressions prepared by Stramma (1981) and by Emery and Dewar (1982) were employed.

A computer programme was developed whose inputs were the co-ordinates of the XBT stations, the historical data grid centers, the observed surface salinities and temperature profiles, and the historical temperature-salinity pairs from each grid. This programme interpolates the historical data for the positions of the XBT stations and provides the salinities corresponding to the observed temperatures. The salinity distributions thus obtained showed good agreement with measured values at approximately the same latitudes (e.g., Roemmich and Wunsch, 1985; Fuglister, 1960).

Baroclinic geostrophic currents were then computed using a reference level at 1200m, chosen on the basis of results obtained recently for the North Atlantic, on the assumption of conservation of total mass, bu Stramma (1984) and Roemmich and Wunsch (1985).

As the XBT measurements made from the *Mauricio de Oliveira* extended only to depths of 800-900m, a computational scheme was applied prior to the geostrophic calculations, in order to extrapolate the temperature and salinity fields down to 1200m, using the available historical data and imposing a matching condition at the end portion of the XBT trace, between the observed and the historical temperatures.

Volume transports were then computed for consecutive pairs of XBT stations for layers 20m thick, from the surface to 1200m, and then added up to obtain:

$$T_{v=} \int_A \int v \, dx \, dz$$

where A represents the vertical area comprised between the stations, from 0 to 1200m, v is the meridional velocity (positive northward), x is the zonal co-ordinate and z is the vertical co-ordinate. Corresponding heat transports were similarly computed as

$$T_h = \int_A \int c_p \, \theta \, \rho \, v \, dx \, dz$$

where c_p is the specific heat at constant pressure of seawater, θ is the potential temperature and ρ the density of seawater.

Results

Thermohaline fields. The positions of the XBT stations made by *Mauricio de Oliveira* are shown in Fig. 1.

The evolution of the surface temperatures and salinities observed during the study period is displayed in Fig. 2. The thermal seasonal cycle is very obvious (Fig. 2a), but there is considerable asymmetry between the eastern and the western basins of the North Atlantic, a smaller amplitude and some lagging being noticeable in the east, probably corresponding to a large-scale manifestation of the Portuguese upwelling.

Figure 1.

1. Positions of XBT stations made by *Mauricio de Oliveira* from September 1983 to June 1985 for the CLIVA Project, (Roman symbols indicate the CLIVA sections identified in Table 1.)

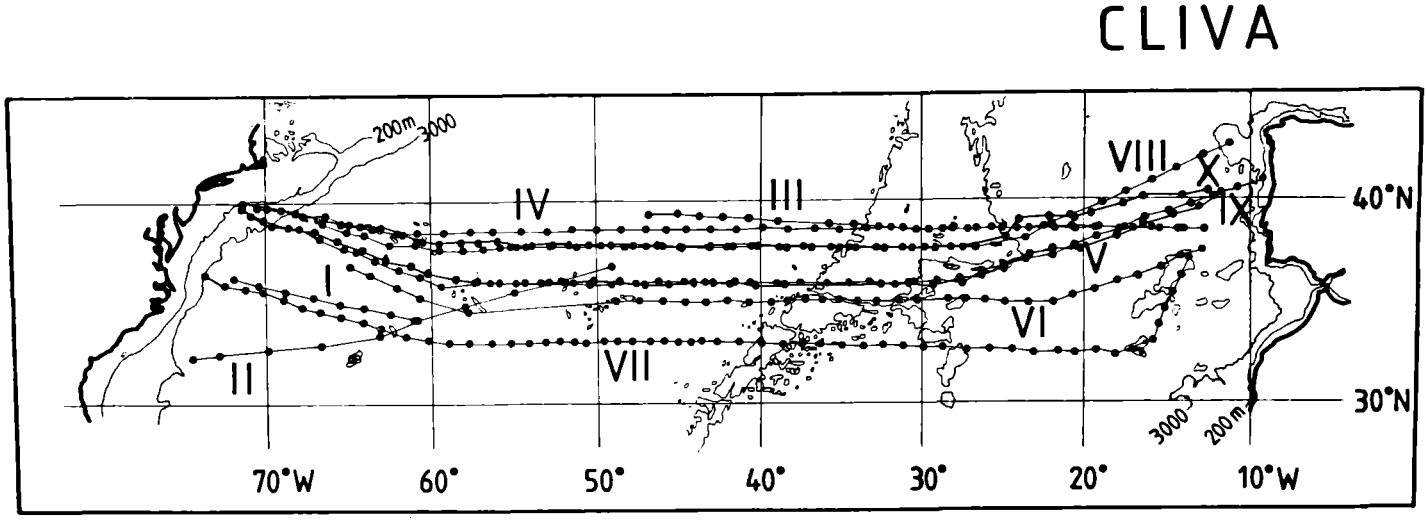

However, the corresponding salinity distribution (Fig. 2b) presents a quite different pattern, with little seasonality, but with a structure in bands of alternating minima and maxima: from Portugal to about 20°W, low salinities prevail (coastal upwelling, large scale southward flows?); from 20° to 35°W and from 45° to 65°W there are bands of high salinities with low values in between, over the western flank of the Mid Atlantic Ridge; west of about 65°W, near North America, salinities decrease reaching extremely low values due to the influence of the Labrador current.

The vertical temperature distributions obtained with th CLIVA sections and illustrated in the examples of Fig. 3, point to two distinct thermal regimes wesrt and east of about 40°W. In the eastern basin and over the Mid Atlantic Ridge the isotherms show a general downward slope to the west, the permanent thermocline is relatively shallow and some thermostads and even tempertature inversions (due to water of Mediterranean origin) are noticable at the greater observed depths. In the western basin, strong horizontal gradients near the American coast indicate the signature of the Gulf Stream, the permanent thermocline is very deep with thick thermostads extending above it as a result of deep convection in late winter (e.g. Fig. 3b) and many cyclonic mesoscale eddies (Gulf Stream "rings") of about 200 km, in diameter were identified through their strong and symmetric lateral gradients.

The transition between those two different thermal structures of the subtropical North Atlantic occurs at about 40°W, near the western flank of the Mid Atlantic Ridge, and was identified in the CLIVA sections as corresponding to an inter-

Figure 2.

Variation of sea surface properties during one year from CLIVA observations:
(a) temperature (b) salinity.

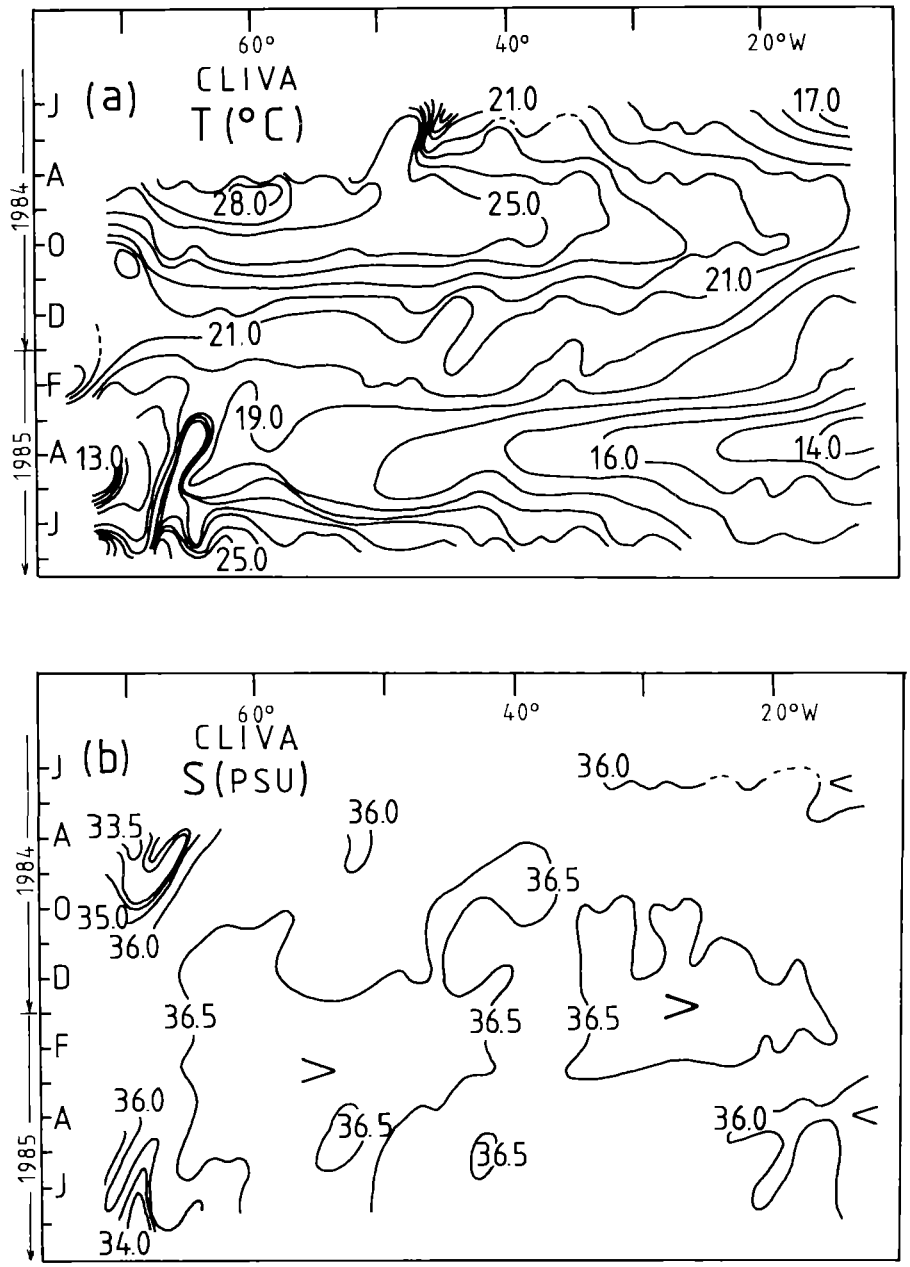

Figure 3.

Examples of vertical temperature distributions obtained during CLIVA:
(a) summer (CLIVA IV: 3-13 August 1984); (b) winter (CLIVA VIII): 14-24 March 1985).

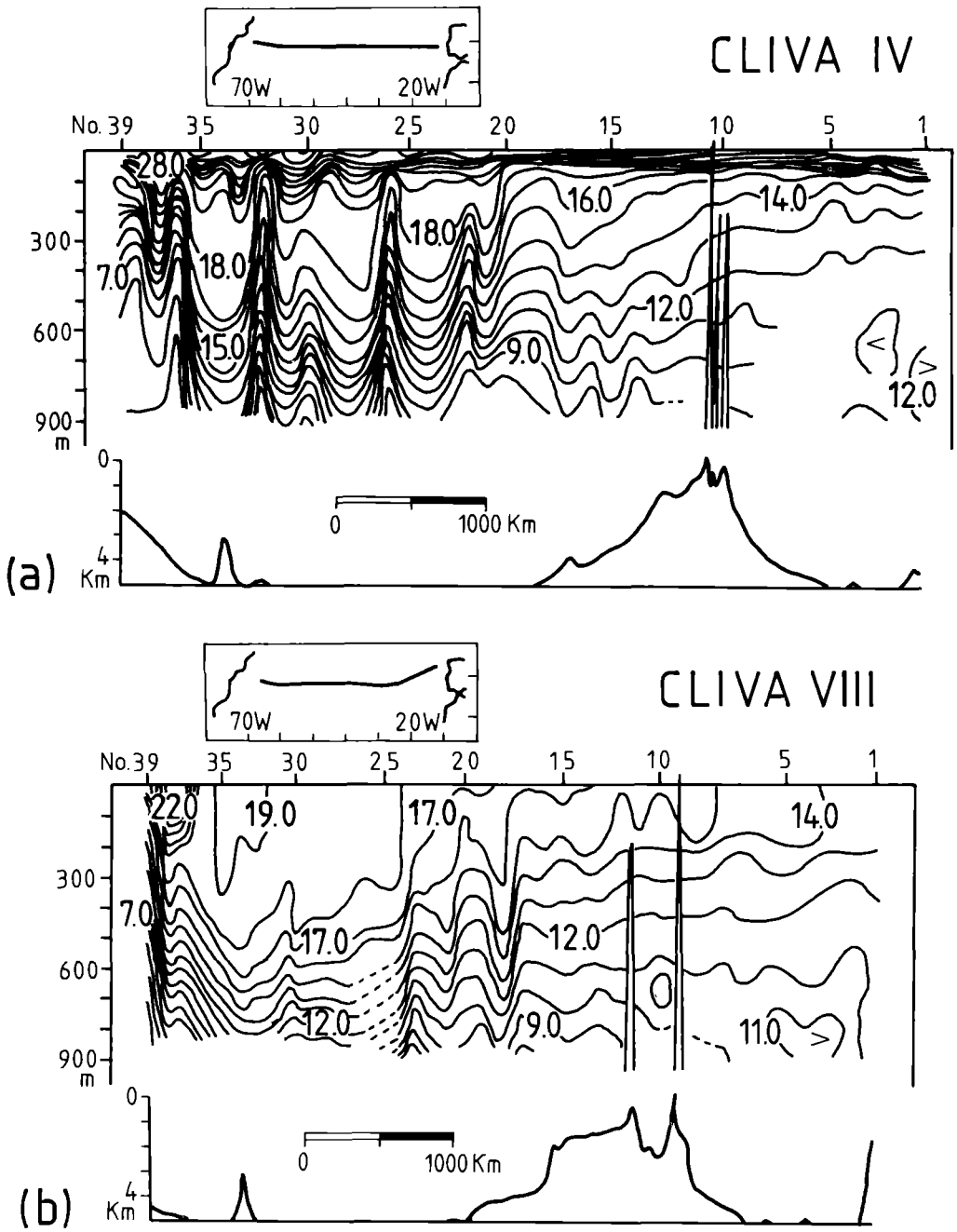

nal front extending vertically for several hundreds of meters in the upper ocean. This structure coincides at the surface with the low-salinity belt identified before.Meridional circulation. Baroclinic geostrophic meridional currents were computed from the observed and calculated thermohaline fields using the methods explained above. As shown in the examples in Fig. 4, their patterns are generally consistent with the temperature distributions already described: (i) in general, weak currents prevail in the eastern basin, with some northward cores being noticeable off Portugal; (ii) a southward current is identified in the vicinity of the western flank of the Mid Atlantic Ridge; (iii) intense currents (~1m/s) of opposed directions are a common feature in the western basin constituting cyclonic circulations associated with the same mesoscale eddies already identified through their thermal signatures; (iv) a strong northward circulation of the Gulf Stream near North America.

The southward circulation west of the Azores is linked to the internal frontal structure identified in the temperature sections. This current seems to bear continuity with mesoscale fronts in a more southward area previously investigated by Gould (1985), and with the sub-tropical front identified south east of the Azores by Kase and Siedler (1982). It corresponds apparently to a strong and individualized recirculation of the Gulf Stream for which we suggest the name "Azores Current".

Meridional transports of mass and heat . The mass transport in the "interior" of the ocean (i.e., away from the effects of the western boundary current) can be decomposed in the Ekman transport, directly induced by wind and stress, and in the geostrophic transport associated with the mass field of the ocean. In the western boundary circulation (the Gulf Stream, in the present study) the role of the Ekman transport is locally neglected and the downstream component of the current is well approximated by the geostrophic hypothesis.

With the CLIVA data (zonal sections) it is only possible to compute meridional geostrophic transport. For the Ekman transport across the zonal section under consideration, we adopted the "climatological" value of 2±2 Sverdrup ($1Sv=10^6 m^3 s^{-1}$) towards the south, obtained at 36°N by Roemmich and Wunsch (1985) from wind data compiled by Hellerman and Rosenstein (1983).

Figure 4.

Examples of the meridional geostrophic currents obtained across CLIVA sections: (a) summer (CLIVA IV); (b) winter (CLIVA VIII). Positive values correspond to northward currents (shaded areas indicate southward components). Units are cm s^{-1}.

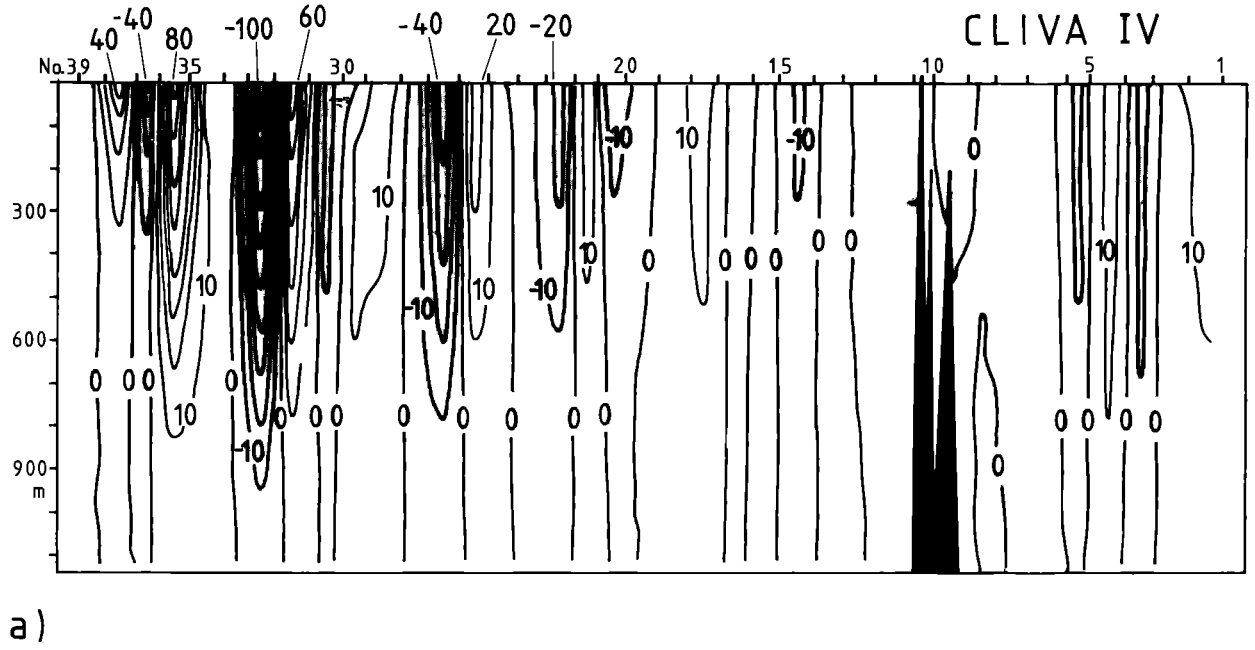

(a)

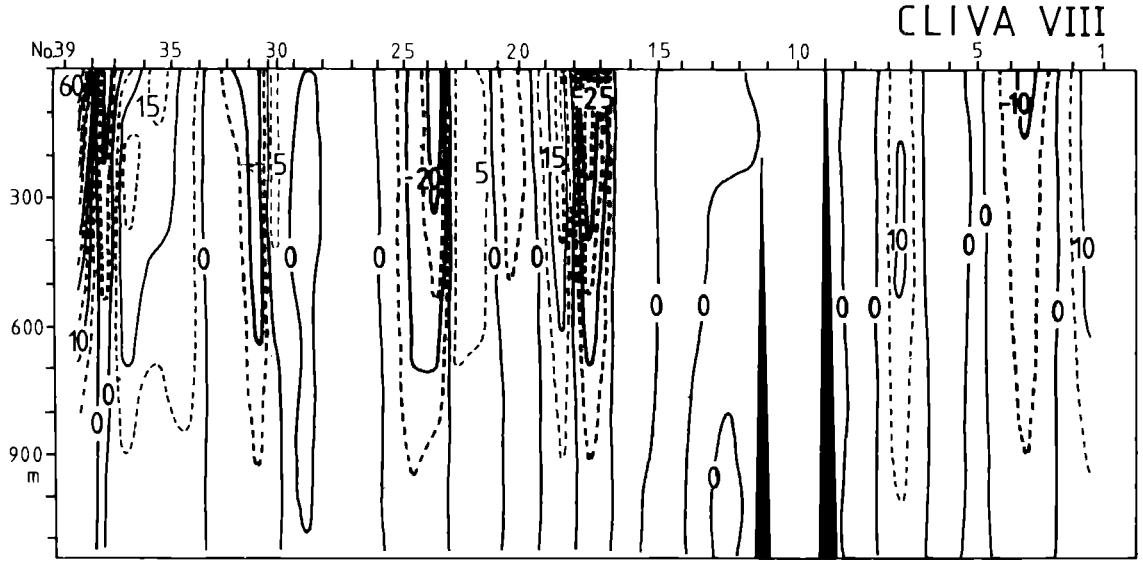

(b)

The meridional volume and heat transport obtained with the data from CLIVA sections are displayed in Table 2 and Fig.5. In order to be able to compare the present results with those from other investigators and also because some CLIVA sections did not extend close enough to the western coast, the contributions from the Gulf Stream and those from the ocean "interior" to the total transport were separately calculated.

The total transports in the layer 0-1200m, have values of about 40 Sv towards the north, resulting from northward contributions of the Gulf Stream ranging from 49 to 66 Sv and southward transports in the "interior" from -10 to -30 Sv.

The only published results that can be compared to the present ones are those of Roemmich and Wunsch (1985). They present volume and heat transport across zonal sections conducted by oceanographic vessels along the 36°N parallel, one during the International Geophysical Year, in 1959, and another in 1981. However, these authors did not consider decomposition of the transports as was done here and they used, as a geostrophic reference the isopycnal σ_2 = 36.82 (σ_2 - density anomaly relative to 2000 db) instead of a level surface; that isopycnal lies at a mean depth of 1300m, across the whole North Atlantic, but may deviate considerably from that depth, particularly in the Gulf Stream precisely where the strongest flows occur and thus exert more influence on the net meridional transports.

For the layer between the sea surface and that isopycnal, Roemmich and Wunsch (1985) obtained northward transports of 18.1 and 19.1 Sv with the 1959 section and of 12.9 and 16.5 Sv with the 1981 section, using two different methods. As can be seen from Table 2, the CLIVA results attain values about twice as high as those from Roemmich and Wunsch (1985). Such a discrepancy may result from the already mentioned difference between the reference surfaces used in the geostrophic computations, or from systematic errors introduced through our methods for calculating salinities from observed temperatures and for extrapolatingdata to 120m, or even to real fluctuations in the transports. However, the CLIVA results show considerable internal coherency and, on the other hand, our computed Gulf Stream

Table 2.

Meridional volume and heat transports in the upper 1200m of the subtropical North Atlantic across CLIVA sections

CLIVA section no.	Volume Transport (10^6 m^3 s^{-1})			Heat Transport (10^{15} W)		
	total	interior	Gulf Stream	total	interior	Gulf Stream
1984:						
IV						
August	43.76	- 10.40	54.16	2.21	- 1.08	3.29
V						
Sept-Oct	44.64	- 13.62	58.26	1.92	- 1.72	3.64
VI						
November		- 29.79			- 2.20	
1985:						
VII						
Jan-Feb	31.44	- 17.79	49.23	1.67	- 1.50	3.17
VIII						
March	38.42	- 27.79	66.24	2.09	- 2.05	4.14
X						
June	31.66	- 23.68	55.34	1.69	- 1.70	3.31

Figure 5.

Meridional transports (total, Gulf Stream and interior) in the upper 1200m of the subtropical North Atlantic obtained from coast to coast CLIVA sections: (a) water volume; (b) heat.

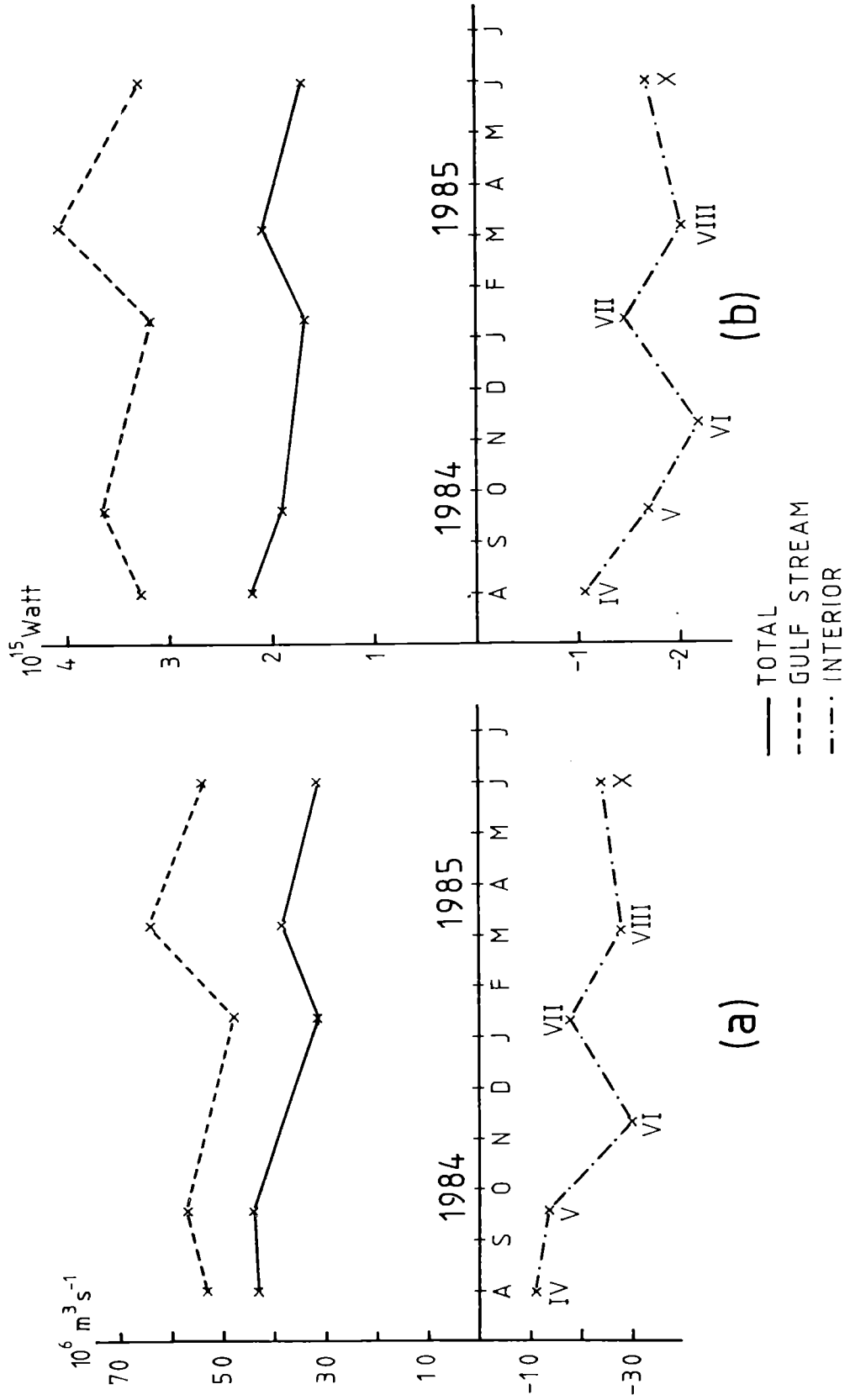

transports are of the same magnitude as those obtained by research ships at corresponding positions (e.g., 60 Sv off Cape-Hatteras and 70 Sv off Woods Hole, according to Worthington, 1976). These considerations indicate that the differences noticed above are probably due to the difference between the reference surfaces used here and by Roemmich and Wunsch (1985).

The credibility of the CLIVA results is also reinforced by the conclusions of Rossby and Rago (1985) on the variability of the Gulf Stream transport, showing that the amplitude of the seasonal signal does not exceed 15% of the yearly mean transport. Adding to this the observational uncertainty, estimated by the mean deviation of the individual values relative to the regression model used by Rossby and Rago, which amounts to 14% of the mean transport, one obtains amplitudes of about 30%. The Gulf Stream fluctuations obtained with the CLIVA data do not reach such values, as can be seen in Table 2 or Fig. 5a.

Meridional heat transports across the sub-tropical North Atlantic were also computed using the CLIVA data. The results are shown in Table 2 and in Fig. 5b. As a result of the calculated values, which range from 1 to 3 petaWatt (1 petaWatt = 10^{15} Watt) it can be concluded that a contribution of 0.2 ± 0.2 petaWatt from the Ekman transport (estimated using CLIVA mean temperatures and an Ekman depth of 50m) is practically negligible for the total heat balance at the latitude of the CLIVA sections (about 35° - 39°N), although it may have some secondary influence in the seasonal variability.

Roemmich and Wunsch (1985) obtained a total heat transport of 0.8 petaWatt to the north between the surface and the bottom of the ocean, through the already mentioned oceanographic sections at 36°N. Since this transport includes the (southward) transport in layers deeper than 1200m, it can be deduced that their result is in qualitative agreement with the present ones.

On the other hand, the computations presented by Lamb and Bunker (1982) from the seasonal evolution of the ocean-atmosphere heat transfer and of the heat content in the upper 500m of the Atlantic, indicate mean northward transports of 0.7 and 1.1 petaWatt, respectively, at 40° and 30°N, in the layer 0-500m, which correspond to less than half of that used in the calculations of the present study. These values show that the results obtained with the voluntary observing ship during CLIVA's first year are in quantitative agreement with the information previously available.

Mean and eddy transports. The CLIVA data were also used to obtain the mean and the "eddy" components of the meridional transports of mass and heat.

The zonal mean operator is defined as

$$[\,(\,)\,] = L_t^{-1} \int_o^{L_t} (\,)\,dx$$

where L_t is the total length of each trans-Atlantic section. Using CLIVA data, zonal means of meridional geostrophic velocity and of temperature were obtained for layers 20m thick, between levels k and k+1: $[v_{gk}]$ and $[T_k.]$ The corresponding deviations from the zonal means, noted with an asterisk, were also calculated

$$T_k^* = T_k - [\,T_k\,] \qquad v^*_{gk} = = v_{gk} - [\,v_{gk}\,]$$

Transports of second order, resulting from the product of two properties, can be decomposed as, for example, for the "heat" (temperature) transport:

$$[\,v_k\,T_k\,] = [\,v_k\,]\,[\,T_k\,] + [\,v_k^*\,T_k^*\,]$$

where the first term on the righthand side represents the product of the zonal means of the two properties and the second term represents the contribution of the space covariance between meridional current and temperature.

In the time domain, the available historical mean values were used as representative of the time means:

$$\bar{(\,)} = \lim_{t\to\infty} \int_o^t (\,)\,dt'$$

Noting with primes the deviations relative to these means, the following relations are obtained:

$$v = \bar{v} + v' \qquad T = \bar{T} + T'$$

and the second order "heat" transport may be written as:

$$vT = \bar{v}\bar{T} + \bar{v}T' + v'\bar{T} + v'T'$$

where there are now, apart from the products of the means and of the perturbations,contributions due to the transport of temperature fluctuations by the mean current and to the transport of the mean temperature by the velocity fluctuations.

Applying the zonal mean operator to the last relation, one obtains:

$$[\,vT\,] = [\,\bar{v}\,\bar{T}\,] + [\,\bar{v}\,T'\,] + [\,v'\,\bar{T}\,] + [\,v'T'\,]$$

$$= [\,\bar{v}\,]\;[\,\bar{T}\,] + [\,\bar{v}^*\,\bar{T}^*\,] + [\,\bar{v}\,T'\,] + [\,v'\,\bar{T}\,] + [\,v'\,T'\,]$$

where the first two terms on the right-hand side (which are time-independent) represent "heat" fluxes resulting respectively from the mean current normal to the section and from stationary perturbations ("standing eddies"); the other terms show the different contributions of the time perturbations.

Using the CLIVA data set, we computed the zonal mean meridional velocities across the total width of the North Atlantic $[v]_t$ and the corresponding contributions due to the "interior" of the ocean $[v]_i$; the results are displayed in Fig. 6a,b. The strong effect of the Gulf Stream and a frequent change in direction of the interior circulation near 600m depth are to be noted. The zonal mean temperatures $[\,T\,]_t$ shown in Fig. 6c illustrate the seasonal evolution in the upper layers (down to about 150m), and indicate a warm anomaly corresponding to Section no. VII conducted more to the south than the other CLIVA transects.

The CLIVA data were also used to calculate the partition of the "heat" transport:

$$[vT]_t = [v]_t[T]_t + [v^*T^*]_t$$

and some examples of the results are shown in Fig. 7. The relatively weak values of the covariance term [v*T*] indicate that heat is essentially transported across the zonal section under study by the mean-velocity field and that the spatial covariance does not play a relevant role in such process.

Computations of the decomposition of the mean heat transports into means and fluctuations in the time domain were carried out for the "interior":

$$[vT]_i = [\bar{v}]_i[\bar{T}]_i + [\bar{v}^*\bar{T}^*]_i + [v'\bar{T}]_i + [\bar{v}T'] + [v'T']_i$$

and several examples of the results are shown in Fig. 8. The main contributions to the meridional heat transport are due to the advection of mean temperature by the mean current $[\bar{v}]_i[\bar{T}]_i$ (what one might call the "climatological" transport) and by the time fluctuations of velocity $[v'\bar{T}]$.

In Fig. 9 examples are given of the results of the calculations of the meridional heat transports including the Gulf Stream. In this case $[v'T]_t$ is, by far, the dominating component, even overcoming the effect of $[\bar{v}]_t[\bar{T}]_t$. This demonstrates that the dominant mechanism in the mean meridional heat flux in the sub-tropical North Atlantic is associated with the transport of the mean temperature by Gulf Stream eddies.

Conclusions

Observations with a single merchant ship across the subtropical North Atlantic provided data of oceanographic value. A set of seven sections conducted during one year permitted a description of the structure and seasonal variability of the hydrography of the upper 800-900m, allowing specifically, the identification of a strong southward current, near 35-40°N, to the west of the Mid Atlantic Ridge the "Azores Current".

The data were used to compute meridional volume transports in the layer 0-1200m, across the whole width of the North Atlantic; values of 30 to $45 \times 10^6 m^3/s$ to the north were obtained, including a northward contribution of 50 to $66 \times 10^6 m^3/s$ from the Gulf Stream and a southward contribution of 10 to $30 \times 10^6 m^3/s$ from the ocean interior.

Meridional heat transports calculated with the data set indicate a net value of 1.9 to 2.2×10^{15} Watts towards the north, with contributions of 3 to 4×10^{15}W (to the north) from the Gulf Stream and 1 to 2×10^{15}W (to the south) from the ocean interior.

The agreement between the present results and those from the literature shows that the methodology developed here is adequate for the description and quantification of phenomena involved in oceanic heat storage and transport.

The decomposition of the transports into zonal means and their perturbations demonstrates that the space covariance between current and temperature does not have a relevant role, and that heat is mainly transported by the zonally averaged meridional velocity. In the interior of the North Atlantic, the prevailing effects are those of the transport of the time-mean temperature by the mean current and by the time fluctuations of velocity; standing eddies have a negligible effect in that process. When the Gulf Stream is included in the computations, however, the dominating mechanism is, by far, the one associated with Gulf Stream transient eddies.

Acknowledgements

This research was partially supported by Junta Nacional de Investigacao Cientifica e Tecnologica (Lisbon) under Contract No. 516.83.51. Some support was also provided by Instituto Nacional de Investigacao Cientifica (Lisbon).

The National Weather Service and the National Ocean Service of the National Oceanic and Atmospheric Administration of the USA provided the XBT probes and the recording/launching system, as a contribution to IGOSS.

The success of the observational programme was only possible due to the effort and professional competence of the captains, officers and crew members of the *Mauricio de Oliveira* and the support of the CTM company (Lisbon).

Figure 6.

Vertical distributions of zonal means obtained from CLIVA data:
(a) meridional velocity across the whole of the North Atlantic;

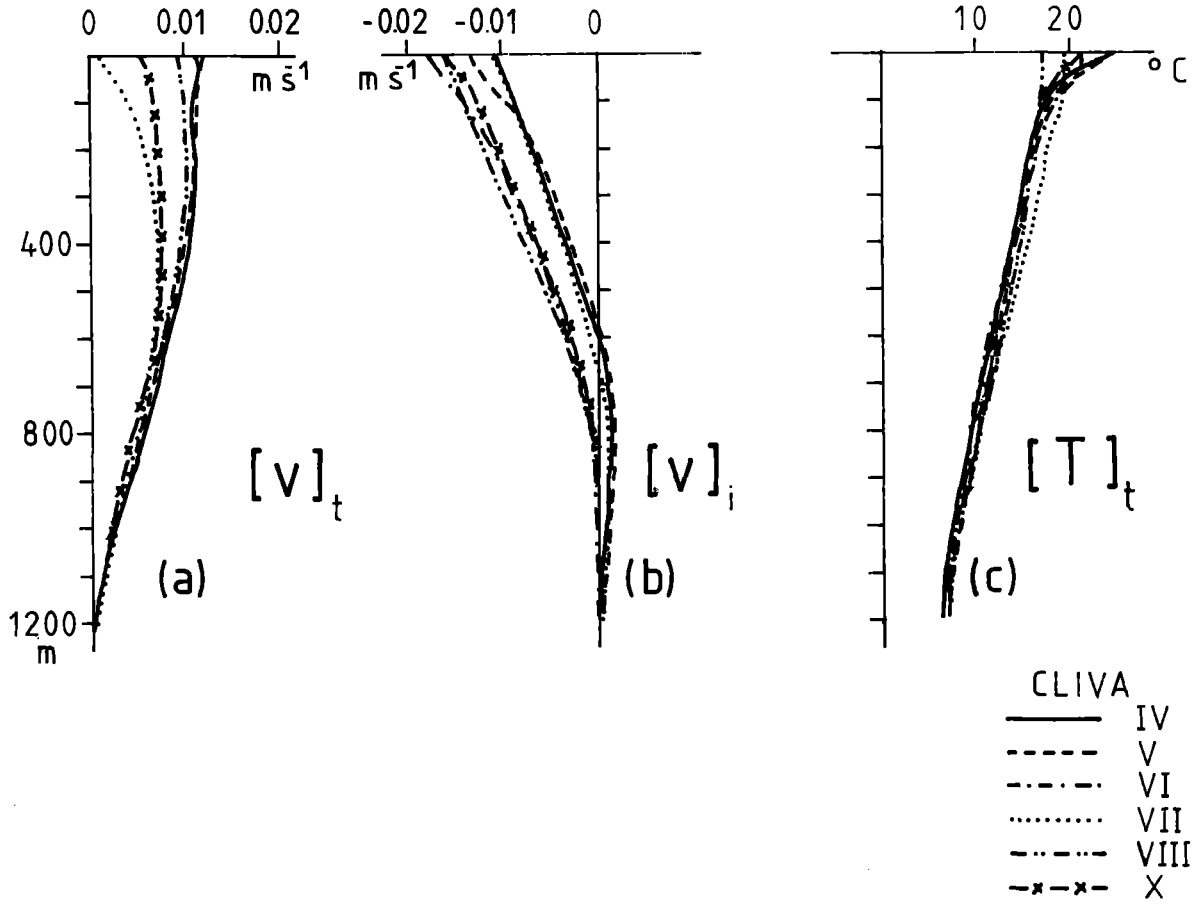

Figure 7.

Vertical distributions of the values of the various terms in
$[vT]_t = [v]_t[T]_t + [v^*T^*]_t$
obtained from coast to coast CLIVA sections (sections identified as in Figure 6).

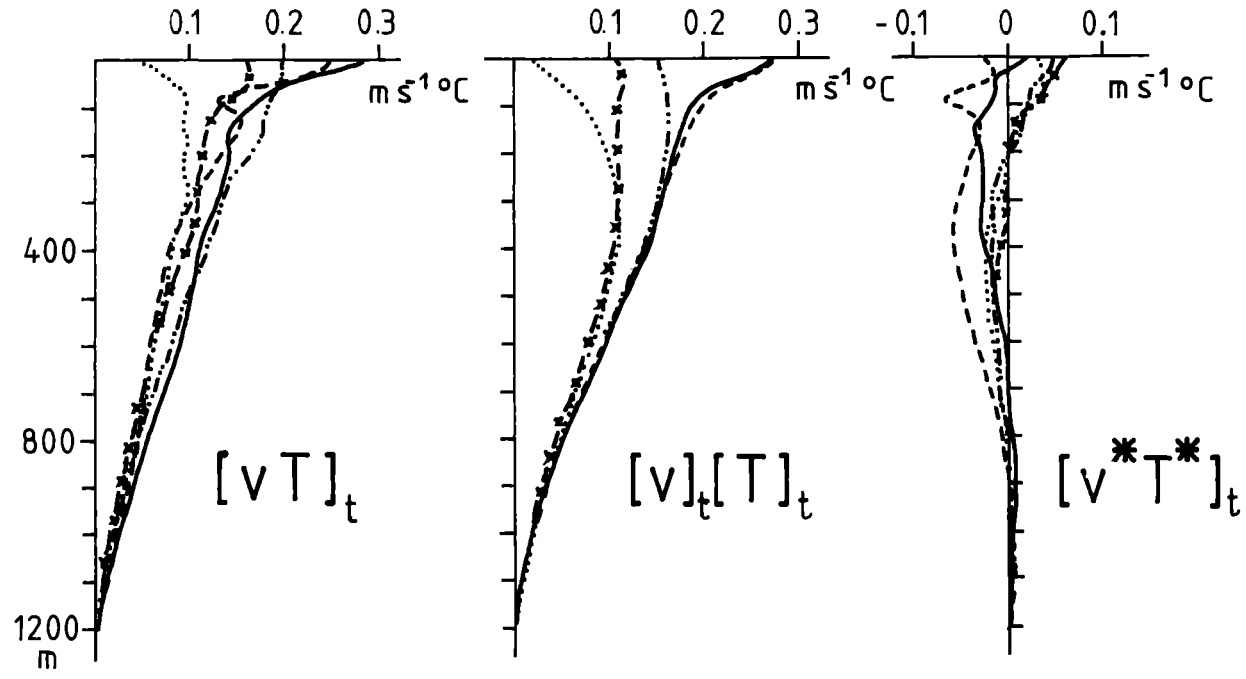

Figure 8.

Vertical distributions of the values of the various terms
in the space-time decomposition of the meridional "heat" transport
in the interior of the North Atlantic, calculated with CLIVA data (see text).

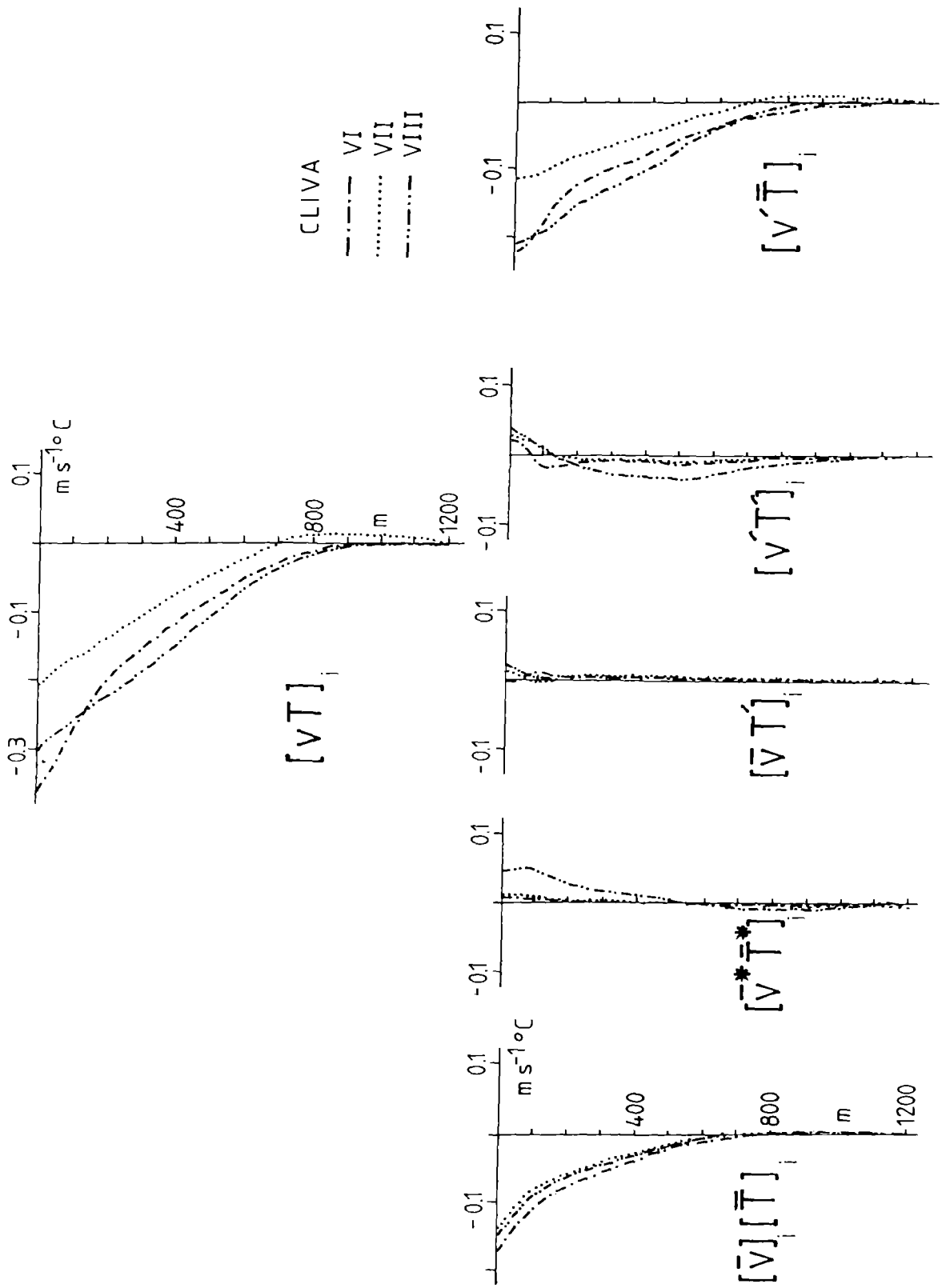

Figure 9.

Vertical distributions of the values of the various terms
in the space-time decomposition of the meridional "heat" transport
in the whole width of the North Atlantic, calculated with CLIVA data (see text).

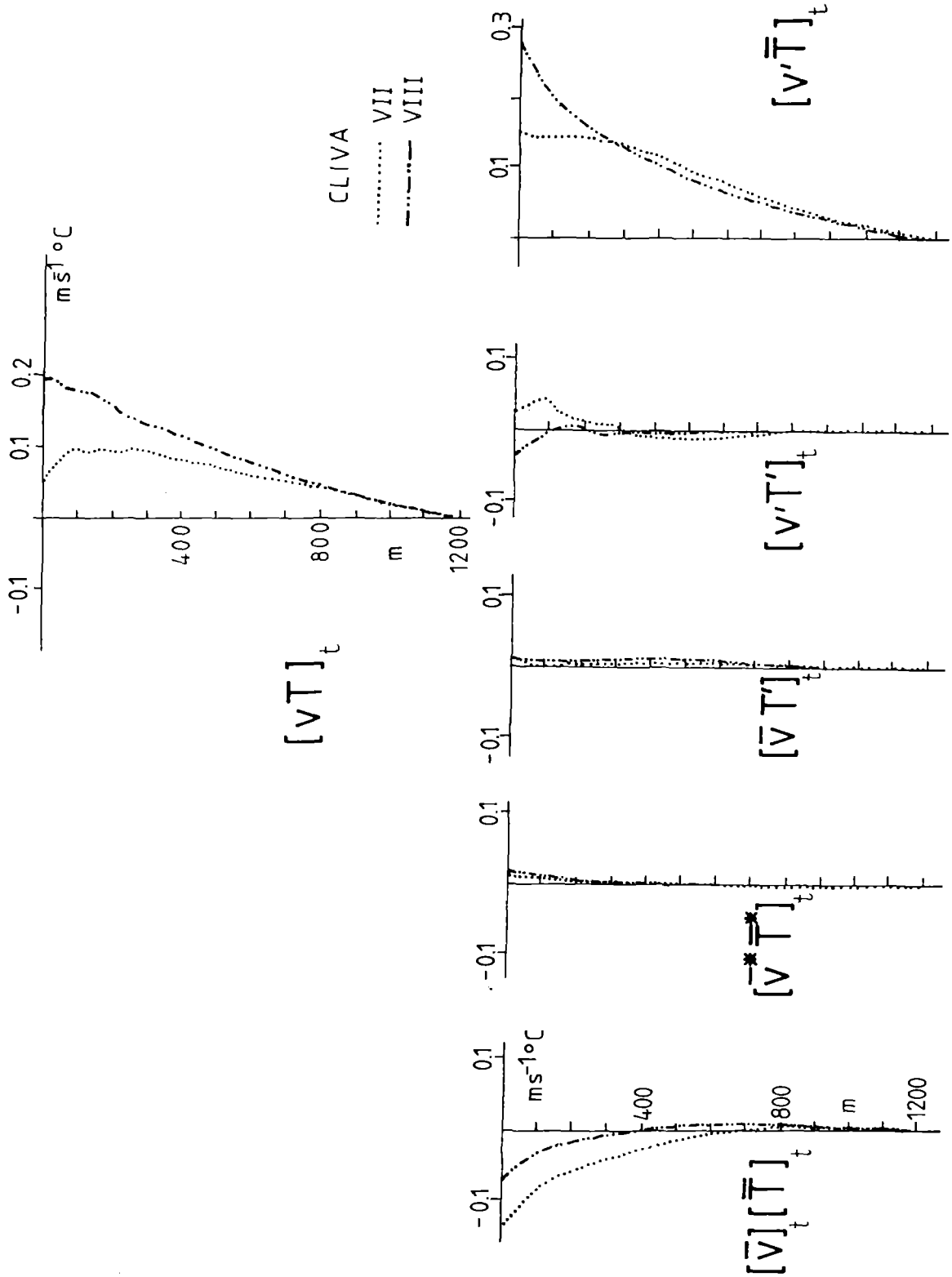

References

1. Emery, W., 1975. Dynamic height from temperature profiles. *J. Phys. Oceanogr.*, 5, (2), pp. 369-375.

2. Emery, W., and Dewar, J., 1982. Mean temperature-salinity, salinity-depth and temperature-depth curves for the North Atlantic and the North Pacific. *Prog Ocean.*, 2, pp. 219-305.

3. Fuglister, F.C., 1960. Atlantic Ocean Atlas. The Woods Hole Oceanographic Institution Atlas Series, Vol.1.

4. Gould, W.J., 1985. Physical oceanography of the Azores Front. *Prog. Ocean.*, 14, pp. 167-190.

5. Hellerman, S., and Rosenstein, M., 1983. Normal monthly wind stress over the world ocean with error estimates. *J. Phys. Oceanogr.* 13, 1093-1104.

6. Kase, R., and Siedler, G., 1982. Meandering of the subtropical front south-east of the Azores. *Nature,* 300, pp. 245-246.

7. Lamb, P.J., and Bunker, A.F., 1982. The annual march of the heat budget of the north and tropical Atlantic Ocean. *J. Phys. Oceanogr.*, 12 (12), 1388-1410.

8. Roemmich, D., and Wunsch, C., 1985. Two Transatlantic sections: Meridional circulation and heat flux in the subtropical North Atlantic Ocean. *Deep-Sea Res.*, 32 (6), pp. 619-664.

9. Rossby, T., and Rago, T., 1985. Hydrographic evidence for seasonal and secular change in the Gulf Stream. IOC Time Series of Ocean Measurements, Vol. 2-1984, pp.25-28, IOC Tech. Ser. 30, Unesco.

10. Stramma L., 1981. Die bestimmung der dynamischen topographie aus temperaturdaten aus dem Morostatlantik. Berichete Institut fur Meereskunde Kiel, 84, 66 pp.

11. Stramma L., 1984. Geostrophic transport in the warm water sphere of the eastern sub-tropical North Atlantic. *J. Mar. Res.*, 42, pp. 537-558.

12. Worthington, L.V., 1976. On the North Atlantic circulation. The Johns Hopkins University Press, 110 pp.

4 . Sea Level Variations in the Tropical Atlantic: The Seasonal Cycle and New Observations in 1983 and 1984

J-M Verstraete

ORSTOM
Laboratoire d'Océanographie Dynamique et Climatologie
Institut Océanographique
Paris, France

Introduction

Very little is known about the importance of the seasonal and interannual heat-storage (or transfer) variability in the oceans because continuous observations of thermal structures and currents are not possible on a basin-wide scale. Even though oceanographic instruments are vastly improved and in spite of many dedicated efforts, the departure from the mean circulation (and the deep circulation) are still not known. Thirty years ago, the authors of the "seasonal oscillation in sea level" (Pattullo et al, 1955) estimated that "The observed seasonal variations in sea level will have to provide much of the necessary empirical guidance for such an understanding". At low latitudes, the meteorological forcing is very regular and the low frequency sea level variations are able to provide a source of information about the internal dynamics of the ocean. It is now well established that for periods from several days to years, changes in sea level are linked to the ocean heat and salt content through the expansion and contraction of the water column which result from changes of the mean thermal and haline structures. Oscillations in the height of the sea surface arising from the seasonal variation in specific volume are called steric oscillations, nearly equal in magnitude to those in dynamic height. The steric sea level is high when the water column is warm, low when it is cold; conversely, a high (low) steric level corresponds to low (high) salinities. As a rough-and-ready rule of thumb, a salinity increase of 1°/oo produces much the same density change as a 4°C decrease in temperature. Close correspondence of the variations in time of direct observations of the daily mean sea surface elevation and the daily dynamic height was demonstrated during three totally independent experiments in 1973 (9 days), 1974 (74 days) and 1977 (160 days) in the Gulf of Guinea (Verstraete and Picaut, 1983). The seasonal cycles of the tropical thermocline, heat content, dynamic height and mean sea level in three upwelling areas of the eastern tropical Atlantic off Dakar, Abidjan and Pointe Noire are well documented (Verstraete, 1982, 1985 a,b and 1987).

Prior to and after the start of the pressure tide gauge experiment which was a part of the FOCAL PROGRAMME (Francais Ocean-Climat Atlantique Equatorial Programme) in the tropical Atlantic, continuous effort allowed us to collect most of the available long-term sea level observations along the western African coastline. With other historical data, we have at our disposal a reference for analyzing both the seasonal and interannual variations of the new sea level data set.

An array of eleven shallow pressure tide gauges (ORSTOM) and five deep-sea pressure recorders (IOS, Bidston) was deployed in a common effort from October 1982 through November 1984 as a prelude to a Tropical Ocean Global Atmosphere project (TOGA)(see Figure 1). The array was designed with two objectives: to observe the oceanic sea level continuously and synoptically on a basin-wide scale from short time scales (2-5 days period) to interannual changes; and (2) to measure the differences in sea level between some selected sites as along the equator, or across large-scale flows as the Canarias Current or the South Equatorial Current terminus near the South American continent.

Instrument Logistics, Data Sources and Processing

All the tide gauges (WLR-5 AANDERAA) were equipped with an ultra precise "Paroscientific" quartz pressure sensor (range 0-67m, resolution 0.7mm, accuracy 0.7cm of water height) and a thermistor fitted in an aluminium block placed inside the pressure sensor housing (range -3°C, +35°C, resolution 0.04°C, accuracy 0.1°C). With a sampling interval of one hour the theoretical autonomy is more than a year. The pressure effects due to surface waves are averaged out over the integration time of the instrument (40 seconds). Performance of the gauges was evaluated upon their reception at the IFREMER centre (Brest) in June 1982 at the 20m deep sea water experimentation basin of the TDI department (Technique et Developpement Industriel) and at the SEQM department (Section Essai Qualification Materiel). We checked particularly for any eventual drift or hysteresis of the pressure sensors by many experimental casts in the basin; the gauges and a Neil Brown probe were operated at exactly the same level so that we had simultaneous, very precise records of temperature, conductivity (salinity) and pressure (depth). The results were very satisfactory for the thirteen tide gauges, for both pressure and temperature records, and we did not find any hysteresis effect in the range of 0-20 metre depths.

Islands are viewed as stable platforms from which it is possible to measure the open-ocean sea level. Assuming that no tectonic activity occurs, three effects are able to contaminate estimates of open-ocean sea level: radiation stress of surface waves in harbours, small-scale variations in wind (Wunsch, 1972) and the pressure difference between the upstream and downstream regions caused by the flow of water around an island. To filter out high frequency surface phe-

nomena, most of our gauges were deployed below 5 metre water depth and as far as possible from swift current areas. Two apparatus were deployed in harbours (at Praia and Lome) in protected areas.

For long-term observations of the sea level, it is absolutely necessary to make sure that: (1) the distance from sea bottom up to the instrument is kept constant; and (2) at each recovery-redeploying operation the new apparatus is put by the diver exactly at the same level as the previous one in its cradle. Each cradle is made of a PVC (plastic) tube which is fixed in a reinforced concrete platform cemented in the rocks of the sea bed. As the pressure cases are made of an aluminium alloy tube, it is essential that no metallic parts be apparent external of the platform to prevent electrolysis. A full description of the cradle and the techniques of deployment were given by J. Labarre (1983) following benevolent counsels kindly provided to us by Roger Lukas of JIMAR (University of Hawaii). Details on positions, depths, time origin and total data records on December 31, 1984 are given in Table 1 and Figure 1. Three stations were installed from the R/V CAPRICORNE (belonging to IFREMER, France), four from the French ORSTOM R/V A. NIZERY, one from the IMPERIAL MARINEIHRO of the Brazilian Navy, and two from the ORSTOM/FOCAL base at Dakar. The tide gauge at Ascension was owned by ORSTOM and deployed by I.O.S., Bidston, Great Britain. Only one cradle was broken, at Fernando de Noronha (for some unknown reason) where we lost one tide-gauge and 9 months of observations. A new cradle was built again from our R/V CAPRICORNE in April 1984. Due to some malfunction of the apparatus, we could get only 2 months of hourly observations at Trindade.

All the records collected at various sites were first processed at the Antenne ORSTOM at the IFREMER centre at Brest, then combined into time series. Copies were given in May 1984 and in July 1985 to D. Cartwright (IOS, Bidston) and in June 1984 to the French Hydrographic Service (EPHSOM, Brest). Temperature and absolute pressure time series were obtained from 5m to 13m depth at ten sites; sea surface elevation was derived from the sea-bed pressure by using values of density computed from the in-situ temperature and a fixed salinity (35°/oo) according to the formula given by Millero and Poisson (1981). No adjustments were made for variations of barometric pressure; only a fixed standard atmospheric pressure (1013.0 mbar or hecto Pascal) was subtracted from the absolute sea-bed pressures.

All the data sets (pressure, temperature, sea-level elevation) obtained at the FOCAL tide gauge network were recorded at one hour intervals. The hourly time series were filtered either with a "Demerliac" filter at Brest (Demerliac, 1973) or with a "Cartwright" filter at Bidston. The virtues of each filter have been described carefully by Cartwright (1984). All the tidal frequencies (diurnal, semi diurnal, third diurnal and higher frequencies) were practically "killed" whereas the long period components (Mf, Msf, Mm, Ssa, Sa) were not reduced. Both filters are symmetrical and preserve phases. Their cut-off frequencies are respectively 0.37 c/d (2.703 days) and 0.65 c/d (1.538 days). The Demerliac filter spans 71 hours of data, whereas the Cartwright filter spans 241 hours. Monthly mean sea level elevations and temperatures were calculated from the daily values, and anomalies from the long-term (means of all the daily means) at each site were derived.

Table 1.

Positions, depths, time origin and total data records at 31 December 1984 of the ORSTOM/τγ tide gauge stations.

Station	Long.	Lat.	Depth (m)	Time origin (U.T.)	Data length (days)	Country
Dakar	14°40.0'N	17°25.8'W	8.38	1300,24Dec1982	738	Sénégal
Praia	14°55.0'N	23°30.0'W	7.03	1800,02Mar1984	303	CVerde
Lomé	6°08.2'N	1°17.4'E	8.35	24Nov1983	37	Togo
Principe	1°39.1'N	7°26.5'E	5.57	0700,09Nov1983	415	RDSTP
Sao Tomé	0°01.1'N	6°30.8'E	7.05	0900.06Feb1983	694	"
Annobom	1°24.5'S	5°38.7'E	11.56	0800,08Feb1983	692	E.Guinea
Ascension	7°55.9'S	14°25.5'W	12.80	0930,22Apr1983	618	G.B.
Natal	5°45.1'S	35°11.7'W	5.96	0900,28Oct1982	795	Brazil
PenedosP.P.	0°55.2'N	29°20.6'W	11.56	1000,05Nov1982	787	"
Fernando N.	3°49.7'S	32°24.2'W	7.91	2000,07Nov1982	487	"
Trindade	20°30.2'S	29°18.6'W	4.70	1900,13Jun1983	57	"

Figure 1.

The FOCAL/TOGAMA (TOGA/Maregraphe/Atlantique) tide-gauge network
(October 1982-December 1987)in the Tropical Atlantic

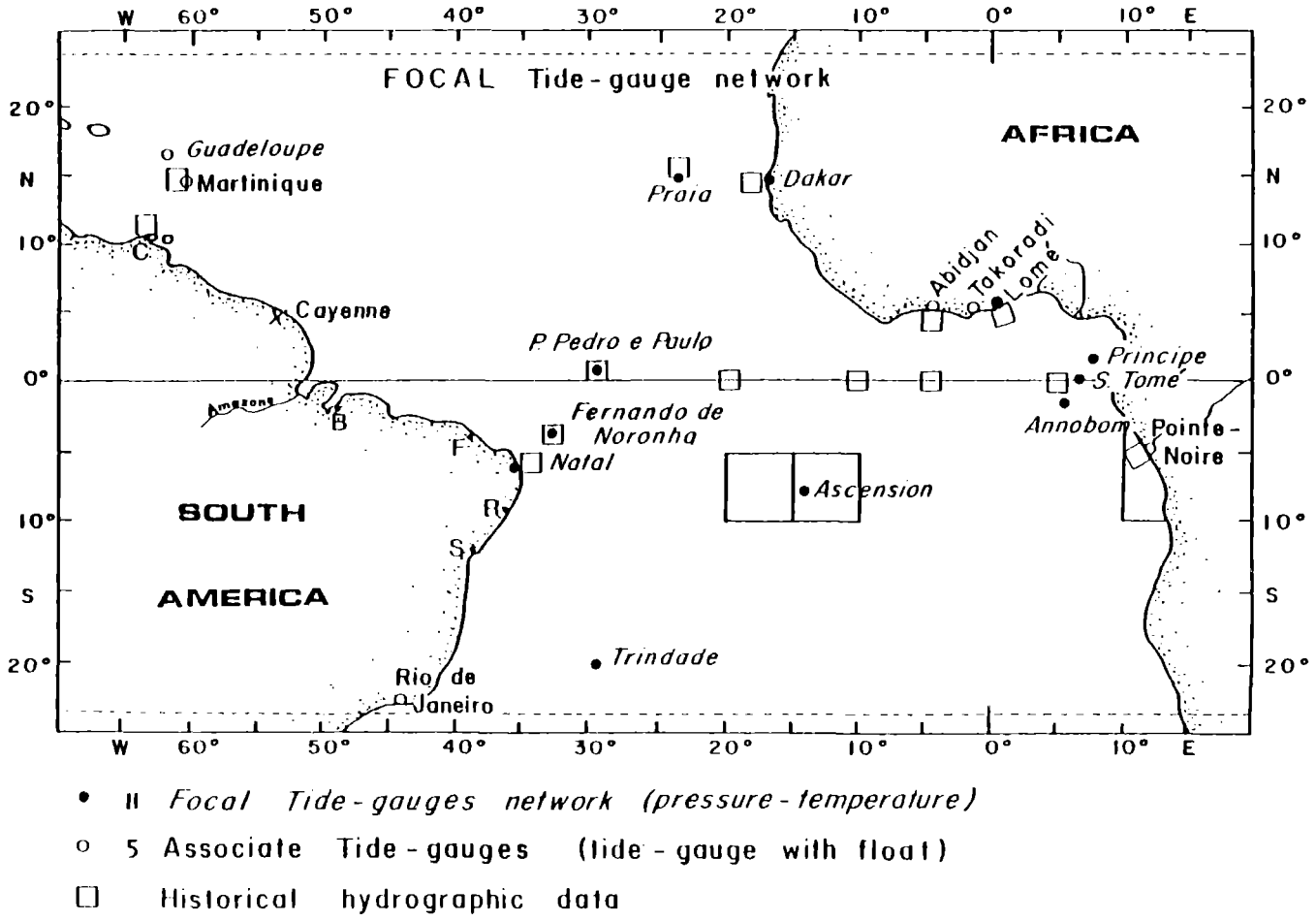

Table 2 gives the locations and sources of the historical monthly sea levels from Casablanca to Walvis Bay (Africa) and from Rio de Janiero to La Guaira (South America). Monthly atmospheric sea level pressures from the archived time series established by Bunker and Goldsmith (1979) from 1948 to 1972 were processed by ORSTOM at Brest to get the annual cycle of the sea level pressures over the tropical Atlantic Ocean. In addition, we used sea level pressures collected by ASECNA (Association Securite Navigation Aerienne) in Africa and by the Meterological Office (London) at St. Helena and Ascension Islands.

Low Frequency Sea Level Variations in the Tropical Atlantic

Harmonic Analyses. To characterize the seasonal cycle, it is necessary to ascertain the relative importance of the long-period tidal components. Harmonic analyses of the hourly values of sea level can be used to check indirectly the quality of the observations by comparing the main tidal components from the shallow records with the pelagic tidal constants given by the deep-sea pressure recorders or the inverted echo-sounders at other sites in the tropical Atlantic (Cartwright, 1982; Cartwright and Zetler, 1985). The diurnal tide K1 has its largest amplitude in the Gulf of Guinea, whereas the semi-diurnal tides M2 and S2 are maximum in the western equatorial part of the basin. This is in agreement with the recent cotidal charts given by Vassie (1982). The amplitude of the third diurnal component is always inferior to 1 cm. At the fortnightly periods (Mf and Msf) only Mf is of significant amplitude, although Msf was observed along the northern coast of the Gulf of Guinea (Picaut and Verstraete, 1979; Verstraete et al, 1980).

The annual and semi-annual components (Sa and Ssa) have their largest amplitudes at the equator in the Gulf of Guinea (Sao Tome). Except for Mf, the observed amplitudes at the Sa and Ssa periods at the shallow recorders are clearly much larger than those observed in the deep sea (Cartwright et al., 1987) or than the theoretical ones given by the equilibrium tides (Lizitzin, 1974). Obviously, current and steric effects in the "warm water sphere" are the main phenomena whereas the amplitudes of the gravitational tides at those periods have only minor effects on the surface layers of the ocean.

In the Gulf of Guinea it is possible to reconstitute the strong baroclinic sea level cycle with only the two first harmonics of the "mean year" (Verstraete et al, 1980). The semi-annual component is of equal importance to the annual term in this area where the seasonal variation of the heat con-

Table 2.

Locations, duration and sources of the monthly sea level historical time series (slashes indicate interruptions).τγ

Location	Time origin		End	Source of the data
AFRICA				
Casablanca	1957	//	1959	PSMSL
Sta Cruz de Tenerife	1927		1935	"
St. Louis	1975		1983	ORSTOM
Dakar	1942	//	1966	EPSHOM
Conakry	1956	//		ORSTOM
Freetown	1926	//		PSMSL
Monrovia	1953		1954	GFDL
San Pedro	1976	//	1979	ORSTOM
Abidjan	1967		1978	"
Takoradi	1929		1969	GB,Survey Department
Tema	1963		1978	Survey Department
Lomé	1970		1978	ORSTOM
Cotonou	1956	//	1981	"
Lagos	1940		1941	PSMSL
Forcados	1969		1972	"
Bonny Jetty	1971		1975	"
Calabar	1962		1964	"
Douala	1955	//	1958	ORSTOM
Libreville	1958		1960	EPSHOM
Port Gentil	1964		1965	"
Pointe Noire	1959	//	1980	ORSTOM
Walvis Bay	1959		1965	"
SOUTH AMERICA				
Rio de Janeiro	1949		1968	PSMSL
Salvador	1949		1968	"
Recife	1948		1968	"
Fortaleza	1948		1968	PSMSL
Belem	1949		1968	"
Carupano	1966		1975	"
La Guaira	1953		1975	"

tent is not confined to the upper layers and comes primarily from advection rather than insolation.

In the equatorial Atlantic, the seasonal cycle changes from being predominantly semi-annual in character in the East to mostly annual in the West. The semi-annual phase is fairly stable at the equator from the Penedos to the three equatorial islands in the Gulf, whereas the annual phase at Sao Tome (6°E) is in quadrature with the one at the Penedos (29°W).

The amplitudes and phases of the annual and semi-annual sea level cycles were also obtained by harmonic analyses of historical hourly values at Abidjan (5 years), Takoradi (1 year) and Lome (1 year). They are nearly equal to the present ones for the Sa component. The Ssa components have the same amplitudes (about 5cm) but the semi-annual phase shifts from 327-351° at 0°,6°E to 50-95° at the three precited harbours, so that the Ssa signal at the equator, 6°E leads the Ssa signal at the northern coast by nearly 1.5 months.

The seasonal cycle from historical data. The annual changes in sea level are not smooth quasi-sinusoidal curves as they would be if the solar annual and semiannual tides were dominant, but are irregular and peaky. In addition, the equilibrium amplitudes of Sa and Ssa, maximum at the equator, are only 0.16 and 0.64cm; yet annual sea level changes of 10cm amplitudes are observed along the African and South American coasts. As sea level responds to barometric variations in an inverted barometer sense (Wunsch, 1972), the analysis of seasonal sea level changes observed by ordinary surface tide gauges requires a careful examination of the atmospheric pressure cycle. We have studied the annual cycle of the sea level pressure between 20°N and 20°S and between Africa and South America in order to evaluate the isostatic changes due to atmospheric pressure changes.

The results are summarized in Figure 2 where the double amplitude (crest to trough) of the annual cycle is given in hPa (or cm) inside the upper right corner and the climatic mean pressure in the lower left corner of each of the 26 Marsden squares. Minimum amplitudes are observed off Senegal (1.5 hPa) and maximum off Brazil (5.7 hPa). The equatorial band (5°N-5°S) is a low pressure zone. High pressures straddle the middle of the "channel" between Africa and South America whereas low pressures run along the continents. Sea level pressures in the southern tropical Atlantic and the Gulf of Guinea are influenced by the St. Helena anticyclone (Figure 3), whereas the northern tropical Atlantic is under the influence of the ITCZ (Intertropical Convergence Zone).

Comparing the above figures (1.5 and 5.7 hPa) with the observed sea level amplitudes, it is safe to claim that at this very low frequency the barometric correction is unnecessary in this area. A crosspectral analysis between five years of adjusted and non-adjusted sea level time series at Abidjan did not reveal any phase difference and shows a very high coherence for periods from 5 to 300 days (Picaut and Verstraete, 1976).

Figure 2.

Annual amplitudes from crest to trough of the sea level pressure over the Tropical Atlantic (1948-1972);
top number in each Marsden square is amplitude in hPa (or cm).
Low number is climatic mean pressure in hPa (add 1000). The double dotted area is a maximum sea surface pressure area.

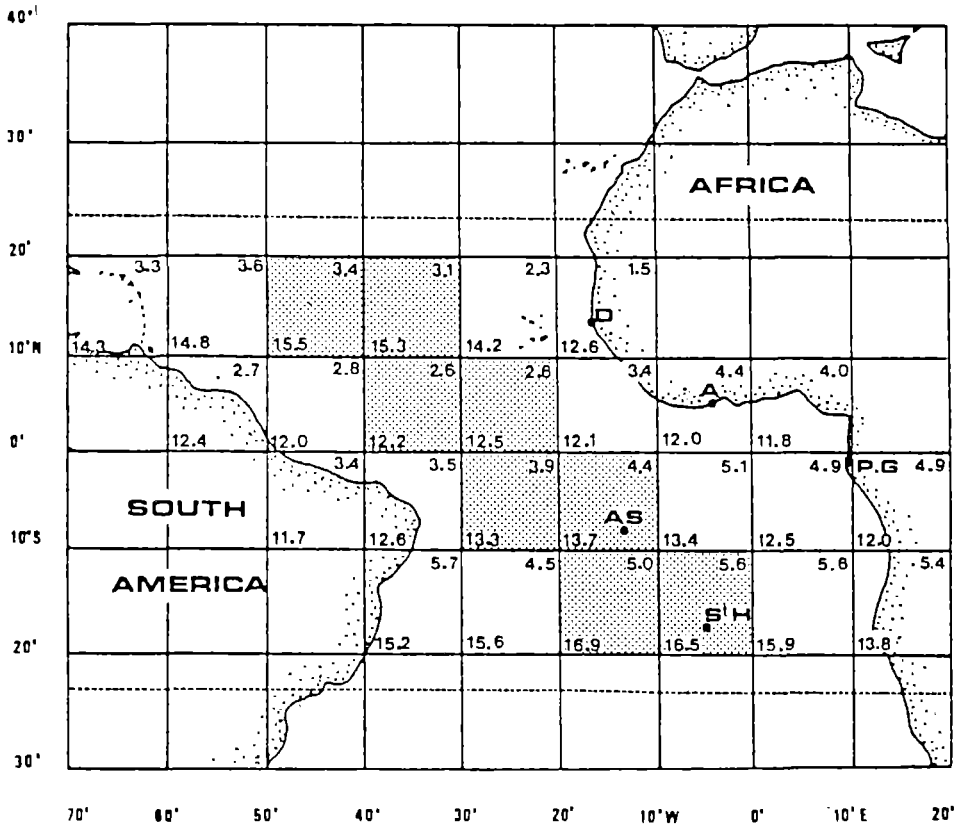

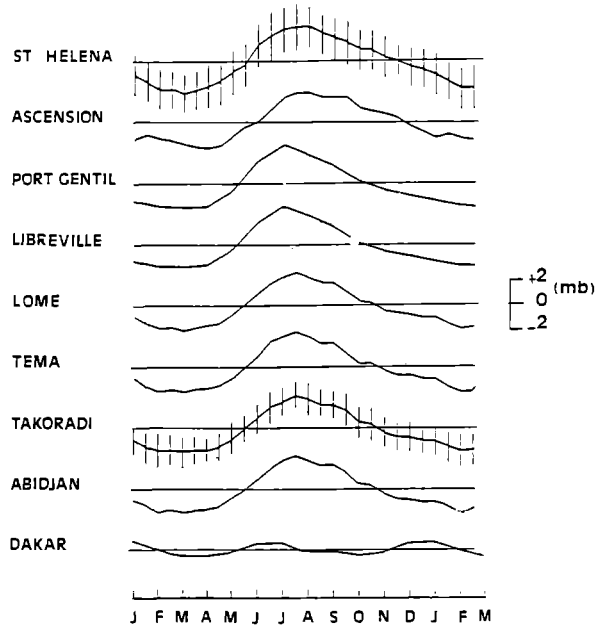

Figure 3. Seasonal cycle of the sea level pressure at selected stations in the central and eastern Tropical Atlantic. Vertical bars show one standard deviation about the mean.

Along the coasts of Brazil and Venezuela, the amplitudes and phases of the annual cycle of the sea level (Figure 4) vary strongly when we compare the stations north of the ITCZ with the southern ones. The ITCZ is the near equatorial trough of low pressure and associated convergence zone of the trade winds flowing toward South America. The march of the seasons in northeast Brazil and French Guyana is dominated by the latitudinal migration of the ITCZ. In northern winter, the convergence zone shifts southwards reaching a southernmost position (3°S) in February-March-April time of the rainy season in Brazil's "Nordeste". In northern summer, the convergence zone reaches 10°N in August-September. We observe indeed a very strong annual signal at Belem (Figure 4) where the sea level is 11.5cm above its climatic mean in March-April. Of course, this is due to the heavy rains and discharges of big rivers into the Rio Para. We do not observe such high levels either at Fortaleza or Georgetown, where for the same months the sea level is slightly below its mean (-1 to -2cm). Belem is the only station where we observe a semi-annual signal (two maxima, in March-April and in September-October), probably due to the fact that the ITCZ crosses the site twice each year. However, it is difficult to explain this strong semiannual signal by the local precipitations which are at minimum in September-October (de Mesquita et al, 1985). The amplitude of the annual cycle is minimum at Fortaleza which is south of the ITCZ.

To the north of 5°N and to the south of 5°S, sea levels vary in phase opposition. Along 2000 km of coastline, from Recife (8°S) to Rio (25°S), the annual cycle of the sea level is very similar, with double amplitudes of about 10cm, high sea levels in April-May and low sea levels from August (Rio) to November (Recife).

Although the three stations south of Cape S. Roque display the same annual pattern, it is difficult to recognize a firm coherence in their monthly anomalies from 1948 to 1968 (Figure 5). Probably the distances between the stations are too large for this study. Even the series of Salvador and Recife, two harbours only 600km distant, do not show a strong coherence, but the amplitudes of their anomalies are weak compared to those of Rio or Fortaleza. We have compared the two series of La Guaira and Carupano, two sites 400km distant along a nearly zonal-oriented coastline (10°N) between 1967 and 1975. Their seasonal cycle (Figure 4) and their anomalies (Figure 6) are very coherent. We note the similarity of the anomalies particularly in 1968-69 and in 1972-73; in 1969, the first peak was in March (+6cm), the second one in October (+8.5cm), simultaneously at the two stations. These peaks had been preceded by a trough of 6.5cm in October-November 1968. For the second event, the first peak occurred from December 1972 to February 1973 (+6.0cm) followed by a very strong peak in August 1973 (+13 cm at La Guaira, +8.8cm at Carupano). Such elevations must be related to large scale atmospheric phenomena and probably to the "El Nino" events which occurred in 1969 (weak) and in 1972-1973 (strong) (Rasmusson, 1984).

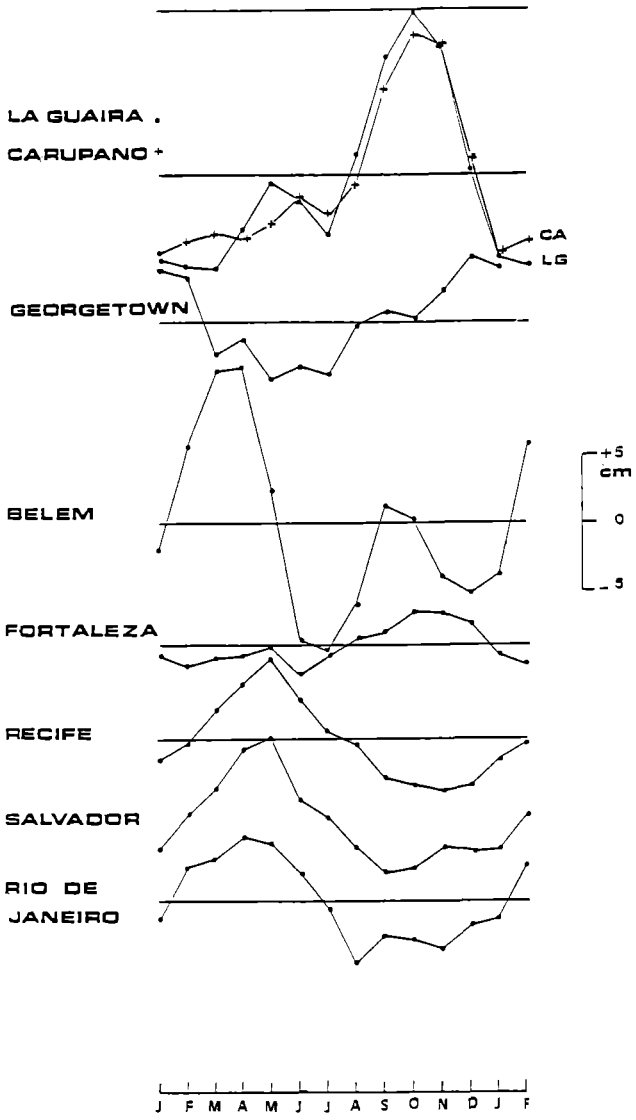

Figure 4. Annual cycle of monthly sea levels from Rio (Brazil) to La Guaira (Venezuela). Reference level is the mean of all observations at each station.

Figure 5.

Monthly sea level anomalies (cm) from Rio to Carupano (1948-1968).

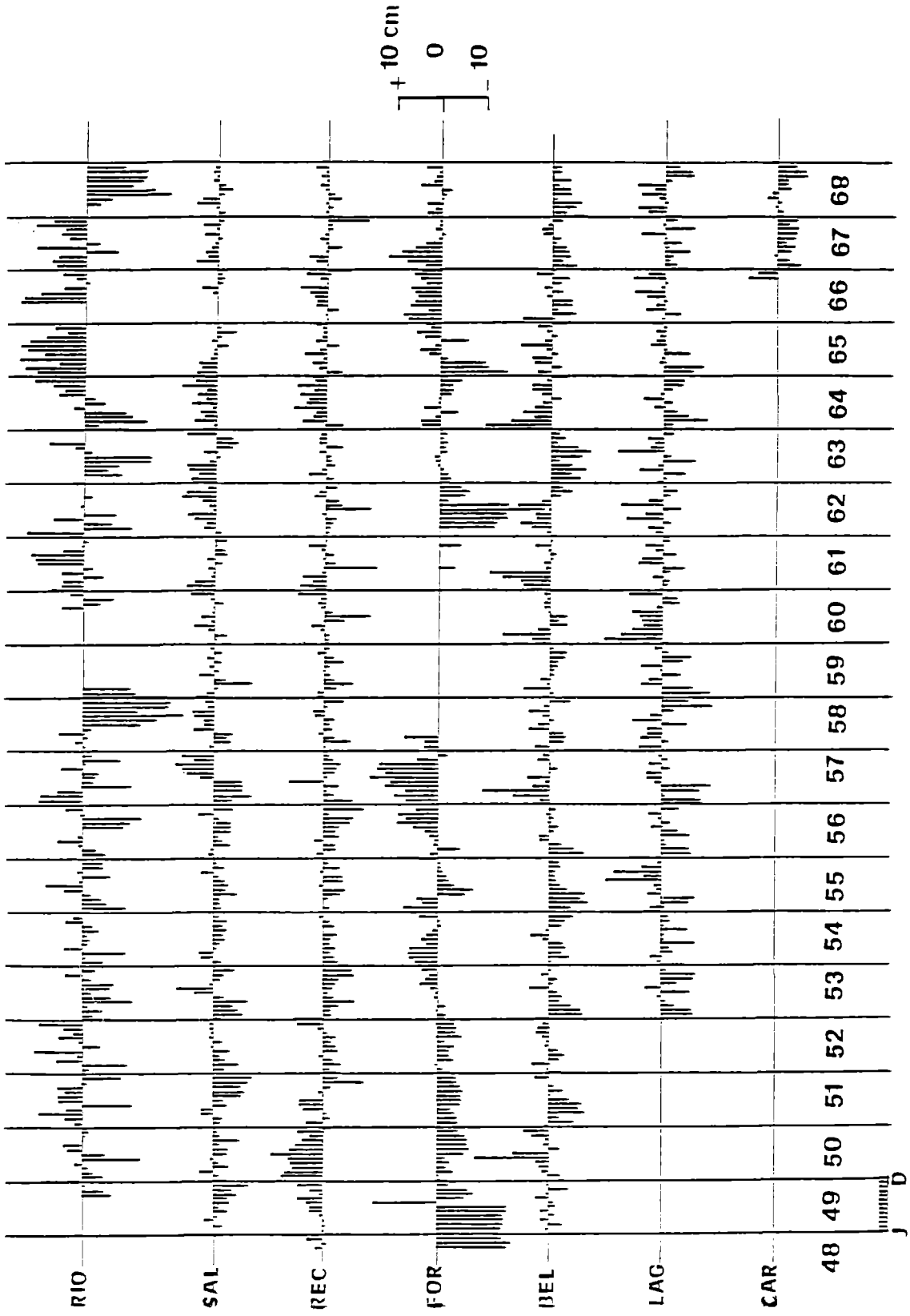

Figure 6.

Same as Figure 5 at La Guaira and Carupano. (1967-1975).

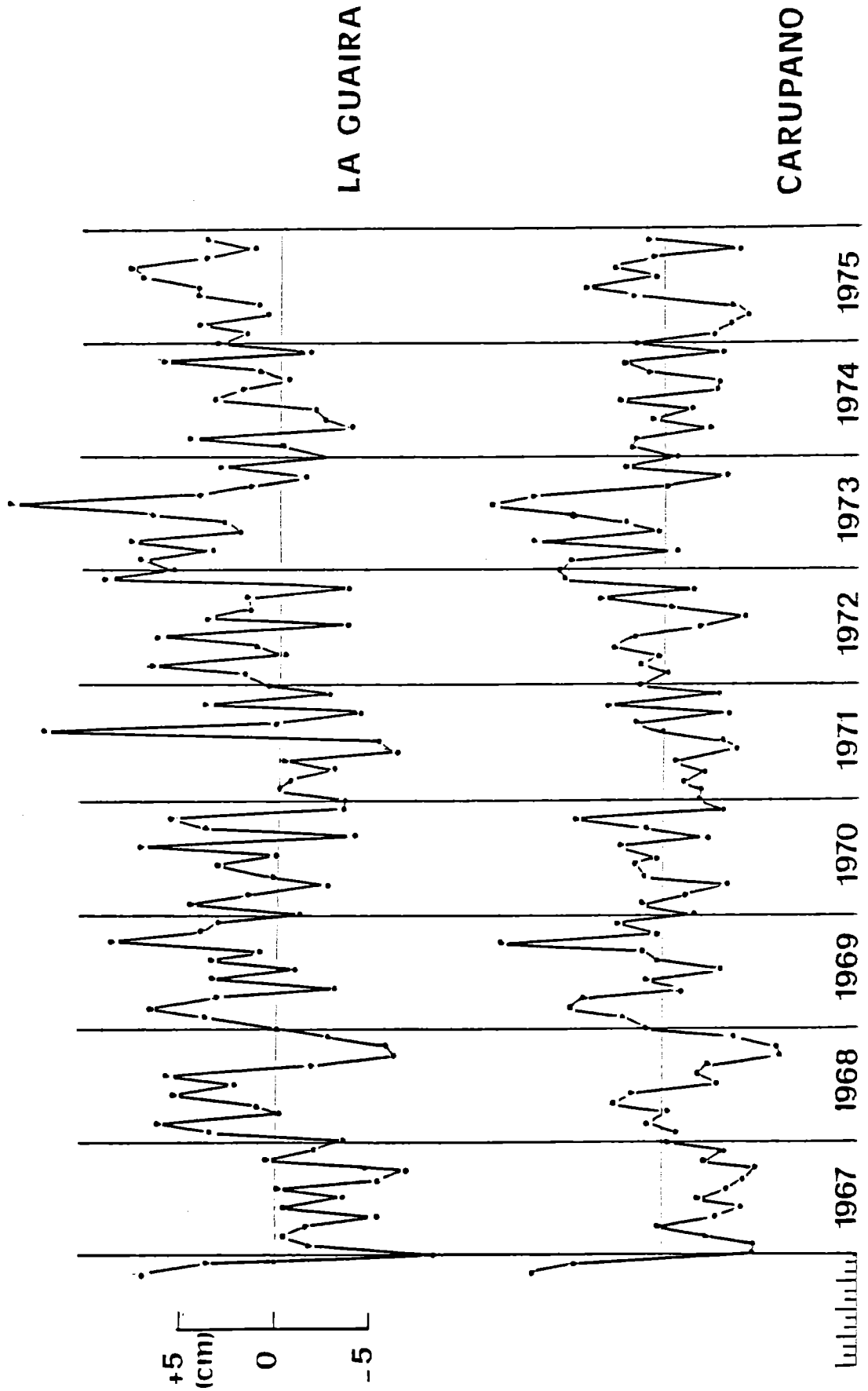

The pattern of the annual cycle of the sea level in the eastern tropical Atlantic is very coherent from a typical southern cycle (Walvis Bay) to a typical northern one (Santa Cruz de Tenerife). In the Gulf of Guinea all the stations reveal a typical southern cycle from Pointe Noire, Port Gentil (Gabon) to San Pedro, Monrovia; at any station, the major event is a sea level drop of about 10cm from the climatic mean sea level (Figure 7). At Walvis Bay (23°S), the cold season is in June-July-August and this is the time period of the African Monsoon in the Gulf of Guinea. We observe the upwelling signal as a sea level drop which does not occur simultaneously along the coastline. According to the historical data set, the upwelling event and minimum sea levels occur between April and June along the North-South boundary of the Gulf, whereas along the East-West boundary, mimima are in July-August, (Verstraete, 1985a). Further north, the cycle is clearly out of phase with the Gulf of Guinea: sea levels are maximum in August at Dakar (+8.2cm above the climatic mean) and at Santa Cruz de Tenerife (+7.0cm). It was not possible to study the monthly sea level anomalies along the African coastline, because we did not find a sufficiently long and simultaneous time series there.

Now, looking at the entire tropical Atlantic basin, we see that outside of the equatorial strip 5°S-8°N low and high sea levels occur on each side of the basin in the winter-spring and in the summer-autumn seasons of each hemisphere. Within the equatorial strip 5°S-8°N, it is the opposite and we note that the amplitude of the annual cycle in the western equatorial Atlantic is very weak (Fortaleza: -2, +2cm; Georgetown: -4, +5cm) compared with the eastern equatorial Atlantic (Pointe Noire: -11, +8cm; Abidjan: -9, +8cm). Belem is not relevant here, because the observations there are heavily contaminated by noisy effects due to river discharges. We note also the asymmetry between the western equatorial cycle, which is an annual cycle with only one maximum and one minimum, and the eastern one, which is a semiannual cycle with two maxima and two minima. In the northern hemisphere, the symmetry of the cycles at Carupano and Dakar is noteworthy with low sea levels in February-March (cold season) and high sea level in August (Dakar) and October (Carupano). In the southern hemisphere, Recife-Salvador-Rio lag Pointe Noire, Walvis Bay by three months (Figures 4 and 7).

Synoptic Sea Level Observations in the Equatorial Atlantic in 1983 and 1984

Daily sea surface elevations and in situ temperatures (at the depth of each instrument, Table 1) at nine pressure tide-gauge stations are shown between November 1982 and December 1984 in Figures 8 and 9. Inspection of Figure 8 shows anomalies at Penedos and Natal in 1983. At the Penedos, the relative sea level (RSL) was above the mean sea level (MSL) computed from two years of observations, whereas at Natal large changes of RSL occurred in March-April, June 1983, followed by a negative trend from August 1983 to January 1984 (-8.2cm). These observations are not bolstered either by the windstress data or by hydrology (which could explain barotropic and (or) baroclinic sea level changes). These two time-series suggest an instrumental error due to an error in the design of the cradles (electrolytic phenomenon took place). A large editing effort was necessary on the Natal and Penedos monthly sea levels, which were adjusted to the ob-

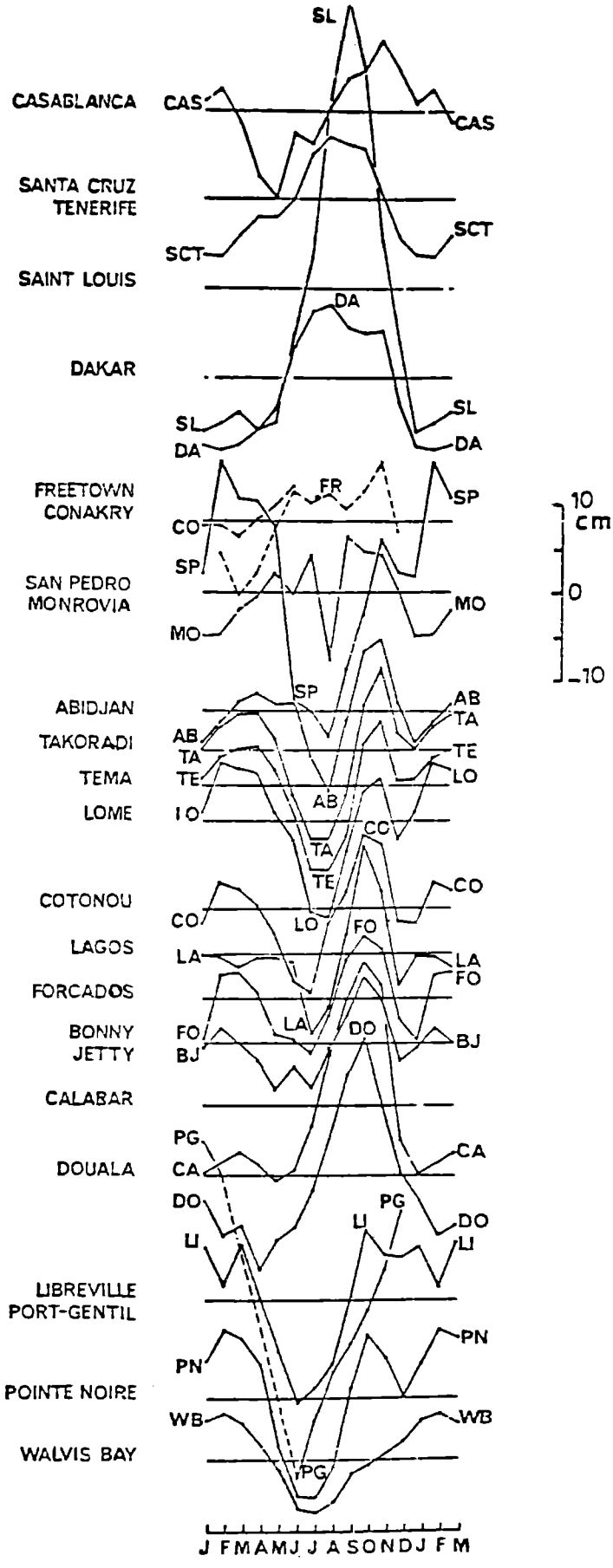

Figure 7. Annual cycle of monthly sea levels from Walvis Bay to Casablanca (cm). Reference level is the mean of all observations at each station.

Table 1.

Positions, depths, time origin and total data records
at 31 December 1984 of the ORSTOM/τγ tide gauge stations.

Station	Long.	Lat.	Depth (m)	Time origin (U.T.)	Data length (days)	Country
Dakar	14°40.0'N	17°25.8'W	8.38	1300,24Dec1982	738	Sénégal
Praïa	14°55.0'N	23°30.0'W	7.03	1800,02Mar1984	303	CVerde
Lomé	6°08.2'N	1°17.4'E	8.35	24Nov1983	37	Togo
Principe	1°39.1'N	7°26.5'E	5.57	0700,09Nov1983	415	RDSTP
Sao Tomé	0°01.1'N	6°30.8'E	7.05	0900.06Feb1983	694	"
Annobom	1°24.5'S	5°38.7'E	11.56	0800,08Feb1983	692	E.Guinea
Ascension	7°55.9'S	14°25.5'W	12.80	0930,22Apr1983	618	G.B.
Natal	5°45.1'S	35°11.7'W	5.96	0900,28Oct1982	795	Brazil
PenedosP.P.	0°55.2'N	29°20.6'W	11.56	1000,05Nov1982	787	"
Fernando N.	3°49.7'S	32°24.2'W	7.91	2000,07Nov1982	487	"
Trindade	20°30.2'S	29°18.6'W	4.70	1900,13Jun1983	57	"

served dynamic heights gathered during eight synoptic cruises (FOCAL Programme October 1982-August 1984). Sea level observations at the other sites were satisfactory. The tide-gauge at Fernando de Noronha island was lost in July 1983, due to the destruction of the cradle.

In the Gulf of Guinea, the tide-gauge array straddles the equator at Sao Tome island; it was completed in early November 1983 at Principe island. Sea levels at the three sites vary in phase remarkably. The annual cycle is very strong, with high sea levels in January-February-March (main warm season) and low sea levels in May-June-July (main upwelling season); then sea levels are high again in September-October and low in November-December. This is in agreement with the seasonal cycle described at Pointe Noire and Libreville from historical data (Figure 7). Along the coastline of the Gulf, this bimodal seasonal cycle was described by Verstraete (1985 a,b). The main cold season and minimum sea levels in the equatorial area (Sao Tome, Libreville) are observed in May-June-July about two months earlier than in the Tema-Takoradi-Abidjan area (minimum sea levels in July-August).

In Figure 8 we observe very regular oscillations of about two weeks in periodicity, superimposed on the seasonal trends. Spectral analyses give evidence of a maximum in energy density at 13-14 day-period; harmonic analyses show precisely that the Mf tidal component (13.6 day-period) is present everywhere in the tropical Atlantic with amplitudes of nearly 2.0cm and no phase propagation along the equator. The ubiquity of this oscillation is noteworthy and its synchronisation can be checked visually by superposing the graphs of stations as distant as Sao Tome and Penedos, for example.

The Warm Event of 1983-1984 in the Tropical Atlantic Ocean

The new sea level data set is far too short in time for establishing the annual cycle at each site. The synoptic data of the years 1983 and 1984 differed from climatology and it is therefore necessary to refer to historical sea level observations (EPSHOM, Brest; PSMSL, Bidston). Monthly levels at Pointe Noire and Recife harbours were used as surrogate climatic references for the nearest new sites, respectively Annobom (near Pointe Noire) and Natal (near Recife). As interannual differences in level can be obscured by the annual signal, we have subtracted the monthly climatic means from the monthly sea levels computed at Annobom and Natal in 1982-1984, to get the monthly anomalies at these two sites. All the sea levels are referred to the Mean Sea Level (MSL) computed from all the observations at each site.

Climatic anomalies in the western and eastern equatorial Atlantic are shown at Natal and Annobom in Figure 10. We observe two opposite trends. At Natal, sea level anomalies decreased from +6cm in September 1983 to -8cm in May 1984, while they rose from nearly 0 to +5cm in the same time at Annobom. These anomalies give evidence of a large basin-wide oceanic event in the equatorial Atlantic ocean

Figure 8.

Daily mean sea level elevation (cm) relative to the mean sea level elevation in 1982-1984 at the FOCAL tide-gauge network.

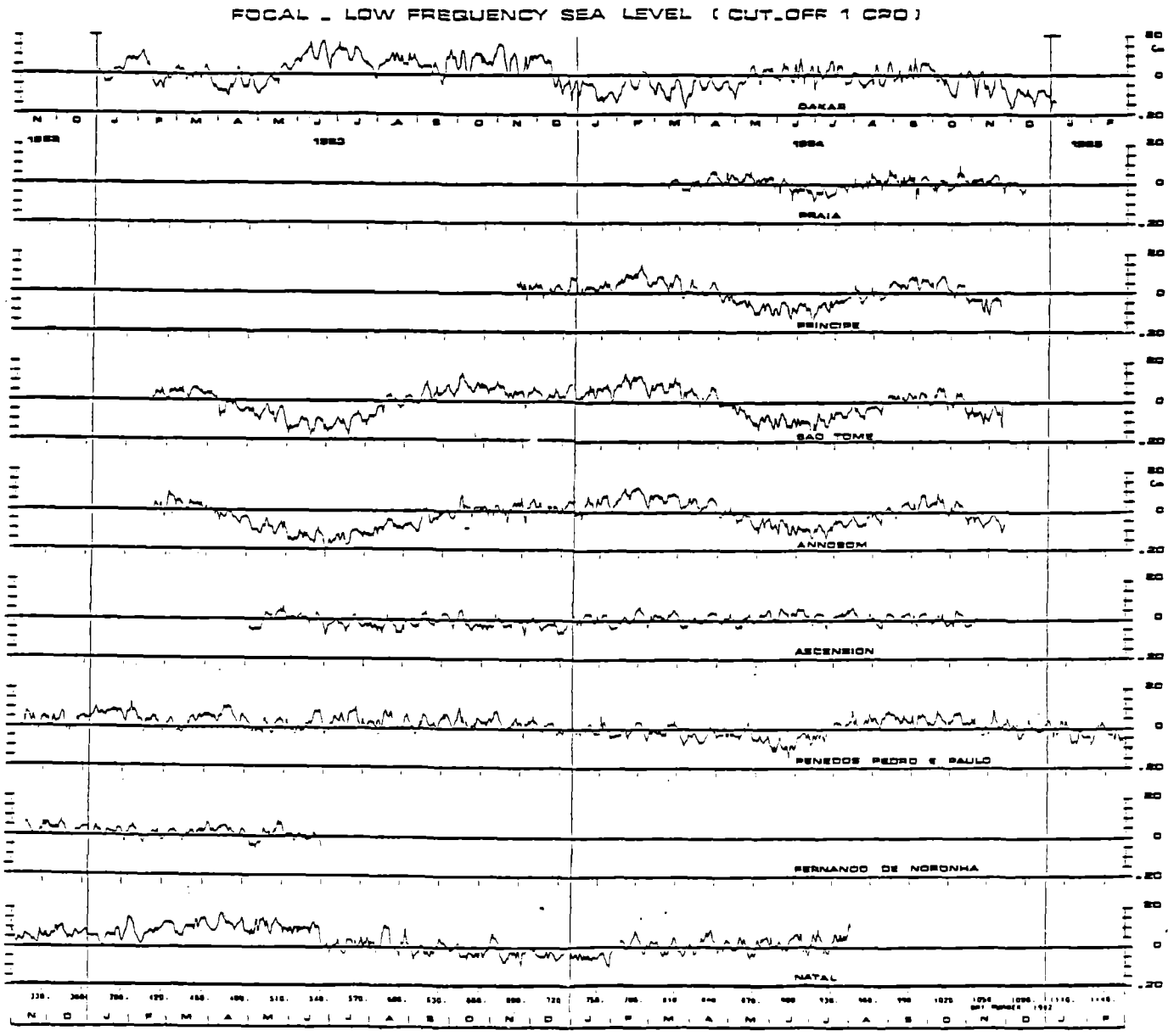

which occurred between the autumn of 1983 and the spring of 1984. Usually, the sea surface along the equatorial Atlantic slopes upward to the west of 10°W, whereas in the Gulf of Guinea it is flat or slopes upward to the east. This pattern is well documented and can be explained by a steady zonal westward windstress to the west of 10°W (Katz et al, 1977; Katz et al, 1986) and northward-eastward windstress in the Gulf. (Verstraete et al., 1980). Numerical modelling works (Philander, 1979; Philander and Pacanowski, 1981) and studies of the seasonal changes of the surface dynamic topography in the 16°S-30°N area (Arnault, 1984; Merle and Arnault, 1985), show that the tropical Atlantic Ocean is in equilibrium with the seasonal winds. Between October 1982 and August 1984, eight synoptic cruises of both the R/V CAPRICORNE and NIZERY between 35°W and 6°E provided data that illustrate the seasonal variability of the zonal and meridional sea surface dynamic topography (relative to 500m), (Hisard and Henin, 1984). Combining this data set with historical hydrographic data at the BNDO data bank, we have established the dynamic sea surface topography along each transect and along the equator. In 1982-1984, the absolute sea surface sloped downward from Natal (100.7, 2.8 dyn-cm) to the Penedos (92.2, 2.6 dyn-cm) and from the Penedos to Sao Tome. In the Gulf of Guinea, during the October 1982 August 1984 time period, the absolute sea surface sloped downward from Principe (88.8, 5.6 dyn-cm) to Sao Tome (86.1, 7.0 dyn-cm) and Annobom (83.9, 7.4 dyn-cm). However, we observed large variations in this pattern and in February 1984 the dynamic height at Sao Tome (101.6 dyn-cm) was higher than at Annobom (100.5) and Principe (99.9), whereas the Penedos were 6.5 dyn-cm "below" Sao Tome.

Figure 9.

Daily mean sea temperature (°C) at each tide-gauge station.
The depth of each station is given in Table 1.

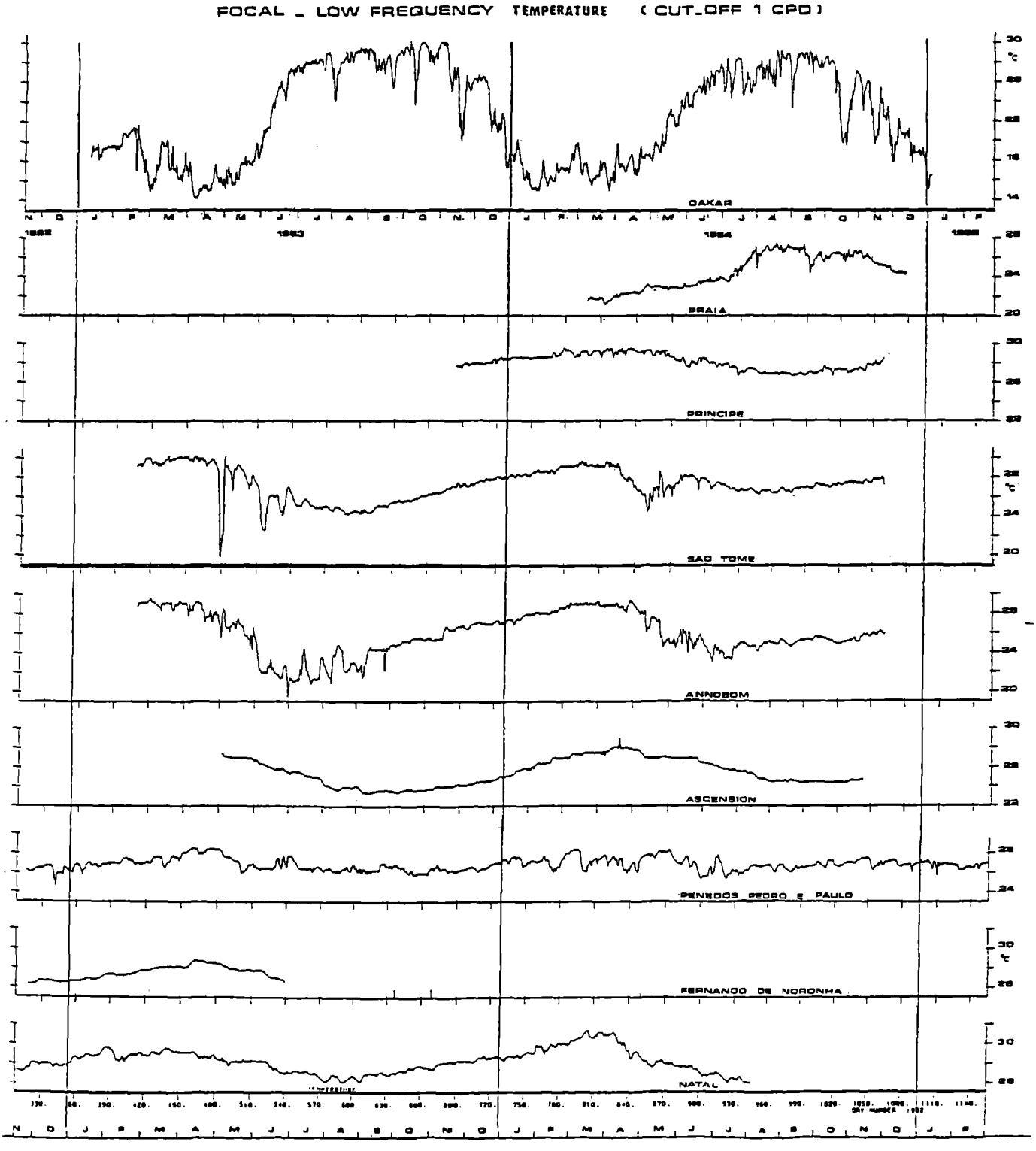

It seems straightforward to compute the mean monthly geostrophic velocity at the mean latitude of each pair of stations between Natal and Penedos. However, the equation of geostrophy does not hold at the equator, and the sign of the Coriolis parameter depends upon the hemisphere (it is positive to the north of the equator, negative to the south). It is therefore necessary to check the sea surface slope between 1°N and 1°S at 29°W, to see if it is possible to substitute the sea surface dynamic height at 0°55'N, 29°W (Penedos) for the sea surface dynamic height at 1°S at 35°W and 29°W. In 1982-1984 it was nearly flat: the mean differences in dynamic heights were 1.1 and 0.8 dyn-cm, respectively. In comparison, the differences Natal less Penedos and FN less Penedos were 8.5 and 3.2 dyn-cm, respectively. Examination of seven transects at 29°W in 1982-1984 reveals that instantaneous dynamic height differences between 1°N and 1°S can reach 2.2 dyn-cm (cruise 6). Indeed, each hydrographic transect essentially represents a "snapshot" of the meridian dynamic topography, contaminated by many high frequency oscillations: i.e., internal tides (Cartwright, 1982), intertial-gravity waves (Garzoli, 1987), Kelvin waves (Katz, 1987), Rossby waves (Weisberg et al, 1979) travelling along the equatorial wave-guide at different phase-speeds. However, the mean sea level derived from hourly time series allows the filtering out of not only internal tides, but also nearly all the sea level variance in the frequency band 1-8 cycles per 40 days. To conclude this discussion, in 1982-1984 the dynamic heights at 0°, 29°W were, in mean, 0.8 dyn-cm below those observed at Penedos. Consequently, we decided to attribute to the position 1°S, 29°W (symmetrical with the Penedos position in reference to the equator), the monthly sea level values observed at Penedos. This pseudo tide-gauge station is denoted "PN" in Figure 11.

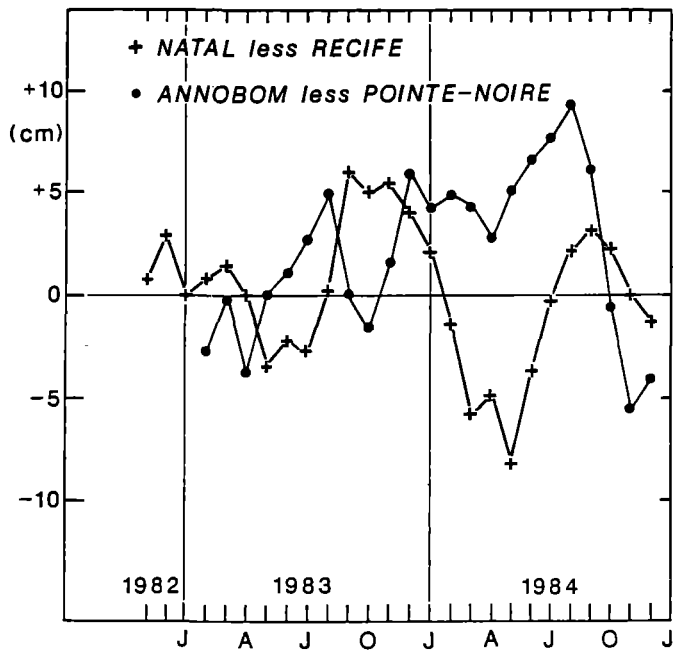

Figure 10. Time series of monthly sea level anomalies at Natal (5°45'S) and Annobom (1°24'S) in 1982-1984. The climatic means are annual cycle of monthly sea levels at Recife (8°03'S) and Pointe Noire (4°49'S) harbours, respectively.

Figure 11.

Monthly sea surface geostrophic currents (in cms-1) computed from the absolute sea surface slope between the tide-gauge stations at the western array. "PN" indicates the surrogate position of the Penedos at 1°S, 29°30'W. Surface geostrophic currents from the 1982/84 hydrocasts and the seasonal geostrophic currents from historical data are also shown.
Mean position for each pair a, b, c is given. Tick marks on the time axis are the fifteenth day of each month.

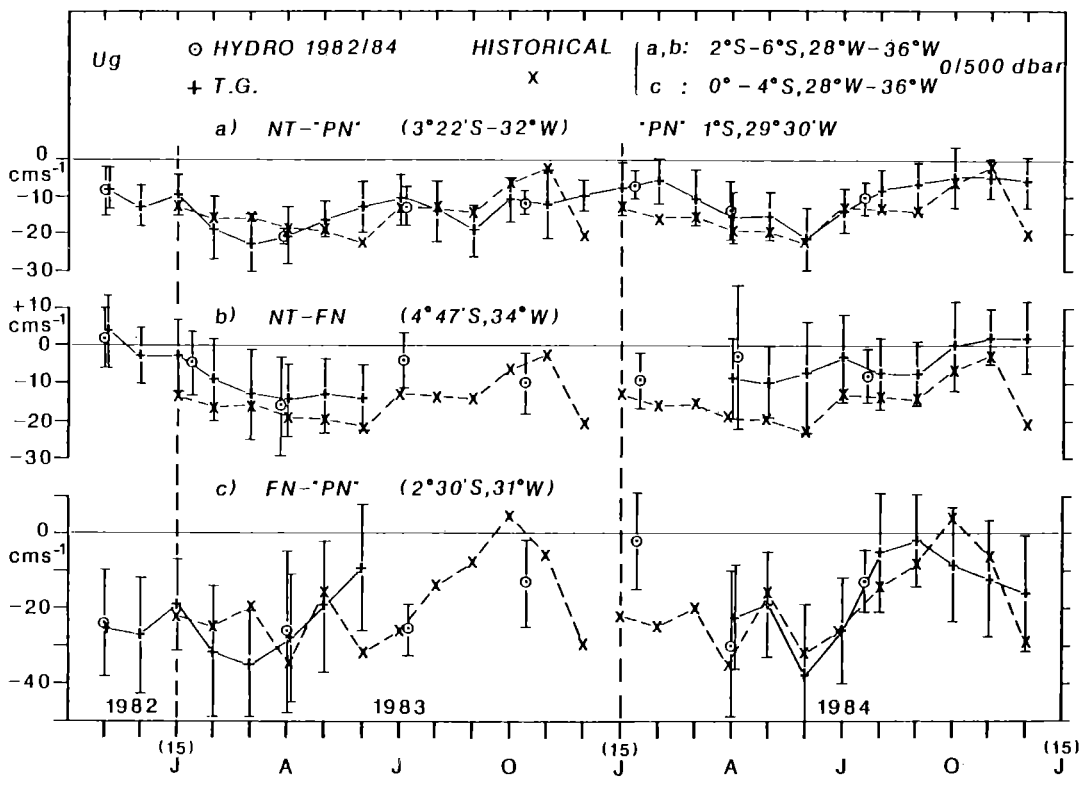

The monthly sea surface geostrophic currents (Ug) computed from the sea surface slopes between Natal, FN and "PN" (surrogate position of the Penedos station) are shown in Figure 11. Although nine months of sea level observations are missing at FN, it is interesting to compare Ug at 3°22'S, 4°47'S and 2°30'S (Fig. 11a,b,c). First, the geostrophic current is faster and its seasonal cycle larger in the Fernando-"PN" area. Second, in 1984, the South Equatorial Current (SEC) between Natal and Fernando was significantly below its historical seasonal cycle (Fig.11b). Third, there is an excellent agreement (seven to eight occurences) between the two types of observations, hydrography and tide-gauge, at the three sites. In the longest time series (Fig.11a), the seasonal variations of Ug appear pretty well, with maximum and minimum velocities in the boreal winter-spring and in autumn, respectively. The inter-annual variability is evident, particularly the changes in the time of the maxima (March in 1983, June in 1984) and the weakness of the SEC in 1984 relative to 1983 and relative to the historical seasonal cycle, described by Arnault (1984), Merle and Arnault (1985) and Arnault (1987). In the area 2°S-6°S, 28°W-36°W, Arnault (personal communication) finds a maximum westward Ug (referred to 500 dbar) in June and a minimum in October-November. In 1983, the mean surface geostrophic SEC at 3°22'S, 32°W was maximum in March, three months earlier than climatology; it decreased faster than climatology until July 1983 and was significantly below its mean value in December 1983-February 1984. In June 1984, the SEC recovered its mean seasonal value, then decreased until October-November; again, it was below its seasonal values in August-September and in December 1984.

A basin-wide perturbation occurred in the equatorial Atlantic Ocean in boreal Autumn 1983-Summer 1984. The slackening of the surface geostrophic component of the SSEC (Southern component of the SEC) at 32°W was accompanied by strong eastward currents at 4°W. Warm and saline waters were advected into the Gulf (Hisard et al, 1986). The surface equatorial seasonal upwelling was inhibited at 6°E as well as at 4°W, as near-sea-surface temperatures were about 3°C warmer in June-August than over the same time period in 1983 (Figure 12, Principe, Sao Tome, Annobom). These much higher than seasonal surface temperatures in the Gulf were associated with unseasonal torrential rains over the islands in June-July-August 1984. According to climatological statistics, these months are dry (they are known as the "Gravana"). It rains 4 mm at Sao Tome (climatic mean over 27 years), and 160 mm at Principe (mean over 17 years). In contrast, in June-August 1984, it rained 290 mm. and 1892 mm, respectively. These facts strongly suggest than an El-Nino-like event occurred in the equatorial and tropical South Atlantic Ocean in 1984. The two tide-gauge arrays at Natal-FN-Penedos and Principe-Sao Tome-Annobom monitored the meridional pressure gradients at 32°W and 6°E across the SEC. The tide-gauges at Penedos (29°W) and Sao Tome (6°E) combined with IES could monitor the eastward and westward zonal pressure gradients (ZPG's) along the equator (Katz el al., 1986). Correlations of the synoptic ZPG with absolute current observations at 28°W and 4°W may provide a means to monitor the equatorial undercurrent volume transport. In future studies, we hope to address this important question as a step towards the objectives of the scheduled altimeter satellite missions (TOPEX/POSEIDON) and WOCE (World Ocean Circulation Experiment). The demonstrated feasibility of monitoring the surface geostrophic component of the SEC terminus between Natal and Penedos is a significant contribution to these long-term programs. The "TOGAMA" (TOGA/Maregraphe/Atlantique) network is scheduled to be equipped in the near future, to transmit sea level observations in real time at 32°W and 6°E (satellite transmission systems such as ARGOS or METEOSAT), before the launch of the TOPEX/POSEIDON altimetry programs in 1990-1991.

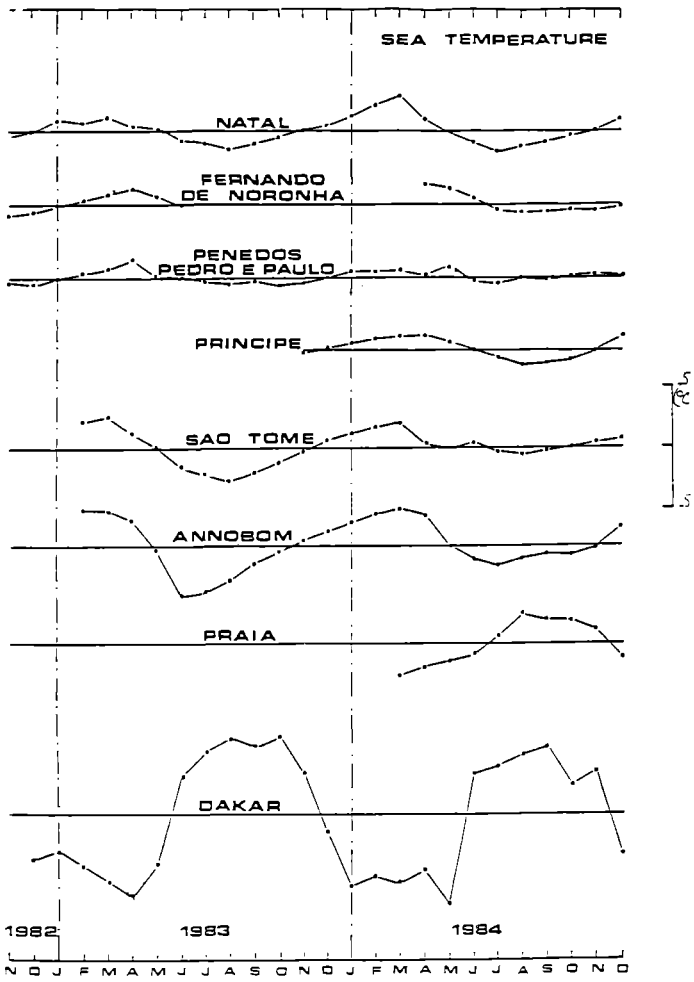

Figure 12. Monthly sea temperature anomalies (°C) at the tide-gauge stations in 1983 and 1984. Anomalies are the differences between the monthly values and the 1982-1984 mean values at each station.

References

1. Arnault, S., Variation saisonniere de la topographie dynamique et de la circulation superficielle de l'ocean Atlantique Tropical; these doctorat 3eme cycle, 198 pp., Universite Pierre et Marie Curie et Musee Nationale d'Histoire Naturelle, Paris, 1984.

2. Arnault, S., Tropical Atlantic geostrophic currents and ship drifts, *J. Geophys.Res.*, 92, 5076-5088, 1987.

3. Bunker, A.F., and Goldsmith, R.A., Archived time-series of Atlantic ocean meteorological variables and surface fluxes. Technical Report WHOI-79-3, 1979.

4. Cartwright, D.E., The tidal signal inverted echo-sounder records, *Deep-Sea Res.*, 29, 767-784, 1982.

5. Cartwright, E.D., A note on the application of smoothing filters to FOCAL/SEQUAL data series. *FOCAL Information*, pp. 6-7 and 14-15, 1984.

6. Cartwright, D.E., and Zetler, B.D., Pelagic tidal constants 2 IAPSO publication scientifique No.33, IUGG, Paris, 59pp., 1985.

7. Cartwright, D.E., Spencer R., and Vassie J., Pressure variations on the Atlantic equator, *J. Geophys.Res.*, 92, pp. 725-741, 1987.

8. Demerliac, A., Le niveau moyen de la mer. Calcul du niveau moyen journalier. 19 pages. EPSHOM, Brest, 1973.

9. De Mesquita, A.R., On mean sea level along the Brazilian coast. Paper presented at the IAMAP/IAPSO Honolulu Assembly (5-16 August 1985).

10. Hisard P., and Henin C., Zonal pressure gradient, velocity and transport in the Atlantic equatorial undercurrent from FOCAL cruises (July 1982-February 1984), *Geophys. Res. Lett.*, 11, pp. 761-764., 1984.

11. Hisard P., Henin C., Houghton, R., Piton B., and Rual P., Oceanic conditions in the tropical Atlantic during 1983 and 1984. *Nature*, 322, pp. 243-245, 1986.

12. Katz, E.J., Dynamic topography of the surface in the equatorial Atlantic, *J. Mar. Res.*, 39, pp. 53-63, 1981.

13. Katz, E.J., Belevich, R., Bruce, J., Bubnov, V., Cochrane, J., Duing, W., Hisard, P., Lass, H.U., Meincke, J., de Mesquita, A., Miller, L., and Rybnikov, A., Zonal pressure gradient along the equatorial Atlantic, J, Mar, Res., 35, pp.293-307, 1977.

14. Katz, E.J., Hisard, P., Verstraete, J-M and Garzoli, S.L., Annual change of the sea surface slope along the equator of the Atlantic Ocean in 1983 and 1984, *Nature*, 322, pp. 245-247, 1986.

15. Labarre, J., Construction d'un support sous-marin permanent pour un maregraphe. Note technique ORSTOM, Dakar-Hann, 10 pages, 1983.

16. Lizitzin, E., Sea level changes, Elsevier, 286 pp., 1974.

17. Merle, J. and Arnault S., Seasonal variability of the surface dynamic topography in the tropical Atlantic Ocean, *J. Mar. Res.*, 43, pp. 267-288, 1985.

18. Millero, F.J., and Poisson, A. International one-atmosphere equation of state sea water, *Deep-sea Res.*, 28A, 6, pp.625-629, 1981.

19. Pattullo, J., Munk, W., Revelle, R., and Strong, E., The seasonal oscillation in sea level, *J. Mar. Res.*, pp. 88-155, 1955.

20. Philander, S.G.H., Variability of the tropical ocean, *Dyn. Atmos. Oceans.*, 3, pp. 191-208, 1979.

21. Philander, S.G.H., and Pacanowski, R.C., The oceanic response to cross equatorial winds (with application to coastal upwelling in low latitudes), *Tellus*, 33, pp. 201-210, 1981.

22. Picaut, J., and Verstraete, J-M., Mise en evidence d'une onde de 40-50 jours de periode sur les cotes du Golfe de Guinee, *Cah. ORSTOM. ser. Oceanogr.*, 14, 3-14, 1976.

23. Picaut, J. and Verstraete, J-M., , Propagation of a 14.7-day wave along the Northern coast of the Gulf of Guinea. *J. Phys. Oceanogr.*, 9, pp. 136-149, 1979.

24. Rasmusson, E.M., El Nino: the Ocean/Atmosphere connection, *Oceanus*, 27, 2, pp. 5-12, 1984.

25. Shannon, L.V., Boyd, A.J., Brundrit, G.B., and Taunton-Clark, J., On the existence of an El Nino-type phenomenon in the Benguela System, *J. Mar. Res.* 44, pp. 495-520, 1986.

26. Vassie, J., Tides and low frequency variations in the equatorial Atlantic, *Oceanologica Acta*, 5, pp.3-6, 1982.

27. Verstraete, J-M., Sea level variation in the Gulf of Guinea, *Trop. Ocean-Atmosphere News*, 9, pp. 5-6, 1982.

28. Verstraete, J-M., Further evidence of poleward propagation of the mean seasonal coastal upwelling in the Gulf of Guinea, *Trop. Ocean-Atmosphere News*, 29, pp. 8-10, 1985a.

29. Verstraete, J-M., Contre-courants equatoriaux et variations saisonnieres du contenu thermique et du niveau moyen dans l'Atlantique tropical Est, *Oceanologica Acta*, 8, 3, pp. 249-262, 1985b.

30. Verstraete, J-M., Seasonal heat content in the eastern Tropical Atlantic, Proc. Int'l Symposium on Equatorial Vertical Motion, Paris, *Oceanologica Acta*, S2, 85-90, 1987.

31. Verstraete, J-M., Picaut, J., and Morliere, A., Atmospheric and tidal observations along the shelf of the Gulf of Guinea, *Deep-Sea Res.*, 26, Supplement, pp. 343-356, 1980.

32. Verstraete, J-M., and Picaut, J., Variations du niveau de la mer, de la temperature de surface et des hauteurs dynamiques le long de la cote Nord du Golfe de Guinee. *Oceanogr. Trop.*, 18, 2, pp. 139-162, 1983.

33. Wunsch, C., Bermuda sea level in relation to tides, weather and baroclinic fluctuations, *Rev. Geophys. Space Phys.*, 10, 1, pp.1-49, 1972.

34. Weisberg, R.H., and Colin C., Equatorial Atlantic ocean temperature and current variations during 1983 and 1984, Nature, 332, pp. 240-243, 1986.

5 . The Southern Oscillation Index Since 1882

J.P. Rebert and J.R. Donguy

Groupe Antenne ORSTOM, Brest, France

Abstract

Atmospheric pressure measurements from Papeete (Tahiti) have been discovered starting as early as 1875. This new data set allows the extension of the Southern Oscillation Index computation back to 1882. Although the reliability of some periods of observation is low, this index appears to be in good accord with historical evidence of El Ninos in the western and central Pacific. We notice once more that the strength of such events in these areas may differ from that observed and currently adopted in the Eastern Pacific.

Introduction

According to Walker and Bliss (1932), "When pressure is high in the Pacific Ocean, it tends to be low in the ocean from Africa to Australia". This feature is called "Southern Oscillation" and the usual index (SOI) is the difference in the sea-level atmospheric pressure between Darwin (12°24'S, 130°48'E, Australia) and Papeete (17°32'S, 149°34'W, Tahiti, central South Pacific). The large-scale pressure variations at these two locations are in opposition to phase (Van Loon and Shea, 1984) and they are usually consistent with the strength of El Ninos.

Monthly pressure at Darwin is available since 1882, but the data file from Papeete officially started in 1935. However, with the gracious help of the "Service des Archives Territoriales de Polynesie Francaise", it has been possible to recover atmospheric pressure measurements from as early as 1875, albeit with some gaps. Accordingly, it is now possible to consider the monthly SOI, from 1882 to the present.

Data

Early atmospheric pressure data at Papeete were recorded as part of a meterological summary found in the official weekly newspaper. Data were available as far back as 1876, though missing for the following periods: 1893 to 1896, 1907 to 1908, 1911 to 1916 and for 1932 and 1934. Data are daily before 1896 and monthly after this date. Daily data were originally issued from direct readings of the barometer at Papeete hospital and given in millimeters of mercury. A mean monthly climatological correction for temperature effects has been first applied to these data which were then converted into millibars and reduced to sea level, knowing the height of the barometer. The monthly data after 1896 had already been corrected and given in millibars.

The monthly means of Darwin's daily average pressure have been kindly provided by the Bureau of Meteorology at Melbourne, Australia, in the form of 9 a.m., and 3 p.m. sea-level reduced presssure at the Darwin Post Office (1882-1942) and Darwin airport (1942-1984).

The Southern Oscillation Index

In order to define the Southern Oscillation Index in the absence of Tahiti data, some authors have utilized closely correlated surrogates. For instance, Quinn et al (1978) substituted the Santiago-Bombay difference before Darwin's pressure was available (1861-1881) and the Santiago-Darwin pressure before Tahiti's pressure was available. Wright (1977) computed a SOI using a combination of the available pressures between Capetown, Bombay, Jakarta, Darwin, Adelaide, Apia, Honolulu and Santiago, and through this method was able to extend the series back to 1851. Trenberth (1984) has discussed the statistical validity of the SOI using the available pressure at Darwin and Papeete.

A 12-month running mean plot of sea level atmospheric pressure (in millibars) at Tahiti and Darwin is presented in Figure 1. The mean pressure at Tahiti for the whole series is 1012.55 mb and 1009.71 at Darwin. The mean of the first series (1875-1935) for Tahiti does not differ significantly from that of the second part, which means that there is probably no bias in this extended time-series. When examining variability, however, it can be seen that the first half of the series is a little noisier than the second half and that very large pressure excursions appear in this series. As we have no reason, however, to suspect the large scale variability to have been more important at this time than after 1935, (as this feature would have appeared in Darwin's pressure variability), one must exercise caution when interpreting these data.

The most questionable feature appears in 1925 when the Tahiti pressure increases by 4 mb and then remains over 1014 mb from 1926 to 1935, without any concomitant decrease in Darwin. Moreover, this higher pressure gradient should have induced a strong anticyclone in the central South Pacific and, consequently, strong trade winds should have existed at this time. However, Bigg et al (1987) observe an abrupt decrease of the trade winds in 1925 which is inconsistent with such a pressure increase. This supports the hypothesis of erroneous measurements between 1925 and 1934. On the other hand, the same authors notice a strong increase of the winds in the same area during the 1940-1945 period,

Figure 1.

Pressure variations for Tahiti (full line) and Darwin (dotted line) filtered by a twelve-month running mean

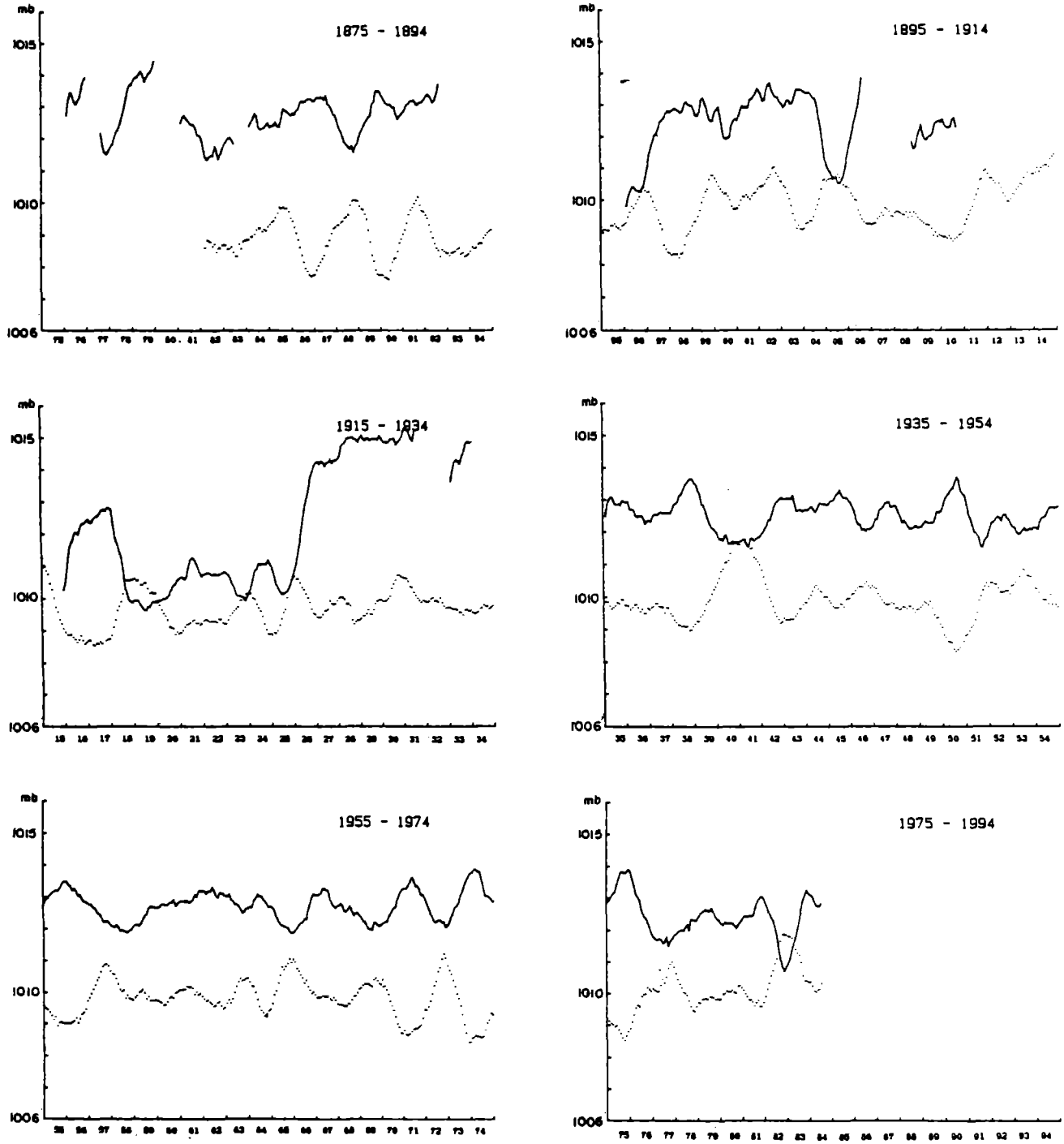

without any modification of the pressures in Darwin and Tahiti, where the measurements were then considered reliable.

It is, therefore, very difficult to draw definite conclusions from such comparison, even where there is no relation between strength of the trade winds and the Tahiti-Darwin pressure gradient (which is quite possible as we have no information on the meridional pressure gradient). Then too, early wind observations in the Pacific may be as questionable as the pressure measurements.

We decided, therefore, as there was no evidence in the documents of any change in the barometer location or of observers at this time, to keep this part of the record for the reader's appraisal.

Figure 2 shows the Southern Oscillation Index (SOI) defined here as the sea level atmospheric pressure difference in millibars between Tahiti and Darwin from 1882 to 1983. The gaps occuring in the record are due to the lack of data at Tahiti. The variations of this SOI are consistent with those shown by Quinn et al (1978) who has used the Santiago-Dar-

Figure 2.

SOI variations expressed as the sea-level pressure difference between Tahiti and Darwin.
A twelve-month running mean has been applied to monthly data

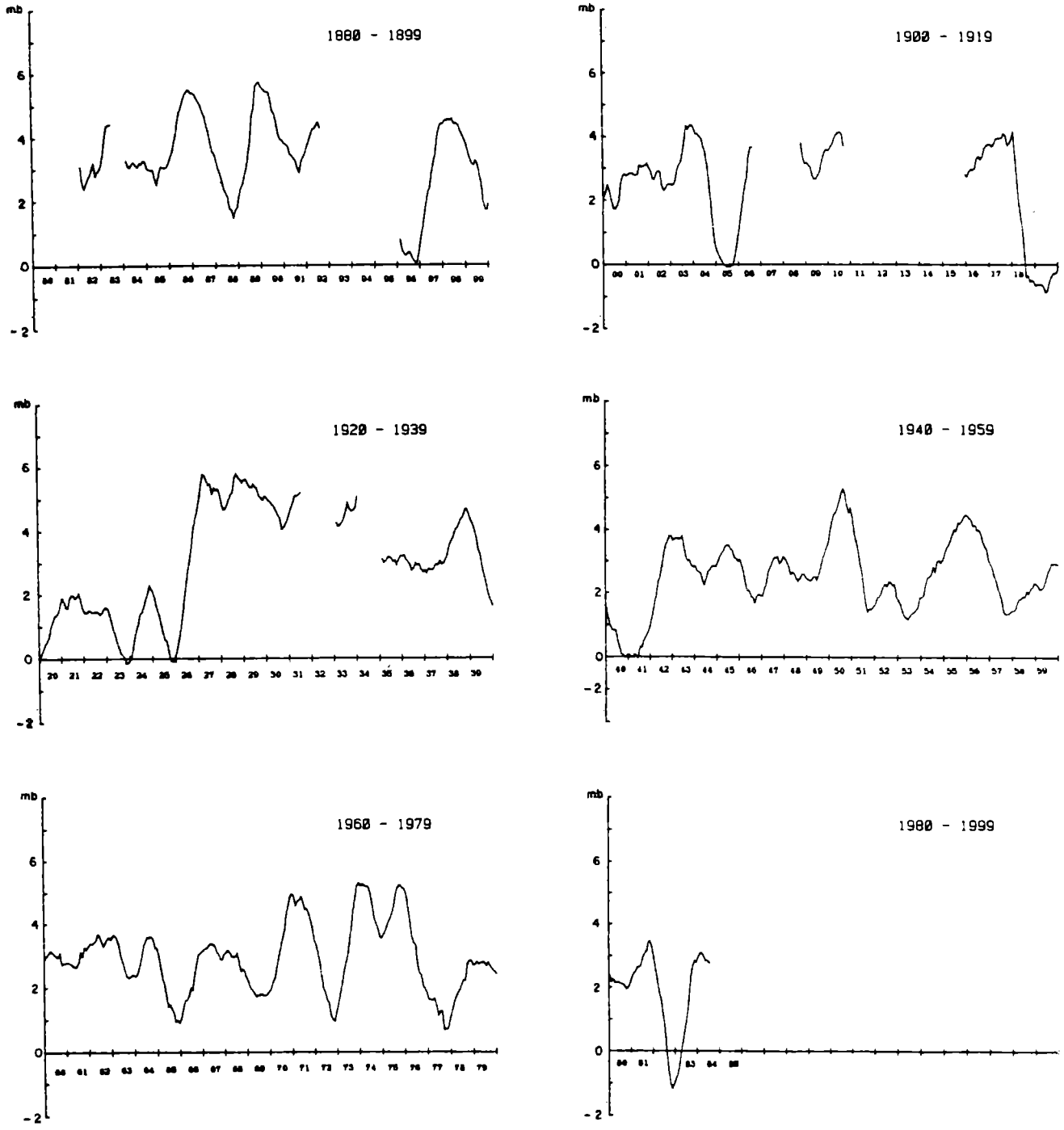

win difference and with those proposed by Wright (1977). However, once again, from 1926 to 1935, the unusual value of this SOI is inconsistent with the other estimates.

The Southern Oscillation Index and El Nino

Another way to assess the reliability of these data is to compare this index to other typical anomalies usually associated with the pressure variability, the most famous being the El Nino phenomenon. Unfortunately, though El Nino events are always associated with a more or less abrupt decrease of the SOI, the intensity of such events cannot be unambiguously related to pressure variations. The intensity of El Nino is, by itself, a poorly defined quantity based on a sum of different types of observations, including physical and biological properties of ocean waters, as well as atmospheric factors such as rainfall.

From eastern Pacific records, El Nino events have been listed by Quinn et al (1986) since the sixteenth century and are classified in four categories: weak (W), moderate (M), strong (S) and very strong (VS) with confidence ratings running from 2 through 5. In Figure 2, most of the listed events correspond to a trough in the SOI curve.

Table 1

	Strength QUINN	Confi-dence		SOI mb	Tahiti	Noumea	Strength W. Pac	Remarks
1877-78	V S	5			Cyclones	Drought	V S	
1884	S	5		+ 3		Drought		
1888-89	M	5		+1.5	Cyclones			
1891	V S	5		+ 3		no		
1896-97	M	4		0			S	
1899-1900	S	5		+ 2		data		
1902	M	4		+2.5				
1905				0	Cyclones	Drought	V S	not cited in QUINN et al (1986)
1907	M	3						
1911-12	S	4		no				
1914	M	5		Tahiti data				
1918-19	M	5		-1		Drought	S	
1923	M	5		0			S	
1925-26	V S	5		0		Drought	S	
1930-31	M	5		+4				
1932	S	5		no data				
1939	M	5						no SOI trough
1940-41	S	5		0	Cyclones	Drought	V S	
1943-44	M	5		+2.5				
1951	M	5		+1.5				
1953	M	5		+1				
1957-58	S	5		+1.5		Drought	S	
1965-66	M	5		+1				
1972-73	S	5		+1		Drought	S	
1976-77	M	5		+1				
1982-83	V S	5		- 1	Cyclones	Drought	V S	

In Table 1, 1877-1983 El Nino evidence has been reported in the eastern Pacific, according to Quinn et al (1986), together with the western and central Pacific from the SOI variations and meteorological events observed in Tahiti (Anon, 1979), and from the 1903-1983 monthly precipitations recorded at Noumea (New Caledonia) by the Service Territorial de Meteorologie de Nouvelle Caledonie. Early data before 1903 are issued from the official weekly newspaper of New Caledonia.

From the western Pacific view, typical manifestations of strong or very strong El Ninos could be characterized by a SOI trough below 1 millibar (Figure 2), accompanied by cyclones at Tahiti (Anon, 1979) and droughts at Noumea (Morliere and Rebert, 1986) or on a wider scale, in the Fiji New Caldeonia area (Ropolewski and Halpert, 1987). Using only the newly discovered data (1875-1935), these features happened in 1877-1878 (according only to Tahiti pressure), 1896-1897, 1905, 1918-1919, 1923, 1925-1926.

From the eastern Pacific view, the 1877-1878 event is effectively classified by Quinn as very strong, but the 1896-1897, 1918-1919 and 1923 events, although characterized by deep SOI troughs are only classified as moderate. The 1925-1926 event is recognized on both sides as at least as strong. The worst case is the 1905 event; Quinn et al (1986) do not notice any El Nino, but in an earlier publication (Quinn et al, 1978), a moderate one was pointed out. However, the Tahiti atmospheric pressure patterns for 1904-1905, 1877-1878 and 1982-1983 (these latter being characterized by a very strong El Nino) are very similar (Figure 3).

It seems, therefore, that the intensity of the same El Nino event can be perceived differently in the eastern and western Pacific. This feature has already been pointed out for the 1979 El Nino-like event observed in the western Pacific, but not noticeable in the eastern Pacific (Donguy et al, 1982; Donguy and Dessier, 1983). However, this 1979 event was weak with a small SOI trough and light meterological conse-

quences. On the other hand, in 1905 the SOI trough was deep and the meteorological consequences, particularly the occurence of ravaging cyclones in Polynesia (Anon, 1979), were as drastic as in 1982-1983. Referring to the work of Ropolewski and Halpert (1987), it is moreover obvious that if the only relation to be considered is that between the SOI and precipitation patterns, the best coherence between these two factors is found in the southwestern tropical Pacific from Australia to Fiji.

Conclusion

The definition of El Nino was first based on anomalous phenomena observed in the eastern Pacific along the South American coast. Such events have been later linked to Pacific-wide modifications of the atmospheric and oceanic circulation, in what are now termed El Nino-Southern Oscillation (ENSO) episodes.

Adding new pressure data from Tahiti allowed us to extend the SOI index back to 1882. Though some parts of this record are questionable due to poor accuracy of these observations and unreliability of the installation, it is possible to use parts of it, if only relative variations on a time-scale ranging from month to year are needed. This record is certainly inadequate for determining long-term trends in the pressures, but quantitites such as phase and intensity of large rises and falls prior to 1935, can be assessed.

The comparison of these results to previous estimations of the strength of historical El Ninos confirms that there is some decorrelation of the intensity of such episodes in the western and eastern Pacific. In particular, the 1877-1878 and 1905-1906 events most probably had an intensity comparable to that of the 1982-1983 event in the western and central Pacific.

References

1. Anonyme, 1979. Vents, cyclones, houles en Polynesie Francaise. *Annales Meteorologiques*. Polynesie Francaise.

2. Bigg, G.R., Whysall, K.D.B., References Cooper N.S., 1987. Long-term trends and a major climate anomaly in the tropical Pacific wind field. *Tropical Ocean-Atmosphere Newsletter*, 37, pp. 1-2.

3. Donguy, J.R., Henin, C., Morliere, A., Rebert, J.P., and Meyers, G., 1982. Appearances in the western Pacific of phenomena induced by El Nino in 1979-1980. *Tropical Ocean-Atmosphere Newsletter*, 10, pp. 1-2.

4. Donguy J.R., and Dessier, A., 1983. El Nino-like events observed in the tropical Pacific. *Monthly Weather Review*. Vol. 111 10, pp. 2136-2139.

5. Morliere, A., and Rebert, J.P., 1986. Rainfall shortage and El Nino-Southern Oscillation in New Caledonia, Southwestern Pacific. *Monthly Weather Review*. Vol. 114, 6, pp. 1131-1137.

6. Quinn, W.H., Zopf, W.O., Short, K.S., and Kuo Yang, R.T.W., 1973. Historical trends and statistics of the Southern Oscillation, El Nino and Indonesian droughts. *Fish. Res. Bull.*, Vol. 76, No.3, pp. 663-678.

7. Quinn, W.H., Neal, V.T., and Antunez de Mayolo, S.E., 1986. Preliminary report on El Nino occurrences over the past four-and-a-half centuries. ref. 86-16. Dec. 1986, N.S.F. ATM 85 15014.

8. Ropelewski, C.C., and Halpert, M.S., 1987. Global and regional scale precitipation patterns associated with the El Nino/Southern Oscillation. *Monthly Weather Review*, Vol. 115, pp. 1606-1626.

9. Trenberth, K.E., 1984. Signal versus noise in the Southern Oscillation. Monthly Weather Review. Vol. 112, pp. 326-332.

10. Van Loon, H., and Shea, D.J., 1984. The origin of a warm event in the Southern Oscillation. *Tropical Ocean-Atmosphere Newsletter*, 27 pp. 1-2.

11. Walker, G.T., and Bliss, E.W., 1932. World weather V. Mem. Roy. Meteor. Soc. 4, pp. 53-84

12. Wright, P.B., 1977. The Southern Oscillation. Patterns and mechanisms of the teleconnections and their persistence. H16 77-13, Hawaii Institute of Geophysics. University of Hawaii, H196844, 107 pp.

6 . Variations of the Mass Field and Currents off the Peru Coast

S. Zuta

Direccion General de Investigaciones Oceanograficas
Instituto del Mar, Callao, Peru

Introduction

The prominent variations off the Peru coast consist of both seasonal and interannual changes, and the two phenomena that regulate the hydrographic regime and the seafood chain are the coastal upwelling and El Nino. The latter is considered a recurrent event with changeable characteristics and associated with the Southern Oscillation.

In normal conditions, the main manifestation of the coastal upwelling is the presence of relatively cold and nutrient-rich waters at the sea surface, in the form of patches or tongues along most of the coastal band which are stronger in aumumn (May-June) and winter (August-September), particularly around 5°S (Paita) in the northern part, and 15°S (San Juan) in the southern part.

El Nino appears off Peru at intervals of 2 to 14 years. Its main effects are the temporal warming of the surface layer, the invasion of low-salinity surface waters from the north and high-salinity surface waters from the west or southwest, both poor in nutrients. Due to its changeable characteristics, several authors distinguish between categories of weak (as 1969), moderate (as 1965, 1976), strong (as 1925-1926, 1940-1941, 1957-1958, 1972-1973), and very strong or extraordinary (as 1982-1983) El Nino events.

Summarized in this paper are the main changes in the horizontal and vertical distribution of temperature and salinity, as well as the currents in the coastal band, with special attention given to observations made in 1976-1977 and 1982-1983, periods of intense field observations.

Data

All available data were included to derive the climatic mean of SST and SSS given in Tables 1 and 2, and corresponding

Table 1.

Climatic means of SST (°C) for the coastal band between 3°S and 19°S, at intervals of one degree latitude. (See shaded squares in Fig.1).

Lat(S°)	Jan.	Feb.	Mar.	Apr.	May.	Jun.	Jul.	Aug.	Sep.	Oct.	Nov.	Dec.	AM	AA
03°30'	23.0	24.9	25.0	24.1	23.0	21.9	20.5	20.2	20.7	20.5	21.3	21.3	22.2	4.8
04°30'	21.8	23.5	23.0	22.2	19.7	19.9	18.6	18.1	18.4	18.7	19.4	20.1	20.3	5.4
05°30'	22.2	23.4	23.4	21.5	20.4	19.6	18.6	17.4	17.4	17.7	18.7	19.6	20.0	6.0
06°30'	22.2	22.9	23.2	21.3	19.6	18.8	18.1	17.6	17.4	17.3	18.4	19.7	19.7	5.9
07°30'	21.1	22.5	22.5	21.0	19.7	18.4	18.0	17.2	17.2	16.7	18.1	18.6	19.2	5.8
08°30'	20.3	21.5	21.7	20.4	19.2	18.5	17.5	17.1	16.8	17.1	17.7	18.4	18.8	4.9
09°30'	20.6	21.4	21.5	20.8	19.3	18.4	18.1	17.5	17.1	17.1	17.9	18.6	19.0	4.4
10°30'	20.7	21.3	21.8	20.9	19.7	18.5	17.5	17.0	16.9	16.7	17.8	18.5	18.9	5.1
11°30'	20.0	21.3	20.9	19.8	19.1	17.7	17.1	16.9	16.2	16.9	17.6	18.4	18.5	5.1
12°30'	20.4	21.1	21.4	19.9	18.3	17.5	17.0	16.3	16.4	16.7	17.6	18.9	18.5	5.1
13°30'	20.6	21.1	21.5	19.3	17.8	17.0	16.7	16.1	16.2	17.0	17.5	18.6	18.3	5.4
14°30'	19.5	19.9	20.0	19.1	17.2	16.5	16.5	15.2	15.0	15.4	16.9	17.9	17.4	5.0
15°30'	20.2	20.4	19.7	19.1	17.5	16.4	16.2	15.3	15.1	15.7	16.9	17.9	17.5	5.3
16°30'	20.5	21.1	20.5	19.8	17.9	16.7	16.4	15.1	15.9	16.5	17.7	19.1	18.1	6.0
17°30'	21.4	22.0	22.2	20.9	19.6	17.3	17.0	15.4	16.2	16.9	18.6	19.8	18.9	6.8
18°30'	21.0	22.3	22.9	20.9	20.2	18.0	17.5	16.7	16.7	17.9	18.7	19.3	19.3	6.2
X	21.0	21.9	22.0	20.7	19.3	18.2	17.6	16.8	16.8	17.2	18.2	19.0	19.1	5.2
	Summer			Autumn			Winter			Spring				

AM= Annual Mean AA= Annual Amplitude

Table 2.

Climatic means of SSS (‰) for the coastal band between 3°S and 19°S at intervals of one degree latitude. (See shaded squares in Fig.1).

Lat.(°S)	Jan.	Feb.	Mar.	Apr.	May.	Jun.	Jul.	Aug.	Sep.	Oct.	Nov.	Dec.	AM	AA
3°30'	33.9	33.8	33.6	33.9	34.1	34.5	34.6	34.3	34.4	34.1	34.2	34.2	34.1	1.0
4°30'	34.0	34.3	34.3	34.5	34.9	35.1	35.0	34.9	34.8	34.9	34.4	34.5	34.6	1.1
5°30'	34.5	34.7	34.6	34.9	35.0	35.1	35.1	35.1	35.1	35.0	34.9	34.8	34.9	0.6
6°30'	34.8	34.8	34.8	35.0	35.0	35.1	35.1	35.1	35.1	35.1	35.0	34.9	35.0	0.3
7°30'	35.0	34.8	34.9	34.8	35.0	35.1	35.1	35.1	35.1	35.1	35.0	34.9	35.0	0.3
8°30'	35.0	34.9	34.9	34.9	35.0	35.1	35.1	35.1	35.0	35.1	35.0	34.9	35.0	0.2
9°30'	35.0	35.0	35.0	35.1	35.1	35.1	35.1	35.1	35.1	35.2	35.1	34.9	35.1	0.3
10°30'	35.1	35.1	35.1	35.1	35.2	35.1	35.1	35.2	35.1	35.2	35.1	35.1	35.1	0.1
11°30'	35.1	35.1	35.0	35.0	35.2	35.2	35.1	35.1	35.0	35.1	35.1	35.0	35.1	0.2
12°30'	35.1	35.0	34.9	35.0	35.1	35.1	35.2	35.1	35.0	35.0	35.1	35.0	35.0	0.3
13°30'	35.0	35.1	34.9	35.0	35.0	35.1	35.1	35.1	35.0	35.1	35.0	34.9	35.0	0.2
14°30'	35.1	35.0	35.1	35.0	35.0	35.0	35.1	35.1	35.0	35.0	35.0	34.9	35.0	0.2
15°30'	35.0	35.0	35.1	35.0	35.0	35.0	35.1	35.1	35.0	35.0	35.0	34.8	35.0	0.3
16°30'	35.0	34.9	35.0	35.1	35.0	35.1	35.0	35.0	35.0	35.0	34.9	35.0	35.0	0.2
17°30'	35.0	35.0	35.1	35.2	35.2	35.1	35.1	35.1	35.0	35.0	35.0	35.0	35.1	0.2
18°30'	35.0	35.1	35.1	35.2	35.1	35.1	35.0	35.1	35.1	35.0	34.9	35.0	35.1	0.3
$\bar{X}$	34.8	34.8	34.8	34.9	35.0	35.1	35.1	35.0	35.0	35.0	34.9	34.9	34.9	0.3
	Summer			Autumn			Winter			Spring				

AM = Annual Mean; AA = Annual Amplitude;

to the coastal band (shaded area) of Fig. 1. Four areas were selected in this band (I, II, III and IV) for establishing the vertical mean distribution of temperature for summer (February-March),autumn (May-June), winter (August-September) and spring (November-December) seasons of the southern hemisphere. They are given in Table 3 at standard levels from 0 to 1000m depth. The monthly-mean changes above 400m depth for areas I and III are presented in Fig. 3.

Some published figures were selected from the Step-I Expedition (Figs. 8 and 9) and El Nino Watch Expedition (Fig. 4), to show macroscale features that influence the coastal regime. To show details in temporal changes in the coastal band, data and figures of ESACAN (Part "a" of Fig. 2) and JOINT-II observations (Figs. 2, 5, 7, 10, 11, 12, 13) were used. The former was a co-operative venture between Peru and the Federal Republic of Germany, and the latter a co-operative and interdisciplinary project with the USA in the CUEA Programme of the IDOE (International Decade of Oceanographic Exploration) and the IBP (International Biological Programme). The ESACAN observations were made at about 5°S, and the JOINT-II mainly at about 15°S, as can be seen in Fig. 2 (a,b). These cover approximately the areas I, II, III and IV of this present study, and include the current observations at 10°S continued subsequently until 1983 as part of the EBUC (Eastern Boundary Undercurrent) project (Smith, personal communication).

Many papers were published with ESACAN (1977) and JOINT-II (1976-77) data. Certain selected features described in them are included in Fig. 2 (c,d) from Huyer et al (1978), Fig. 5 (a,b,c) from Huyer and Gilbert (1979), Fig. 7 from Brink et al (1979). Fig. 10 from Brockmann et al (1980), Fig. 11 from Smith (1978), Fig. 12 from Brink et al (1987b), Fig. 13 from Brink et al (1978a). The preparation of Fig. 14 was facilitated by R. Smith.

Also presented are features from the El Nino Watch Expedition (Fig. 4 from GEOSECS Operations Group, SIO, 1975), from the period 1971-73 (Fig. 6 from Zuta et al, 1976) and from the Step-1 Expedition (Fig. 8 from Wooster and Gilmartin, 1961; Fig. 9 from Wyrtki, 1963).

Temperature and Salinity at the Sea Surface

The greatest seasonal and interannual changes take place at the sea surface, particularly in the area of the Peru Current System where a strongly developed tongue of warm water appears from December of one year to March of the next year, east of 90°W, with temperatures of 23 to 27°C in March. An opposite feature occurs in September when a tongue of cold water with temperatures of 17 to 23°C extends westward up to 140°W between 0 and 3°S. This is shown in the monthly maps of Wyrtki (1964) and Reynolds (1982). The 25°C and 23°C isotherm displacements are good indicators of these fluctuations with an average annual variation of up to 7°C, far from the coast, along the axis of the warm tongue (about 270 nm from the coast at 6°S and about 120 nm at 20°S).

The data in Tables 1 and 2 are derived from the coastal band of about 120 nm wide (shaded area of Fig. 1), which is under the influence of the coastal upwelling in normal conditions, and where the highest anomalies during El Nino events take place. In "normal or mean conditions", the highest tem-

Figure 1.

Location of the selected coastal band (shaded) and areas I, II, III and IV (double shaded), as well as stations of Step I Expedition (dots) and El Nino Watch Expedition (circles).

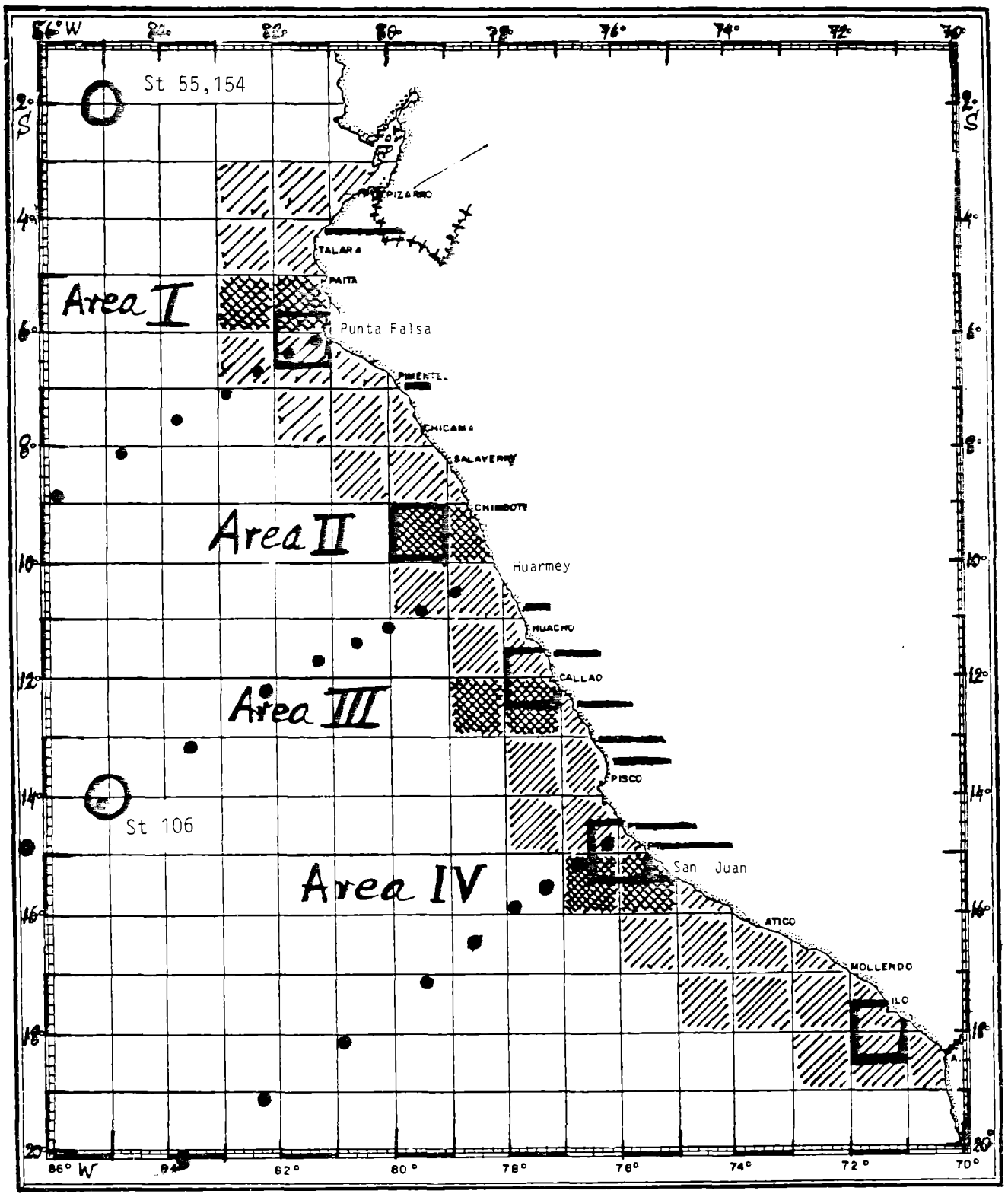

Figure 2.

Location of the areas covered during the cooperative studies of 1976-77 (a,b): ESACAN (MAM-77), ICANE (ND-77) and JOINT-II (March 1976-March 1977), and composite T-S diagrams for Paita (c) and for C-line of Cabo Nazca (d).

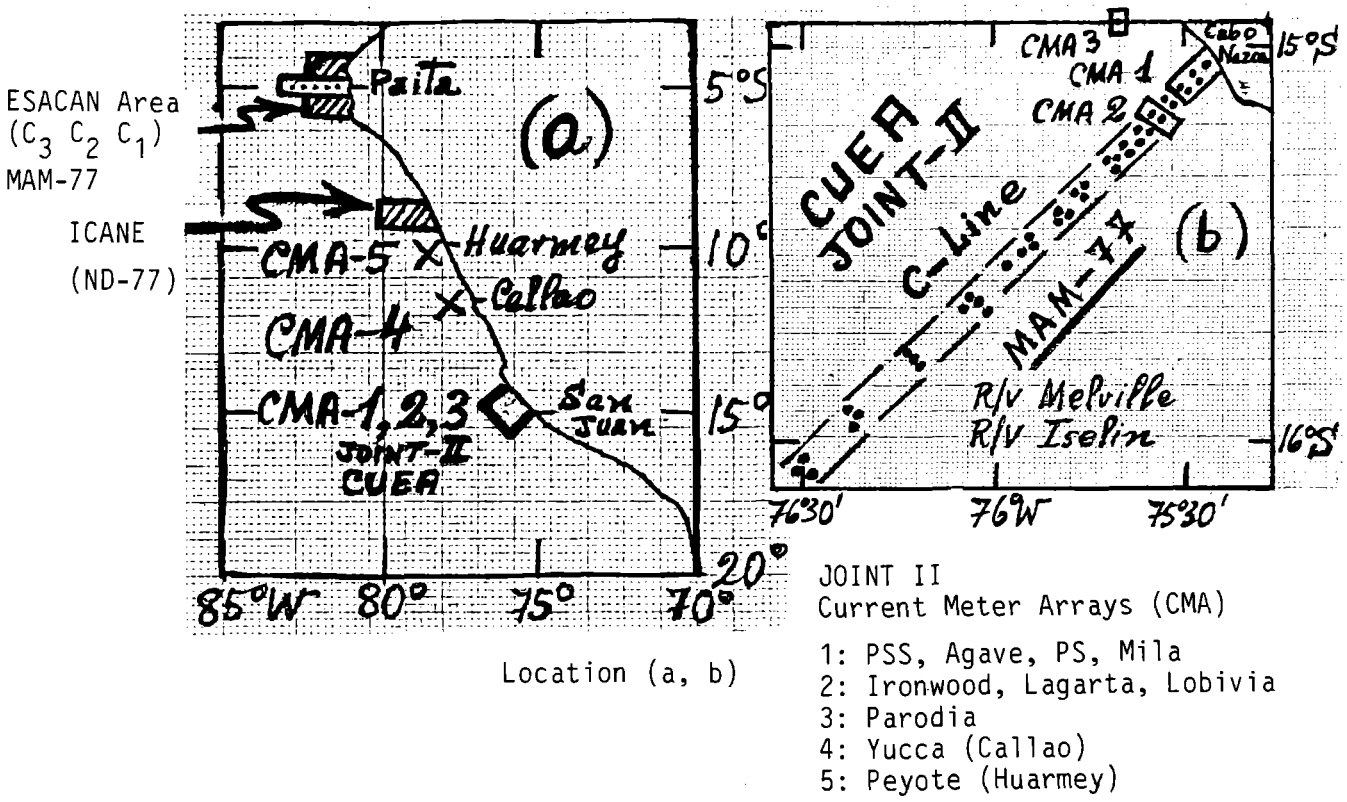

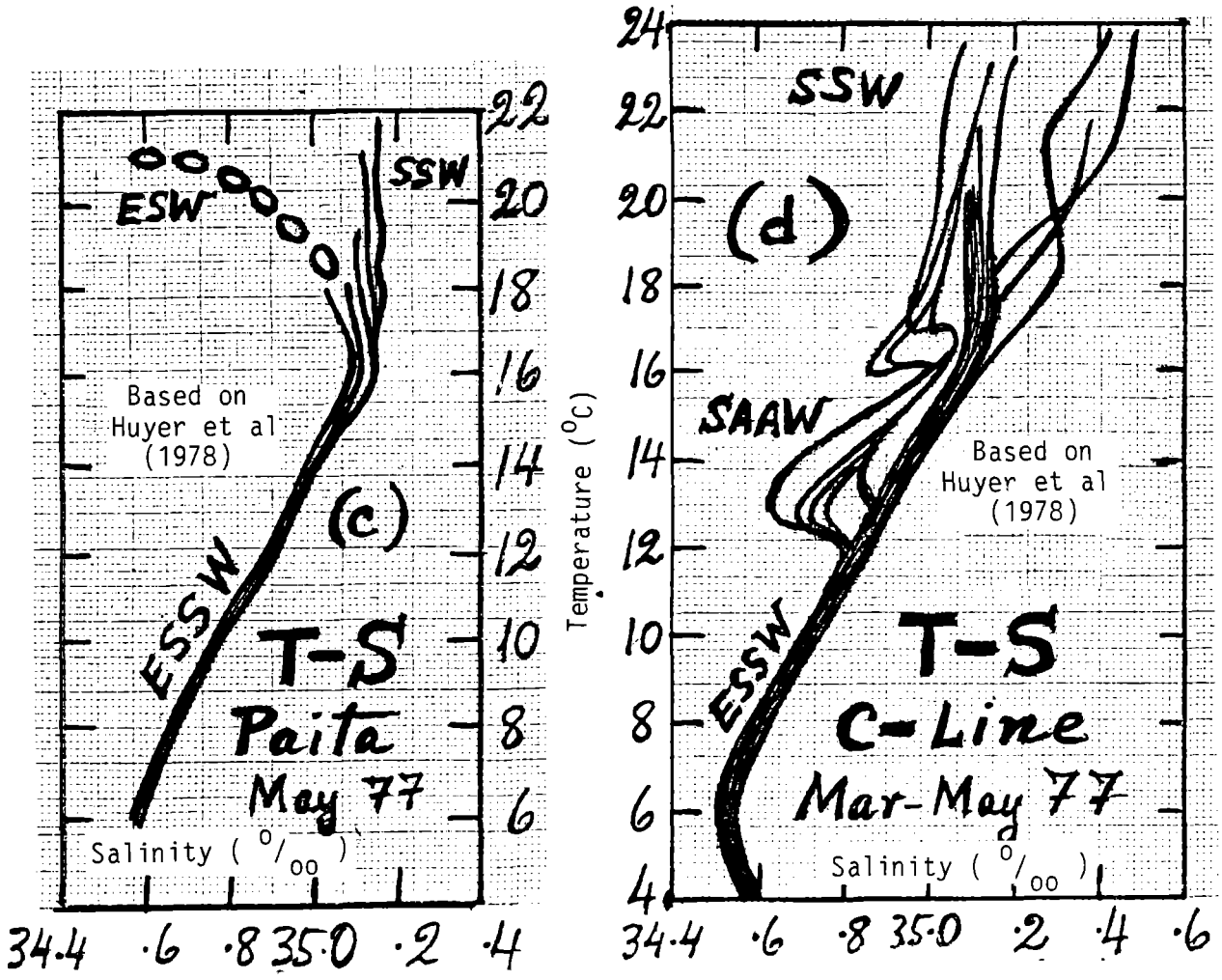

peratures are present in February-March, with values of 20 to 25°C; and the lowest temperatures occur around a representative value of 19.1°C for the whole coastal band. The cold waters, with temperatures below 17°C, are dominant south of 10°S. The surface salinity (Table 2) shows the predominance of low salinity waters north of 5°S, which used to extend southward to 8°S in summer (S.H.). The high salinity waters, with values of 35.0 to 35.2°/oo, are dominant south of 9°S, and in winter and part of spring could extend northward up to 4°S. South of 14°S, the salinities below 34.9°/oo are related mostly with sub-antarctic waters that upwell in the southern part, and eventually with discharge of the rivers in summer (S.H.) time.

The annual salinity variations are high north of 6°S, due to the displacement southward of equatorial and tropical surface waters during spring and summer, and the displacement northward of sub-tropical surface waters during late autumn and winter months. South of 6°S, the annual variation is small, of the order of 0.1 to 0.3°/oo, and the representative value for the whole coastal band is 34.9°/oo.

Vertical Distribution of Temperature and Salinity

Table 3 gives the mean seasonal values of temperature for the column above 1000m depth at areas I, II, III and IV of the coastal band shaded in Fig. 1. The most representative values are those of areas I, III and IV, particularly I and III. The autumn and winter values of area II are affected by the abnormal years of 1972 and 1976. In all of them, very small changes occur normally below 200m depth, and particularly below 400m depth, where the vertical range of temperature is from 4 to 10°C. The significant seasonal changes occur above 100m, where the thermocline and the mixed layer are developed; the former is stronger in summer and in the northern part, and the latter much thicker in winter. The 17°C isotherm is a good indicator of the lower side of the thermocline. Fig. 3 shows the monthly changes above 400m depth, particularly the vertical gradient changes during the year.

Zuta et al (1978) gave the mean seasonal changes of temperature, salinity, sigma-T and dissolved oxygen at two places, approximately close to areas I and IV and for the column above 250m depth. The oxycline is associated with the pycnocline and the thermocline, while the salinity shows appreciable changes above 50m depth in the summer time.

Typical features of the thermal structure are given in Figs. 4 and 5. Besides the mixed layer and the thermocline, two thermal layers are evident, one related to the southern extension of the Cromwell current between 50 and 350m depth with temperatures of 11° to 15°C, and the other between 80 and 125m depth with temperatures of 16° to 19°C, corresponding to the sub-tropical region. These thermal layers give rise to a shallow and a deep thermocline, yielding a chairlike profile in an XBT-trace. Fig. 4 also shows little change of salinity below 50m depth in waters of the equatorial region (St. 55 and 154), and sharp changes between 125-175m depth in open waters of the subtropical region (St. 24 and 126), associated with the sub-surface thermocline and the sub-antarctic water. Evidently there are places like San Juan (Fig. 5), where one finds case "a" in August 1976, case "b" in March 1977 and case "c" in May 1977, with clear changes in the vertical pattern of temperature and salinity. The layer with temperatures of 8-11°C has fluctuations possibly associated with the propagation southward of coastally trapped waves, as was stated by Huyer (1980), during El Nino events. The layer above 300m depth is subject to great changes during El Nino events. This is shown in Fig. 6 during the event of 1972-1973 by a strong deepening of the isotherms at 6°S, 9°S, 15°S and 18°S, particularly north of 9°S (Zuta et al, 1976), and a shallowing of the layer with 8-11°C isotherms near the coast at about 6°S in February 1983 with oscillations at 18°S in November 1982 (Zuta et al, 1984).

It seems that both currents and water masses are affected, at least down to 600m depth during El Nino events. The composite T-S diagram of Fig. 2 shows the dominant features along the Peru coast. At Paita, one finds the equatorial subsurface water, (ESSW) with temperatures of 6-16°C and salinities of 34.6-35.1°/oo. At San Juan the ESSW is still

Table 3.

Seasonal changes of temperature at standard levels down to 1000m depth.
We have taken February and March for Summer (S), May and June for Autumn (A),
August and September for Winter (W), and November and December for Spring (S) of the Southern Hemisphere.

	AREA I : PAITA (5-6°S, 81-83°W)				AREA II: CHIMBOTE (9-10°S, 78-80°W)				AREA III: CALLAO (12-13°S,77-79°W)				AREA IV : SAN JUAN (15-16°S,75-77°W)				
Z (m)	S FM	A MJ	W AS	S ND	S FM	A MJ	W AS	S ND	S FM	A MJ	W AS	S ND	S FM	A MJ	W AS	S ND	Z (m)
0	24.7	18.5	17.8	19.2	22.5	17.5	19.6	17.5	23.0	18.4	16.2	21.1	20.7	18.8	16.8	18.5	0
10	23.8	18.3	17.6	18.5	21.9	17.2	19.6	17.3	21.9	17.6	16.2	21.0	19.9	18.5	16.8	18.6	10
20	22.5	18.0	17.3	17.2	20.6	16.8	19.4	16.3	19.5	17.4	15.9	20.8	18.4	18.0	16.7	18.6	20
30	21.3	17.6	16.9	16.4	19.4	16.3	19.4	15.7	18.2	15.5	15.6	20.2	16.8	17.2	16.5	17.8	30
50	19.3	15.9	16.2	15.6	17.5	15.3	18.3	15.0	16.0	14.5	14.9	18.5	15.3	16.1	15.8	17.0	50
75	17.6	14.9	15.6	14.9	16.1	14.5	16.2	14.4	14.7	13.8	14.2	16.3	14.4	15.0	14.7	16.5	75
100	16.3	14.5	15.2	14.4	15.3	14.4	15.2	13.7	13.9	13.5	13.7	14.8	13.7	14.2	13.9	16.2	100
125	14.3	14.2	14.8	13.5	13.9	14.2	14.6	13.3	13.5	13.2	13.4	14.0	13.2	13.5	13.4	14.8	125
150	13.9	13.9	14.3	13.5	13.6	13.8	14.0	13.0	13.1	12.9	12.8	13.1	12.8	13.0	13.0	13.4	150
200	13.2	13.3	13.6	13.0	13.0	13.5	12.9	13.0	12.4	12.4	12.2	12.3	12.2	12.3	12.4	12.5	200
250	12.6	12.8	12.9	12.3	12.6	12.9	12.4	12.4	11.9	11.8	11.5	11.8	11.6	11.8	11.9	12.1	250
300	11.5	12.1	11.9	11.6	11.8	12.1		12.0	11.1	11.1	10.8	11.2	11.2	11.2	11.3	11.7	300
400	9.4	9.5	9.9	9.3	9.8	9.8		10.4	9.2	9.8	9.3	9.7	9.4	9.8	9.8	10.6	400
500	8.1	8.2	8.2	8.3	8.2	8.6		8.9	7.9	8.6	7.8	8.3	7.9	8.1	8.6	9.3	500
600	7.1	7.6	7.5	7.3	7.2	7.4		7.6	7.0	7.8	6.8	7.3	6.9	7.0	7.3	8.0	600
800	5.6	6.2	5.8	5.7	5.6	5.8		6.1	5.5		5.4	6.0	5.3	5.3	5.5	5.7	800
1000	4.7	5.0	4.5	4.6		4.6		4.9	4.5		4.3	4.6	4.4	4.4	4.9	4.9	1000

Figure 3.

Mean seasonal changes of thermal structure in the upper part above 400m depth at Area I (Paita) and Area III (Callao).

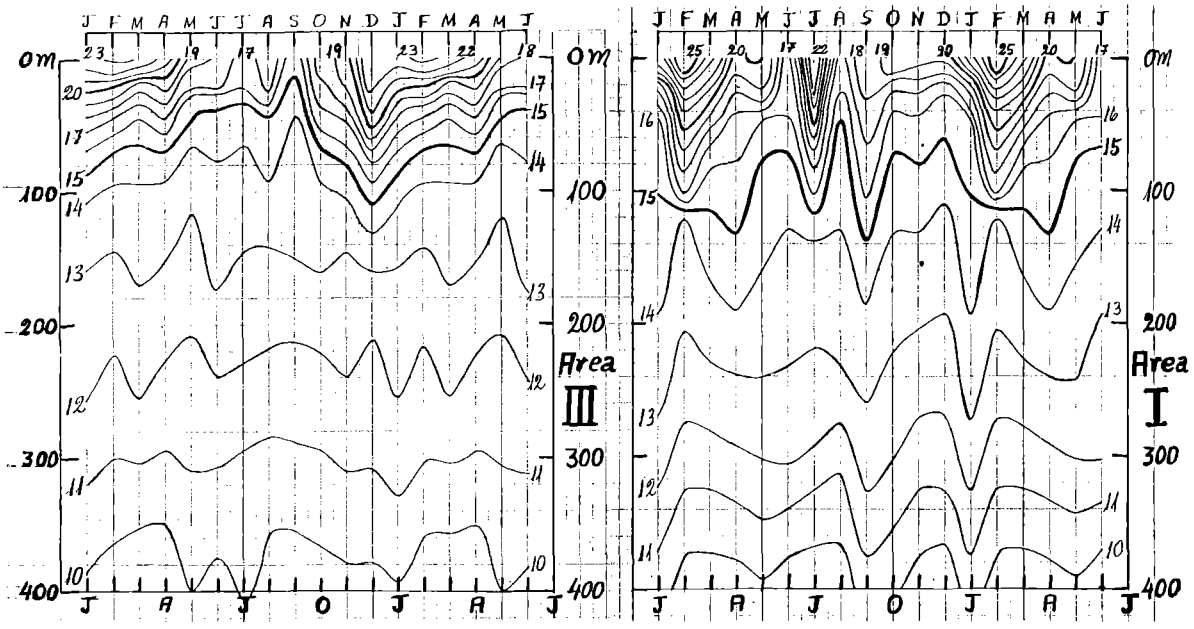

dominant (straight line), but here the Sub-Antarctic Water (SAAW) appears with its characteristic minimum salinity.

The vertical changes of the isotherms are not well understood. It seems that high-frequency phenomena play an important role in the vertical fluctuations, as indicated in March, April and May 1977 off San Juan, by the fluctuations of 13°C and 15°C isotherms presented in Fig. 7 (Brink et al, 1979).

Predominant Flows

We still have a poor knowledge of the surface and sub-surface flows and their changes in space and time, particularly far from the continental margin. On the basis of Step-I Expedition data (October-November 1960, Spring), Wooster and Gilmartin (1961) and Wyrtki (1963) discussed the main flows into the region of the Peru Current system. Figures 8 and 9 show the main surface and sub-surface flows down to 800m depth, evidently for the spring season of a normal year as in 1960 (Zuta et al, 1983).

Using in part the names given by Gunther (1936), Wyrtki (1963) distinguishes the Peru Oceanic Current (POC) west of 82° W and which reaches to about 700m depth, and the Peru Coastal Current (PCC) east of 78°W. In the sub-surface flows he distinguishes the Peru Coastal Undercurrent (PCUC) (or Peru-Chile Undercurrent according to Wooster and Gilmartin (1961)), and the Peru Countercurrent (PCC) located between the PCC and the POC. Between 5°S and 8°S can be found the extension of the South Equatorial Countercurrent (SECC) discussed by Reid (1959), Wooster (1961) and Tsuchiya (1975). The PCUC, underlying the PCC at a depth of several hundred meters, is associated with a divergence of the isopycnals (isotherms) shoreward, a characteristic of the coastal upwelling (Wooster and Reid, 1963). Similar divergence is presented along the equator, associated with the Equatorial Undercurrent or Cromwell Current (Knauss, 1960).

The similarity in the distribution of mass and circulation in the equatorial and eastern boundary regions has been noted by Yoshida and collaborators (Yoshida, 1955; Yoshida and Tsuchiya, 1957; Yoshida, 1958, 1959). Wooster and Gilmartin (1961) were the first to measure the coastal undercurrent and to observe the physical and chemical features associated with it, such as a tongue of relatively high salinity and low oxygen content off Peru, and phosphate and silicate maxima off Chile. The oxygen minimum is evident south of 6°S, but north of this latitude there is a relative oxygen maximum in the upper part of the mixed layer (Cochrane and Zuta, 1968). The density follows the temperature pattern, and the isotherms and isopycnals have a similar distribution with the values in the reverse sense.

The PCUC is a poleward sub-surface flow. Its strength varies from location to location and is stronger over the continental shelf (Brockman et al, 1980). It has fluctuations in different scales without correlation to the local wind (Figs. 10, 11 and 12), in contrast to the coastal upwelling of Oregon and North West Africa (Smith, 1978); its fluctuations are in coherence with the wave propagation at 200 km/day, as in El Nino 1976-1977 and in El Nino 1982-1983 (Smith 1978; Brockmann et al, 1980; Brink et al, 1978).

The observations at about 5°S and 10°S during 1982-1983 (Smith, personal communication) are presented in Fig. 14; they show great changes in the flows northward and southward, without a clear correlation down to at least 450m depth. We need to understand better the non-correlation with temperature at least at the early appearance of El Nino 1982-1983.

Figure 4.

Vertical profiles of temperature (T) and salinity (S) in the upper part above 500m depth at selected stations of El Nino Watch Expedition, in summer (a,b) and autumn (a1, b1) of the Southern Hemisphere.

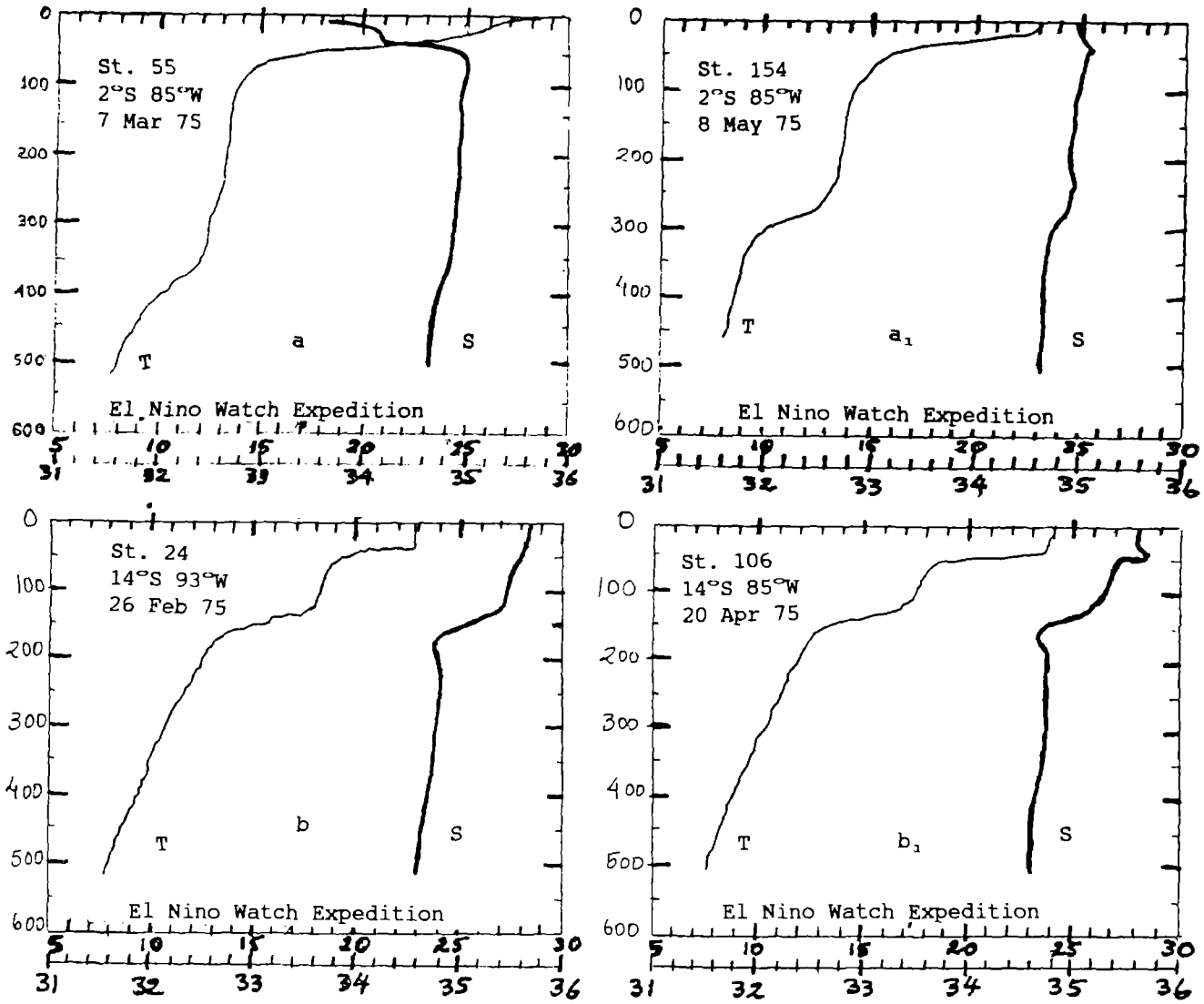

Taken from GEOSECS Operations Group, SIO, 1975

Figure 5.

Sections of temperature (a_1, b_1, c_1) and salinity (a_2, b_2, c_2) off Cabo Nazca (C-line) or San Juan, corresponding to 12-13 August 1976, (a_1, a_2), 18-19 March 1977 (b_1, b_2) and 5-6 May 1977 (c_1, c_2). (From Huyer and Gilbert, 1979).

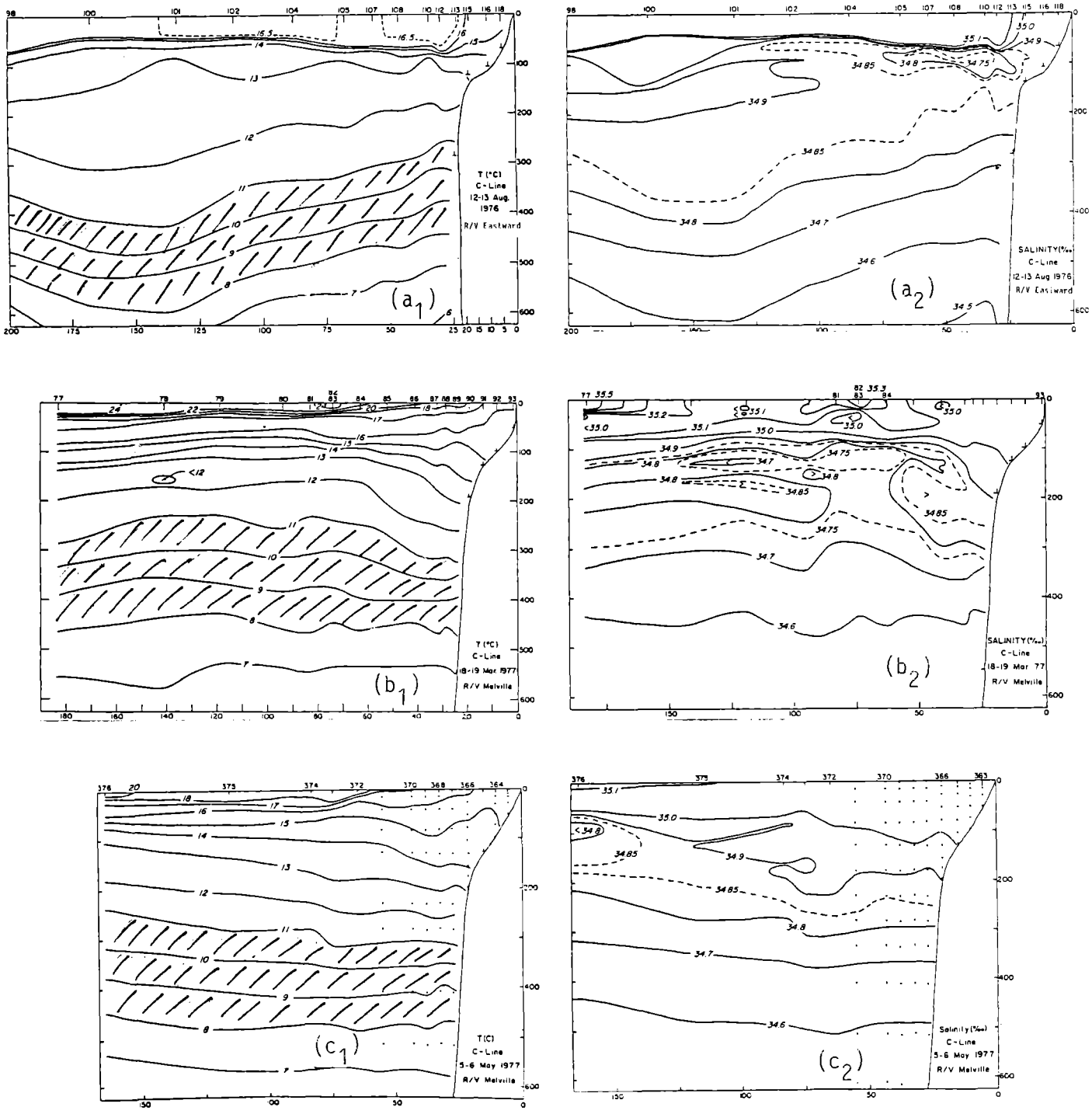

Figure 6.

Seasonal changes of temperature (a, b, c, d)
and salinity (a_1, b_1, c_1, d_1) at Punta Falsa (a, a_1) Chimbote (b, b_1),
San Juan (c, c_1) and Ilo (d, d_1), from July 1971 to July 1973).

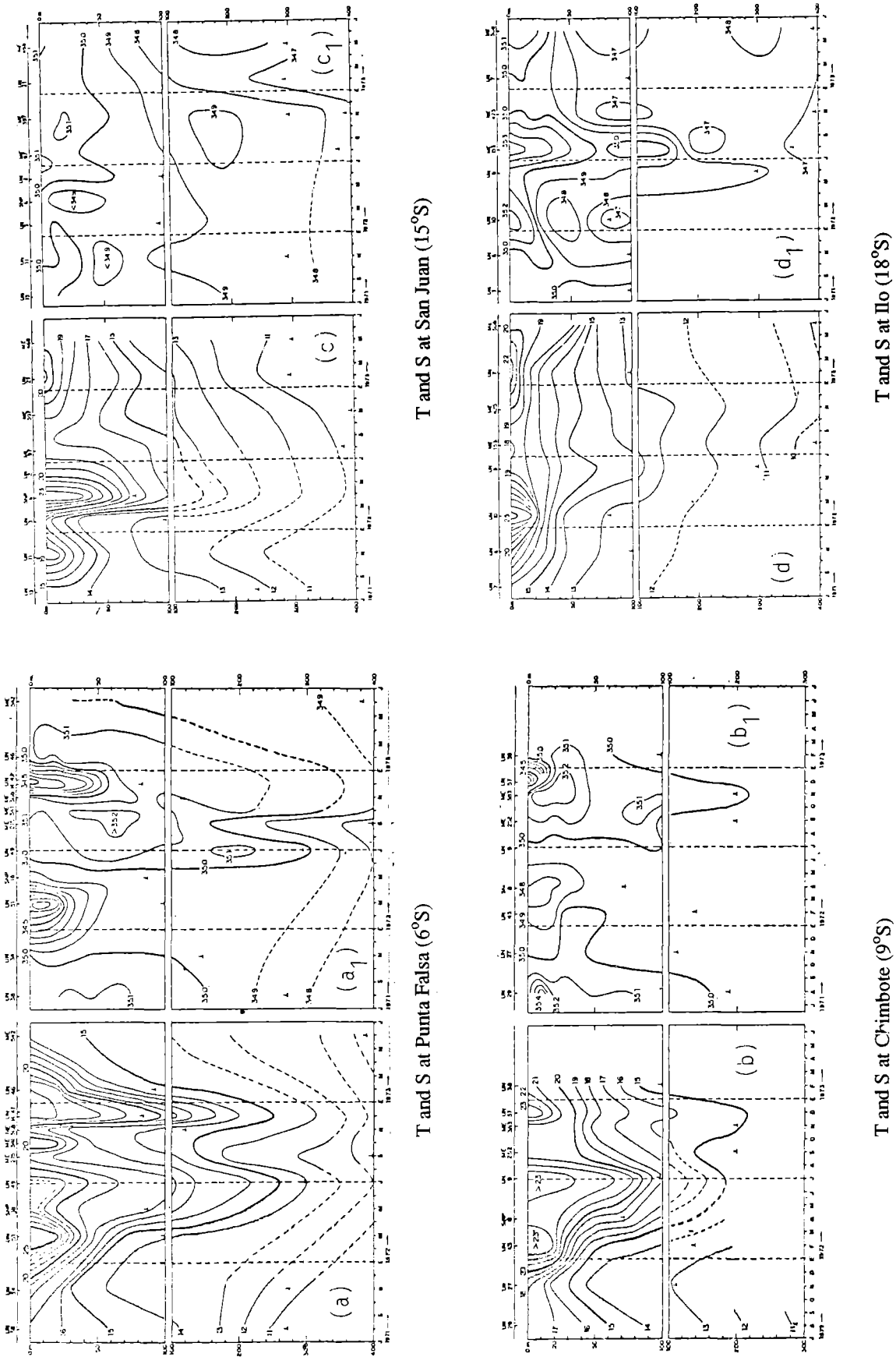

Figure 7.

Changes at C-line (a) of the 15°C and 13°C isotherm in March (b), April (c) and May (d) of 1977, during the intensive observations of JOINT-II (from Brink et al, 1979).

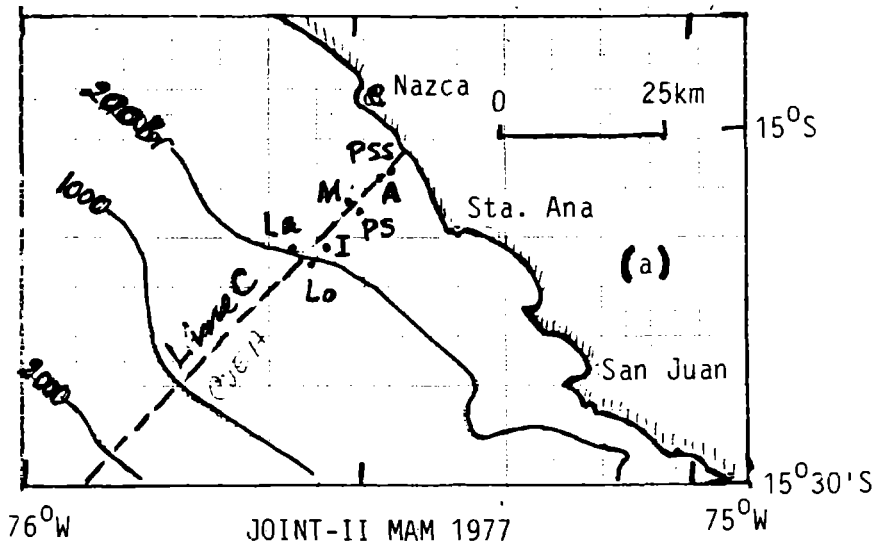

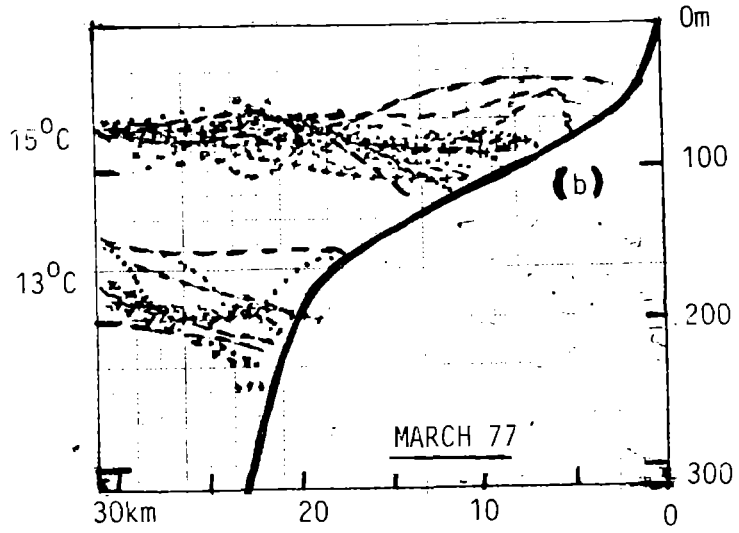

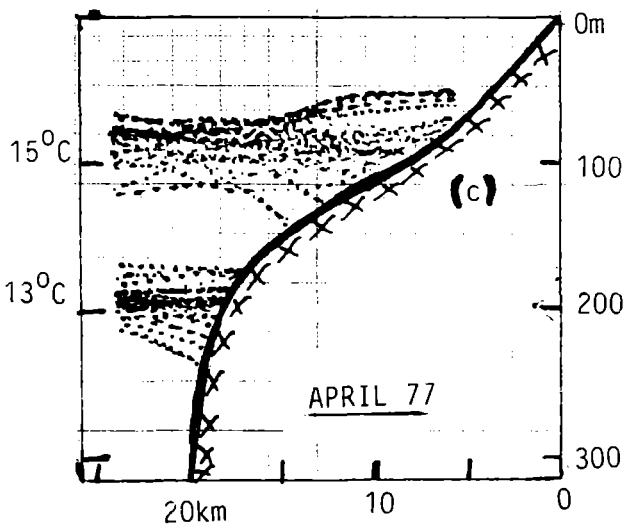

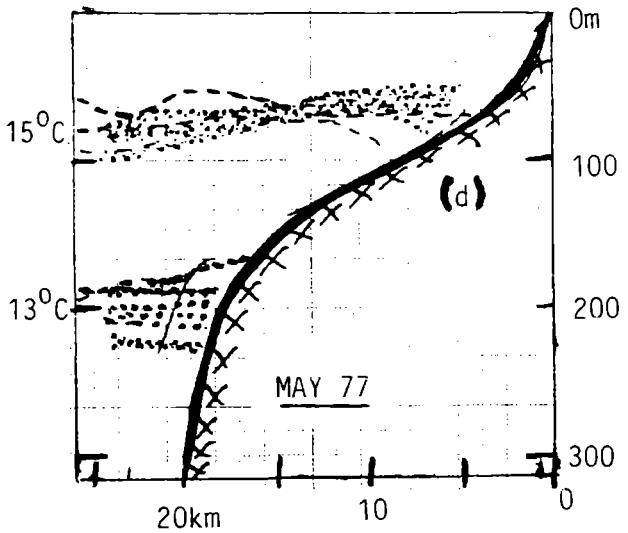

Figure 8.

Geostrophic speed off Punta Falsa (a), Huarmey (b) and San Juan (c) on 8-13 October, 14-18 October and 28 October-2 November 1960, corresponding to data of Step-I Expedition.

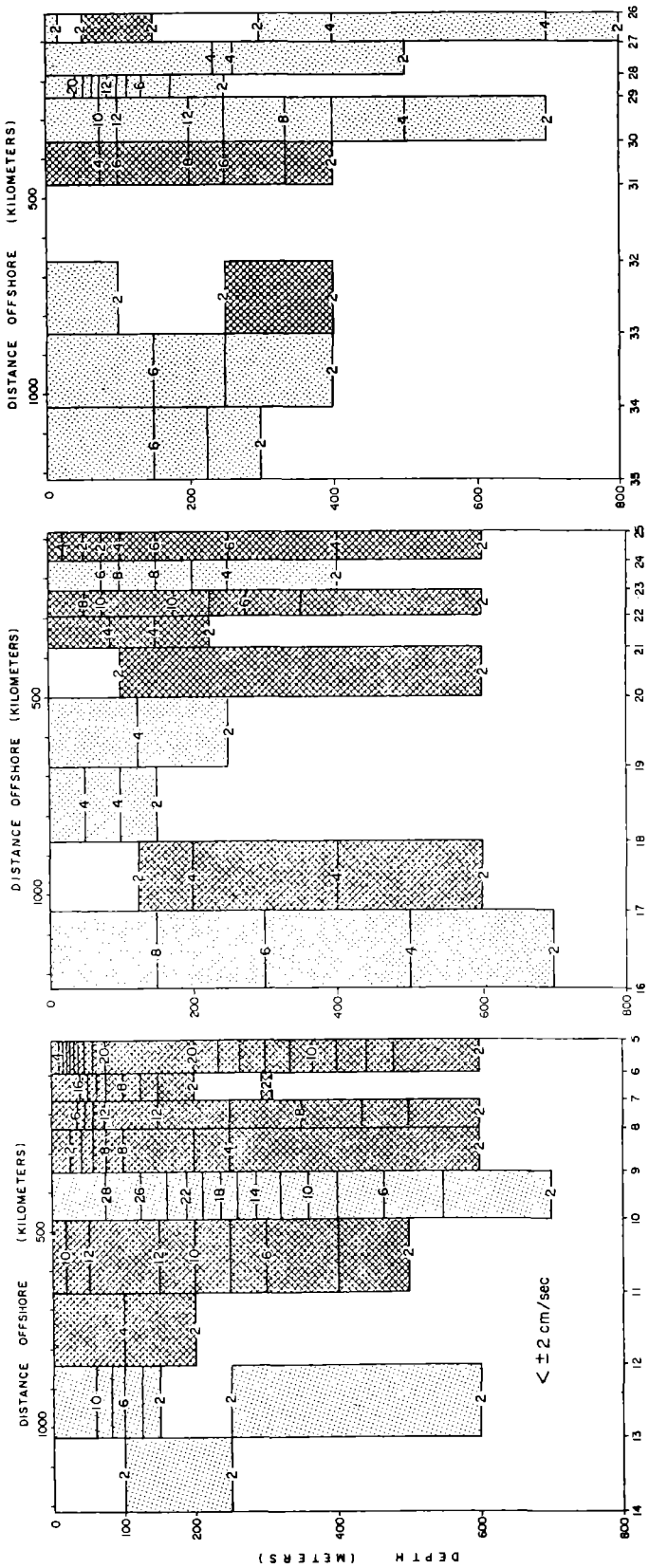

Geostrophic Speed (cm/sec) Darker shading represents southward motion
(from W. S. Wooster and M. Gilmartin, 1961)

Figure 9.

Geopotential topography of the sea surface (a) and 100-decibar surface, (b) in dynamic centimeters, relative to 1000-decibar surface, based on data of Step-1 Expedition (from Wyrtki, 1963).

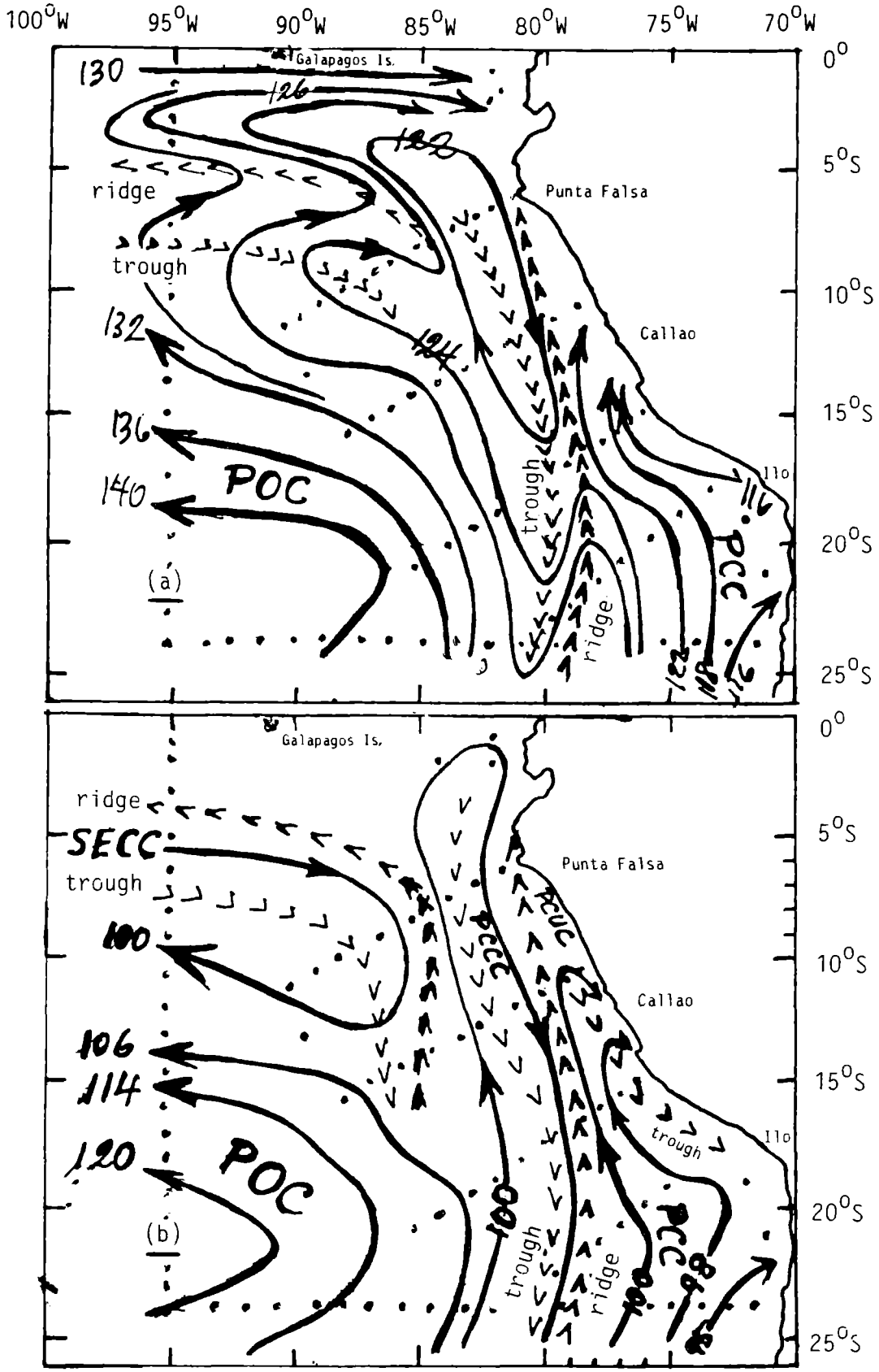

Figure 10.

Mean surface wind (a) and current vectors at several locations along the Peru coast, at 40m (b), 90m (c) and 200m (d) depth, during April-May 1977, based on data of ESACAN and JOINT-II (from Brockman et al, 1980)

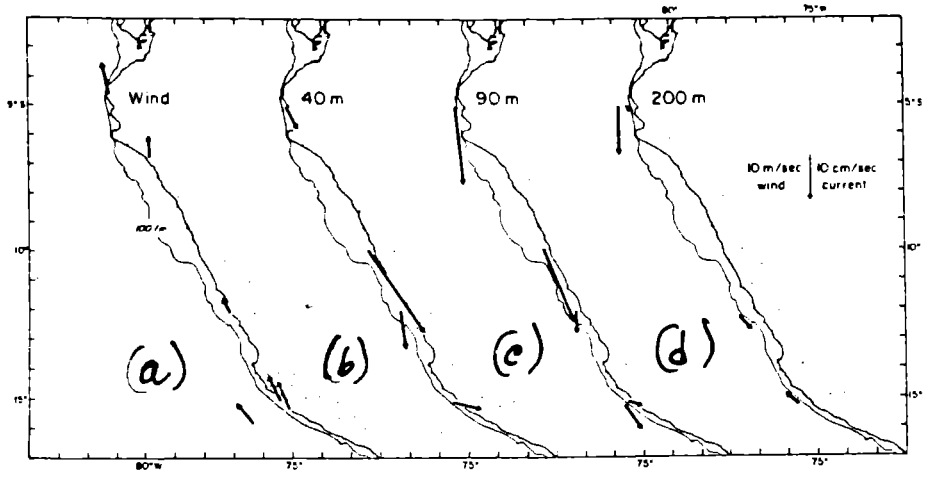

Figure 11.

Time series of surface wind vectors (a),
sea level variations (b), and current vectors at 80-84m depth (c),
at San Juan and Callao in May-August 1976, based on data of JOINT-II (from R.L. Smith, 1978).

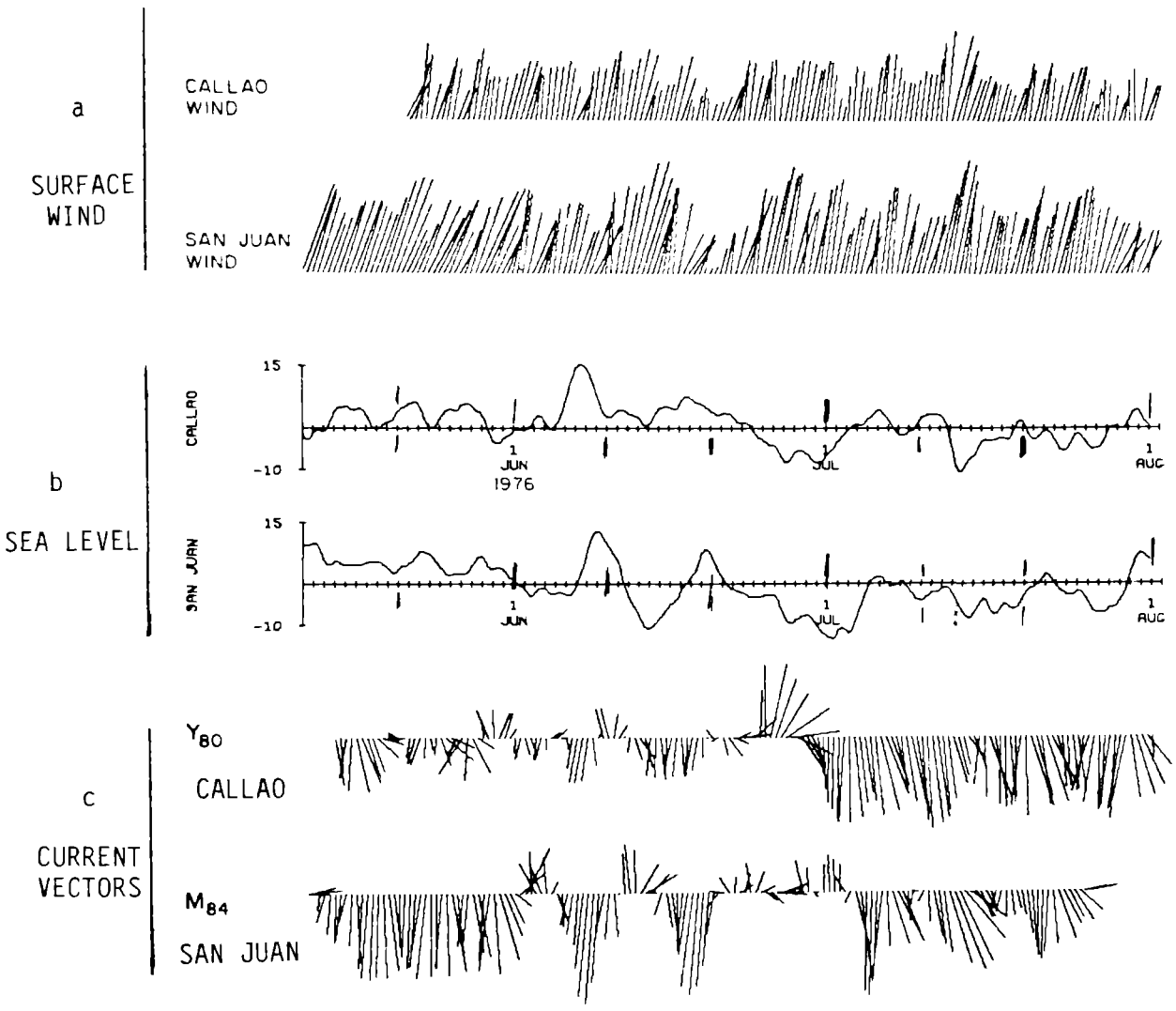

Figure 12.

Time series of surface wind velocities, sea level and current meter velocities during Phase I (28 March-5 June 1976) at Mila-I and Lobivia (a), during Phase II (15 May-26 July 1976) at Mila-II and Lagarta (b), and during Phase-III (29 July-29 September 1976) at Mila-III (c), of JOINT-II 1976.

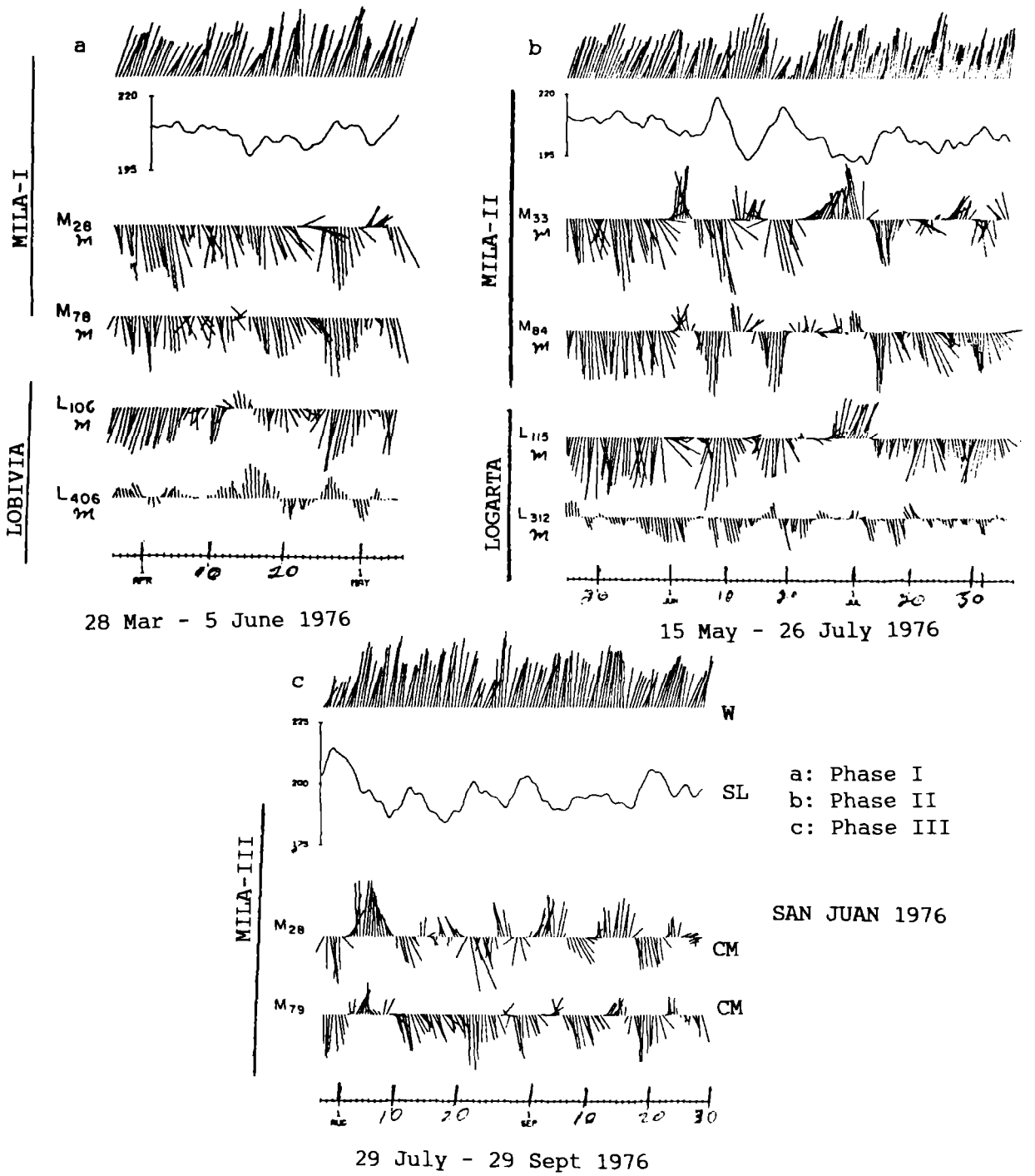

(From K.H. Brink, J.S. Allen and R.L. Smith, 1978)

Figure 13.

Vertical profiles of U and V components for S/Mila
current meter data from 8 March to 13 April 1977 at two days interval.
The upper scale is for U, and the lower scale for V, both in cm/sec.

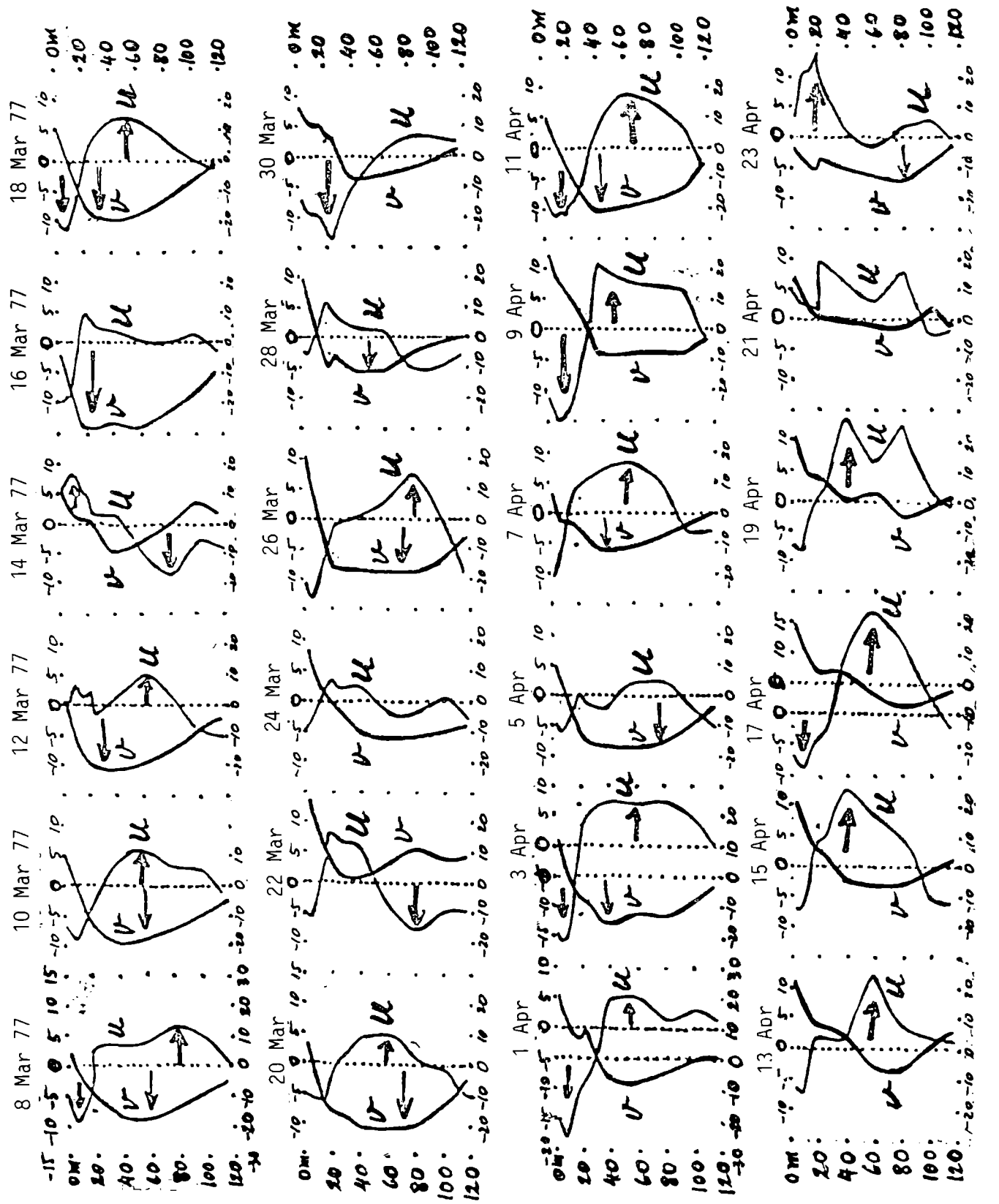

Figure 14.

Time series of temperature of 50 and 100m depth (a,b) at the continental shelf for Paita (5°S), and time series of temperature and current vectors (cm/sec) for Huarmey (10°S), at the continental shelf at 50 and 100m depths (a1, a2; b1, b2) and the continental slope at 160, 290 and 430M depths (a,b,c; a_1,b_1,c_1), for March-November 1982.

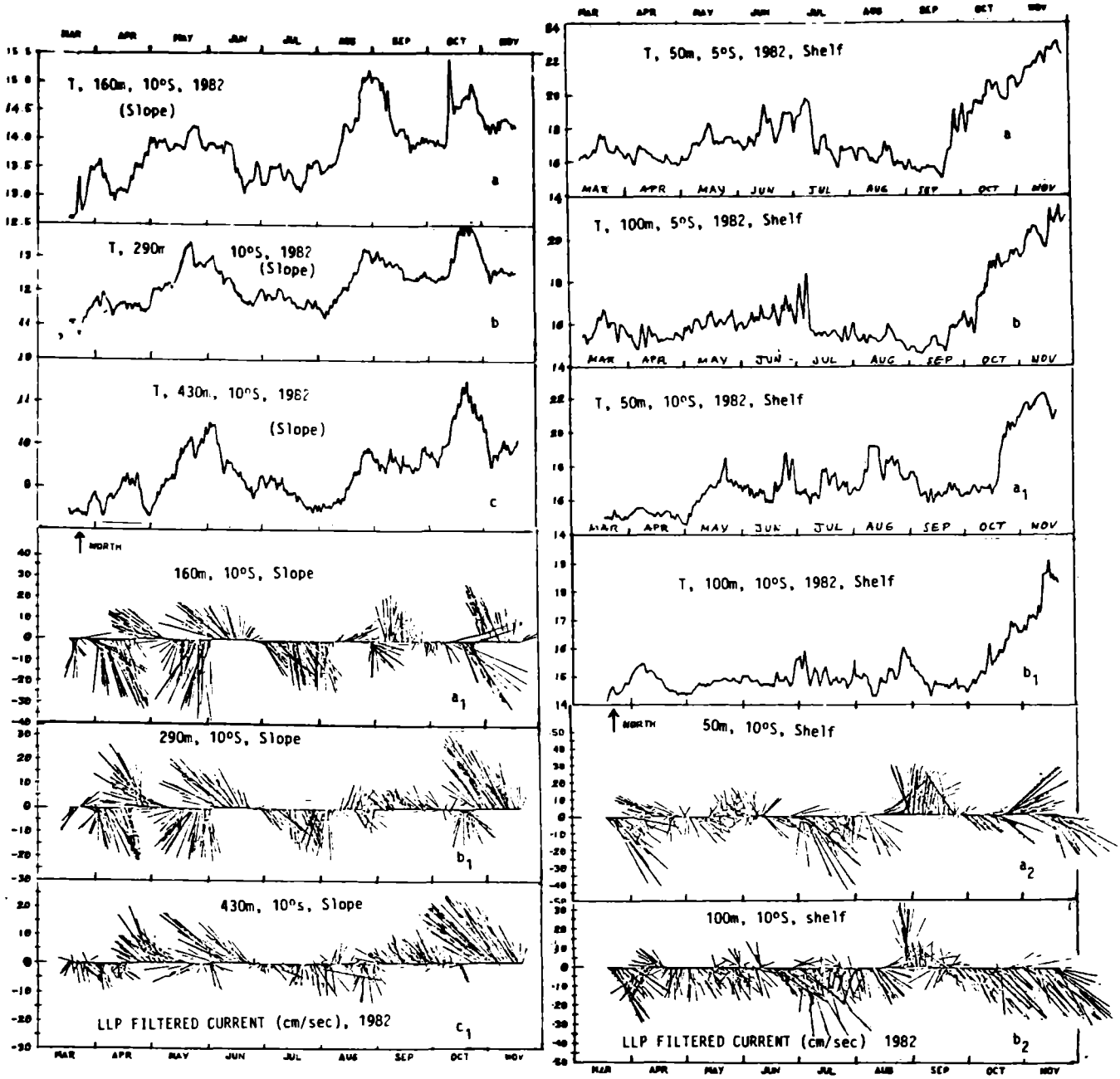

Water Masses

The composite T-S diagram of Fig. 2 (c,d) illustrates the main water masses associated with the circulation off the Peru coast. The main ones are the Equatorial Surface Waters (ESW) of low salinity and high temperatures; the Subtropical Surface Water (SSW), of salinities much higher than 35.0°/oo and temperatures higher than 17°C; the Equatorial Subsurface Water (ESSW), with salinity a little higher than 35.0°/oo and temperatures from 6 to 17° C. The Sub-Antarctic Water (SAAW), with relative low salinity, is situated in the lower part of the discontinuity layer and spreads northward mainly very far from the coast. Only south of 12°S is it found near the coast and below the Subtropical Surface Water (SSW).

The oxygen-minimum layer (OML), with oxygen content less than 0.5 ml/L, extends between 50 and 800m depth, rising much closer to the surface near the coast, and becoming much more notable between 12°S and 18°S, associated with the ESSW, as described by Zuta and Guillen (1970).

Coastal Upwelling

The occurrence of the coastal upwelling along the Peru coast under the persistent southeast trade winds and the resulting high biological productivity in the region are well known. The JOINT-II Expedition (March 1976-May 1977) made intensive physical and biological experiments centered on the continental shelf near Cabo Nazca or San Juan, about 15°S (Fig. 2a,b), an area of persistent strong upwelling (Zuta and Guillen, 1970; Walsh et al 1971; Zuta et al, 1978). The results of such experiments are given in several papers, from which Figures 2, 5, 7, 10, 12 and 13 are taken. These figures show important features, although the observational field coincided with the 1976-1977 El Nino event discussed among others by Wyrtki (1979). A summary of the main characteristics is given in the findings of the following authors, starting with Brink et al (1978, 1983), who state the following:

1. The dynamics and mass balance are strongly three-dimensional and time-dependent, with the biota affected by phenomena ranging from the diurnal sea-breeze to the irregular quasidecadal El Nino. The poleward flowing undercurrent supplies the upwelled water off Peru.
2. The mean offshore flow pattern definitely reflects local wind-driven features in the system, and the time-variability of onshore flow is coupled to fluctuations in the strength of the local winds.
3. The alongshore velocity shows a direct wind effect only near the surface, and much of the time variability at depth can be explained in terms of low frequency, free, coastally trapped waves
4. The temperature field in the upper 30m or so is largely governed by the wind, with upwelling and mixed layer deepening being important processes; below 50m depth, the temperature field is largely controlled by the trapped waves whose effects on the temperature field extend to several hundred meters.
5. The variability of temperature and alongshore velocity are closely coupled through the geostrophic balance.
6. The considerable time variability and spatial structure of the physical regime requires that caution needs to be taken in interpreting observations.

Huyer (1980) analyzed more than 35 repeated hydrographic sections made off Cabo Nazca in 1976-1977 as well as sea level measured continuously at San Juan, and found among other things that the mean undercurrent is not observed 100km from shore, that the sea-level variations are a manifestation of a poleward-propagating internal Kelvin wave with the interface at a depth of 300-500m, and are associated with changes in the depth of the subthermocline isotherms at such depths.

Smith (1978), using the measurement made in 1976-1977, states that the fluctuations in currents were not well correlated with the local wind, and that analyses of current, water-temperature and sea-level time series suggest that the baroclinic Kelvin waves propagate poleward along the coastal boundary coherently at 200 km/day at an offshore scale of 70 km, consistent with a coastally trapped baroclinic wave (i.e., an internal Kelvin wave) in which topography and stratification are important (Wang and Moores, 1976).

The months of most intense upwelling along the Peru coast are May-June and August-September, as stated by Zuta et al (1978) and as also shown in Figures 3 and 5.

The main source of upwelling waters is the Peru Coastal Undercurrent (PCUC) along most of the Peru coast. South of 12°S, the source is the Sub-Antarctic Water (SAAW) in some months of the year, as in February 1968, September 1967, August 1976, November 1960, etc., according to papers by Zuta and Guillen (1970), Wooster and Gilmartin (1961). This is also shown in Fig. 5(a).

On the other hand, Brink et al (1978) have shown a coincidence of a very strong coastally trapped wave with a strong upwelling event during 10-31 March 1976. There is continuing discussion regarding the real role that the local wind and the southeast tradewinds play in the regime of the coastal upwelling in periods of El Nino and non-El Nino conditions. Some people assert that during an El Nino event, the coastal upwelling is stronger than normal; but the cross vertical sections of temperature from November 1982 to May 1983 do not support this idea (see Zuta et al, 1984; Zuta, 1986), especially north of 14°S.

El Nino and the Southern Oscillation

The Southern Oscillation (SO) in the atmosphere and an El Nino (EN) in the ocean, represent the largest interannual climate signal fluctuations, and their close correlations were recognized by J. Bjerknes in 1960 (Wyrtki, 1986). This fact became more evident during the 1982-1983 ENSO event. In describing the physical aspects of the 1982-1983 event, Cane (1983) states on the one hand that El Nino events are the most spectacular instances of interannual variability in the ocean and have profound consequences for climate and the ocean ecosystem. On the other hand, Rasmusson and Wallace (1983) state that the single most prominent signal in year to year climate variability is the Southern Oscillation, which is associated with fluctuations in atmospheric pressure at sea level in the tropics, monsoon rainfall, and winter-time circulation over North America and other parts of the extra-tropics, and that the theoretical understanding of its relationships with the oceanic El Nino phenomenon has begun

to emerge only during the past few years. The world ocean possesses a large heat capacity, but it is sluggish and therefore plays a considerable role in short-range climatic variations, short-range being a period of one month to several years (Sarkisyan, 1986).

El Nino is then a large anomaly of the ocean associated with the year-to-year fluctuations of the ocean-atmosphere system and its large scale process involves most of the Pacific Ocean as stated by Enfield (1980), with spectacular changes across the entire tropical Pacific. It got its name historically from the local fishermen of northern Peru (Paita), who considered El Nino as a local feature, which we now know is not local, but a large scale phenomenon that has one of the strongest and spectacular impacts off Peru.

El Nino is an oceanic response to the changes in the equatorial wind field described by Sadler and Kilonsky (1983) and Gill and Rasmusson (1983). Its occurrence is characterized by changes in sea level, zonal redistribution of water masses, changes in surface and sub-surface currents, redistribution of heat and large temperature anomalies. At the end of an El Nino, the equatorial Pacific is depleted of warm water, which is lost toward higher latitudes. The duration of a complete El Nino cycle is determined by the time required for the slow accumulation of warm water in the western Pacific (Wyrtki, 1985). The redistribution of heat in the ocean has also been studied and modelled by Gill and Rasmusson (1983) and by Philander et al (1984). According to Lucas et al (1984), the first and second vertical modes of the Kelvin waves play an important role during the onset of El Nino conditions and the long Rossby waves during the early phase of the event. White et al (1985) also show interesting features regarding baroclinic long waves at 10°N, 10°S, and Sarkisyan (1986) points out the importance of extra-tropic features.

El Nino events have been documented as far back as 1726 (Quinn et al, 1978), who describe their occurrence at intervals of 2 to 10 years with categories of very weak, weak, moderate and strong El Nino events. The 1982-1983 El Nino will be held in special regard requiring a new category of very strong or extraordinary event (Zuta et al, 1984).

In the last two decades there were four events, 1972-1973, 1976-1977, 1982-1983 and 1986-1987, with the categories of strong, moderate, extraordinary and weak, respectively, at least with respect to the Peru coast. The more documented are 1972-1973 and 1982-1983, described and theoretized by several scientists (see Mariategui et al, 1985). Table 5 shows deviations from the long term mean for the period 1985-1987.

Fig. 6 shows the changes of temperature and salinity at 6°S, 9°S, 15°S and 18°S during the 1972-1973 El Nino, much stronger and deeper at 6°S and 9°S. For reference, Table 4 lists the monthly changes in the depth of the 15°C isotherm at various places. In Fig 10, taken from Brockmann et al (1980) and corresponding to the beginning of 1977, the subsurface flow southward (SSCU) seems to be stronger, at least above 200m depth. In Figs. 11 and 12 taken from Smith (1978) other important features of the 1976-1977 El Nino are shown.

Acknowledgements

I wish to thank Miss Carmen Grados and Mr Eduardo Llata for processing the data, and Miss Eva Ramirez for typing this manuscript. My special thanks to A.G. Alexiou for his patience and long waiting.

Table 4.

Monthly mean of the depth (m) of 15°C isotherm at five places along the Peruvian coast.
The numbers below indicate numbers of years and total observations in such years.
The locations are given with thick squares in Fig.1.
The subindices a and b for April, indicate El Nino data of 1965.

AREA	Jan	Feb	Mar	Apr	May	Jun	Jul	Aug	Sep	Oct	Nov	Dec
Pta. Falsa	36	81	80	151a	69	99	129	78	54	43	46	84
6°S, 81°30'W	2,11	4,11	1,1	1,4	5,14	2,2	4,9	3,10	6,13	3,5	4,8	6,28
Chimbote	63	69	90	138b	74	74	73	70	55	18	59	58
9°30' S,79°30W	2,4	6,15	1,1	2,3	3,4	3,7	2,3	3,8	4,14	1,1	6,17	4,10
Callao	44	66	66	69	44	64	51	37	89	36	39	50
12°S,77°30' W	3,5	6,20	5,9	3,7	6,12	6,9	4,10	4,10	3,5	4,9	9,17	2,5
San Juan	=	46	35	47	28	49	=	=	68	16	36	22
15°S, 76°W		7,18	2,3	2,5	2,3	3,3			1,1	1,4	5,21	1,3
Ilo	=	38	47	=	27	32	=	25	27	24	31	18
18°S, 71°30'W		5,11	3,7		3,5	4,9		1,1	3,5	3,7	4,10	1,3

Table 5.

Monthly mean of SST and the deviations from the long term mean, period 1985-1987.

MONTH	PTO. PAITA			PTO. CHICAMA			PTO. CHIMBOTE			I. DON MARTIN			PTO. CALLAO		
	1985	1986	1987	1985	1986	1987	1985	1986	1987	1985	1986	1987	1985	1986	1987
Jan	18.9	21.6	21.9	15.8	17.1	17.7	19.5	20.0	21.6	17.4	16.7	18.9	15.0	14.7	17.7
	-1.0	+1.7	+2.0	-1.8	-0.5	+0.1	-1.5	-1.0	+0.6	-0.4	-1.1	+1.1	-1.8	-2.1	+0.9
Feb	21.0	22.3	25.9	15.7	17.5	21.7	18.8	21.2	24.8	17.3	18.3	21.0	15.2	17.0	19.1
	-0.5	+0.8	+4.4	-3.5	-1.7	+2.5	-3.3	-0.9	+2.7	-1.5	+0.6	+2.2	-2.5	-0.7	+1.4
Mar	22.7	20.7	25.5	17.1	17.2	22.5	20.3	20.0	26.1	17.2	17.6	22.3	15.6	15.9	20.7
	+1.1	-0.9	+3.9	-1.7	-1.6	+3.7	-2.0	-2.3	+3.8	-1.8	-1.4	+3.3	-2.7	-2.4	+2.4
Apr	19.0	18.1	22.2	15.7	16.1	20.4	18.5	19.5	23.9	16.2	16.5	20.3	15.0	15.4	19.5
	-0.9	-1.8	+2.3	-2.4	-2.0	+2.3	-2.8	-1.8	+2.6	-1.9	-1.5	+2.3	-2.9	-2.5	+1.6
May	16.0	18.0	20.5	15.7	16.7	19.0	17.6	18.5	20.7	15.8	16.2	18.3	14.9	15.3	17.9
	-2.9	-0.9	+1.6	-2.0	-1.0	+1.3	-2.6	-1.7	+0.5	-1.6	-1.2	+0.9	-2.6	-2.2	+0.4
Jun	17.8	16.9	18.9	15.4	16.6	18.2	17.6	17.8	20.2	15.7	15.7	18.7	14.9	15.5	18.1
	-0.7	-1.3	+0.7	-2.0	-0.8	+0.8	-1.4	-1.2	+1.2	-1.1	-1.1	+1.9	-2.0	-1.4	+1.2
Jul	16.4	17.9	18.3	15.8	16.6	17.6	17.1	17.8	19.5	15.4	14.8	17.6	15.1	15.5	17.3
	-0.8	+0.7	+1.1	-1.1	-0.3	+0.7	-1.3	-0.6	+1.1	-1.0	-1.6	+1.2	-1.3	-0.9	+0.9
Aug	15.7	17.5	17.3	15.7	16.8	16.8	17.1	18.7	18.8	15.1	14.5	16.6	14.7	16.1	16.4
	-0.7	+1.1	+0.9	-0.7	+0.4	+0.4	-0.9	+0.7	+0.8	-0.9	-1.5	+0.6	-1.2	+0.2	+0.5
Sept	15.9	16.1		15.5	15.9		17.5	18.6		14.9	14.5		14.5	15.7	
	-1.0	-0.8		-0.5	-0.1		-0.1	+1.0		-0.5	-0.9		-0.9	+0.3	
Oct	16.1	18.4		15.3	15.2		18.2	18.4		15.6	15.8		14.6	15.1	
	+0.4	+1.6		-0.4	-0.5		-0.2	+0.0		0.0	+0.2		-0.7	-0.2	
Nov	16.7	19.3		15.3	17.1		18.3	20.3		15.8	16.7		14.3	15.8	
	-0.6	+2.3		-0.5	+1.3		-0.9	+1.1		-0.3	+0.6		-1.4	+0.1	
Dec	18.1	20.0		15.5	17.9		19.1	21.5		16.2	18.2		14.7	16.6	
	-0.5	+1.4		-1.0	+1.4		-0.7	+1.7		-0.8	+1.2		-1.7	+0.2	

References

1. Bjerknes J., 1961. El Nino study based on analysis of ocean surface temperature 1935 to 1957. *Inter-Amer. Trop Tuna Comm., Bull.*, 5 (3), pp. 217-307.

2. Brink, K.H., Allen, J.S. and Smith, R.L., 1978. A study of low-frequency fluctuations near the Peru coast. *J. Phys. Oceanogr.*, Vol.8, No.6, pp. 1025-1041.

3. Brink, K.H., Halpern D., Huyer A., and Smith R.L., 1983. The physical environment of the Peruvian upwelling system. *Prog. Oceanogr.*, Vol.12, pp. 285-305.

4. Brockmann, C., Fahrbach, E., Huyer A., and Smith R.L., 1980. The poleward undercurrent along the Peru coast: 5 to 15oS. *Deep-Sea Res.*, Vol. 27A, pp. 847-856.

5. Cane, M.A., 1983. Oceanographic events during El Nino. *Science*, Vol. 222, No.4629, pp. 1189-1195.

6. Climate Analysis Center, NMC/NOAA, 1986. *Climate Diagnostics Bulletin*, Nos. 86/10, 86/12 and 86/13.

7. Climate Analysis Center, NMC/NOAA, 1987. *Climate Diagnostics Bulletin*, Nos. 87/1, 87/2, 87/3, 87/4 and 87/5.

8. Cochrane, J.D., and Zuta S., 1968. Equatorial currents east of the Galapagos Islands during February-March 1967. Unpublished manuscript.

9. Enfield, D.B., 1980. El Nino Pacific eastern boundary response to interannual forcing. Resource Management and Environmental Uncertainty. Edited by M.H. Glantz, John Wiley & Sons, Inc., pp. 213-254.

10. Gunther, E.R., 1936. A report on oceanographical investigations in the Peru Coastal current. *Discovery Rep.*, 13, pp. 107-276.

11. Huyer, A., 1980. The offshore structure and sub-surface expression of sea level variations off Peru, 1976-1977. *J. Phys. Oceanogr.*, Vol. 10, No.11, pp. 1755-1768.

12. Knauss, J.A., 1960. Measurements of the Cromwell Current. *Deep-Sea Res.*, 6 (4): pp. 265-286.

13. Lukas, R., Hayes, S.P., and Wyrtki, K, 1984. Equatorial sea level response during the 1982-1983 El Nino. *J. Geophys. Res.*, Vol.89, no. C6, pp. 10425-10430.

14. Mariategui, J., de Vildoso Ch. y Velez J., 1985. Bibliografia sobre el fenomeno El Nino desde 1981 a 1985. *Bol. Inst. Mar Peru-Callao.*, Vol. Extraordinario, pp. 1-136.

15. Pazan, S.E. and White W.B., 1986. Off-equatorial influence upon Pacific equatorial dynamic height variability during the 1982-1983 El Nino/Southern Oscillation event. *J. Geophys. Res.* Vol. 91, No. C7, pp. 8437-8449.

16. Philander, S.G.H., Yamagata, T., and Pacanowski, R.C., 1984. Unstable air-sea interactions in the tropics. *J. Atmos. Sci.*, 41, pp. 604-613.

17. Quinn, W., Zopt, H.D.O., Short, K.S., and Yang, R.K., 1978. Historical trends and statistics of the Southern Oscillation, El Nino and Indonesian droughts. *Fish Bull.*, 76, pp. 663-678.

18. Rasmusson, E.M., and Wallace, J.M., 1983. Meteorological aspects of the El Nino/Southern Oscillation. *Science,* Vol. 222, No. 4629, pp. 1195-1202.

19. Reid, J.L., Jr., 1959. Evidence of a south equatorial counter current in the Pacific Ocean. *Nature,* Lond., 184, pp. 209-210.

20. Reynolds, R.W., 1982. A Monthly averaged climatology of the sea surface temperature. *NOAA Technical Report* NWS 31, pp. 1-35.

21. Sadler, J.C., and Kilonsky, J.C., 1983. Meteorological events during evolution of positive SST anomalies in the equatorial Pacific in 1982. *Trop. Ocean Atmos. Newsletter, 16.*

22. Sarkisyan, A.S., 1986. El Nino-Southern Oscillation and investigations of short-range climate variations according to the "Sections" Programme. WMO No. 649, pp. 42-46.

23. Shaffer, G., 1982. On the upwelling circulation over the wide shelf off Peru. 1. Circulation *J. Mar. Res.*, Vol. 40, 2 pp. 293-314.

24. Smith, R.L., 1978. Poleward propagating perturbations in currents and sea level along the Peru coast. *J. Geophys. Res.* Vol. 83, No. C12, pp. 6083-6092.

25. Tsuchiya, M., 1975. Subsurface countercurrents in the eastern equatorial Pacific Ocean. *J. Mar. Res.*, Vol. 33, pp. 145-175.

26. Walsh, J.J., Kelley, J.C., Dugdale, R.C., and Frost, B.W., 1971. Gross features of the Peruvian upwelling system with special reference to possible diel variation. Investigation Pesquera, 35, pp. 25-42.

27. Wang, D.P., and Mooers, C.N.K., 1976. Coastal trapped waves in continuously stratified ocean. *J. Phys. Oceanogr.*, 6, pp. 853-863.

28. White, W.B., Meyers, G.A., Donguy, J.R., and Pazan, S.E., 1985. Short-term climatic variability in the thermal structure of the Pacific Ocean during 1979-1982. *J. Phys. Oceanogr.*, Vol. 15, No.7, pp. 917-935.

29. Wooster W.S., 1961. Further evidence of a Pacific south equatorial countercurrent. *Deep-Sea Res.*, 8, 3/4. pp. 294-297.

30. Wooster, W.S., and Gilmartin, M., 1961. The Peru-Chile undercurrent. *J. Mar. Res.*, Vol. 19, No. 3, pp. 97-122.

31. Wooster, W.S. and Reid, J.L., 1963. Eastern boundary currents. In The Sea, ed., by M.N. Hill et al. Vol. 2, pp. 253-280, New York, London: Interscience Publishers.

32. Wyrtki, K., 1963. The horizontal and vertical field of motion in the Peru current. Bull. S10. Vol.8, No.4, pp. 313-346.

33. Wyrtki, K., 1964. The thermal structure of the Eastern Pacific Ocean. Deutsches Hydrographisches Institut-Hamburg. Reihe A (8o). Nr. 6, pp. 1-84.

34. Wyrtki, K., 1979. The response of sea surface topography to the 1976 El Nino. *J. Phys. Oceanogr.*, Vol.9, No. 6, pp. 1223-1231.

35. Wyrtki, K., 1982. The Southern Oscillation, ocean-atmosphere interaction and El Nino, *Mar. Technol. Soc. Jour.*, Vol. 16, No.1, pp. 3-10.

36. Wyrtki, K., 1985. Water displacements in the Pacific and the genesis of El Nino cycles. *J. Geophys. Res.*, Vol. 90, No. C4, pp. 7129-7132.

37. Yoshida, K., 1955. Coastal upwelling of the California coast. *Rec. Oceanogr. Wks.*, Japan, 2(2): 13 pp.

38. Yoshida, K., 1958. Coastal upwelling, coastal currents and their variations. *Rec. Oceanogr. Wks.* Japan, Sp. No.2: pp. 85-87.

39. Yoshida, K., 1959. A theory of the Cromwell Current (The Equatorial Current) and of the equatorial upwelling an interpretation in a similarity for a coastal circulation. *J. Oceanogr. Soc. Japan,* 15 (4): pp. 159-170.

40. Yoshida, K. and M. Tsuhiya, 1957. Northward flow in the lower layers as an indicator of coastal upwelling. *Rec. Oceanogr. Wks. Japan,* 4 (1) : 14-22.

41. Zuta, S., 1986. The characteristics of the 1982-83 El Nino off the Pacific coast of South America, WMO No. 649., pp 1-17.

42. Zuta, S., 1987 a. Condiciones Oceanograficas frente al Peru en 1986, Informe Interno, 5 febrero 1987 DGIO/IMARPE.

43. Zuta, S., 1987b. Sumario de las Observaciones oceanograficas frente al Peru en enero-febrero de 1987. Informe Interno, 24 febrero 1987. DGIO/IMARPE.

44. Zuta, S., D. Enfield, J. Valdivia, P. Lagos y C. Blandin, 1976. Aspectos Fisicos del Fenomeno El Nino 1972-73. FAO Informes de Pesca No.185. Actas, Reunion de Trabajo sobre el Fenomeno conocido como el Nino, pp 3-61.

45. Zuta, S., M. FarFan y O. Moron, 1984. Caracteristicas principales del mar frente a Peru durante la evolucion del evento El Nino 1982-83. Rev. Com. Perm. Pacifico Sur, (15): 141-178.

46. Zuta, S., M. FarFan y O. Moron, 1985. Fluctuaciones de la TSM y SSM durante el evento El Nino 1982-83, Ciencia, Tecnologia y Agresion Ambiental: El Fenomeno El Nino, CONCYTEC, Lima-Peru, pp 57-94.

47. Zuta, S. y O. Guillen, 1970. Oceanografia de las aguas costeras del Peru. Bol. Inst. Mar Peru-Callao, Vol. 2, No. 5, pp 157-324.

48. Zuta, S. and J. Quispe, 1981. Hydrographic features off Peru 1979-1980. Recent Progress in Equatorial Oceanography: A report of the final meeting of SCOR-WG47 in Venice, Italy, April 27-30, 1981. Published by Nova University/N.Y.I.T. Press., pp 61-73. 49.Zuta, S., T. Rivera and A. Bustamante, 1978. Hydrologic aspects of the main upwelling areas off Peru. Upwelling Ecosystems, edited by R. Boie and M. Tomezak. Springer-Verlag Berlin Heidelberg New York, pp 235-257.

50. Zuta, S., I. Tsukayama y R. Villanueva, 1983. El ambiente marino y las fluctuaciones de las principales poblaciones pelagicas de la costa peruana. FAO, Informes de Pesca, 291 (2) 179-253.

51. Zuta, S., y W. Urquizo, 1972. Temperature promedio de la superficie del mar frente a la costa peruana, Periodo 1928-1969. Bol. Inst. Mar Peru-Callao, Vol. 2, no.8, pp 459-520.